MODEL PREDICTIVE CONTROLLER BASED OPTIMAL ENERGY MANAGEMENT STRATEGY FOR A FUEL CELL HYBRID VEHICLE

by
ALI KEREM YALÇIN

Submitted to the Graduate School of Engineering and Natural Sciences
in partial fulfilment of
the requirements for the degree of
Master of Science

Sabancı University
April 2024

MODEL PREDICTIVE CONTROLLER BASED OPTIMAL ENERGY MANAGEMENT STRATEGY FOR A FUEL CELL HYBRID VEHICLE

Approved by:

Asst. Prof. Dr. Tuğçe Yüksel ....
(Thesis Supervisor)

Prof. Dr. Serhat Yeşilyurt ....

Assoc. Prof. Dr. Ahmet Onat ....

Date of Approval:

ABSTRACT

MODEL PREDICTIVE CONTROLLER BASED OPTIMAL ENERGY MANAGEMENT STRATEGY FOR A FUEL CELL HYBRID VEHICLE

Ali Kerem Yalçın

Mechatronics Engineering, Master's Thesis, April 2024

Thesis Supervisor: Asst. Prof. Dr. Tuğçe Yüksel

Keywords: fuel cell hybrid electric vehicles, electrical powertrain modeling, energy management strategy, model predictive control, rule-based control

In today's world, the environmental pollution and climate issues caused by fossil-fuel vehicles have made it a necessity to develop alternative technologies capable of being more environmentally friendly. Electric and hybrid vehicles have emerged as alternative technologies to fossil-fuel vehicles within this context, as they offer energy sources with less environmental impact. Despite the importance of electric vehicles due to zero tailpipe emissions, challenges such as limited range, long charging times, lower prevalence of charging stations compared to gas stations, and shorter battery life have led to increased research on hybrid vehicles based on the principle of utilizing multiple energy sources simultaneously. Internal combustion engine-based hybrid vehicles are not environmentally friendly due to their use of fossil fuels. In this regard, fuel cell hybrid electric vehicles draw attention due to several advantages such as zero carbon emissions, longer lifespan of the fuel cell compared to the battery, and shorter charging times. However, the distinct dynamics of batteries and fuel cells reveal the necessity of an energy management strategy that can efficiently and harmoniously utilize these sources in fuel cell hybrid electric vehicles.

In this thesis, the energy management problem in a fuel cell hybrid electric vehicle is addressed. Firstly, in the study, an electrical powertrain model of a fuel cell hybrid electric vehicle is developed in the Cruise-M simulation environment, providing a realistic platform for testing energy management strategies using its comprehensive components. The specifications of the first-generation Toyota Mirai are considered for the designed plant model. Subsequently, a rule-based energy management strat-

egy (RB-EMS) is developed not only to be a benchmark method, but also to assess the representability of the presented plant model. Furthermore, a model predictive control-based energy management strategy (MPC-based EMS) is designed and employed to solve the energy management problem in an optimization-based manner. The developed strategy can adjust the weight factors of the cost function in real-time and improves the the controller performance by enhancing the effectiveness of the optimization. It is observed that the designed plant model can produce realistic results considering the experimental outputs of the power sources presented in the dynamometer test results conducted on a Toyota Mirai. According to the simulation results, it is revealed that the power allocation performance of the MPC-based EMS is more satisfactory compared to the RB-EMS. The strategy has improved fuel economy by reducing fuel consumption overall by 3% compared to the RB-EMS and has been able to keep the battery's state of charge within a certain range. Ultimately, it is understood that the presented powertrain model has the potential to be a realistic virtual platform for studying different energy management strategies extensively. Additionally, the real-time adjustability of controller parameters based on the system's instantaneous conditions via a feedback mechanism in the model predictive control approach demonstrates its potential for further enhancement in such an application.

ÖZET

HİDROJEN YAKIT HÜCRELİ ELEKTRİKLİ ARAÇLAR İÇİN MODEL ÖNGÖRÜLÜ KONTROL TEMELLİ ENERJİ YÖNETİMİ STRATEJİSİ

Ali Kerem Yalçın

Mekatronik Mühendisliği, Yüksek Lisans Tezi, Nisan 2024

Tez Danışmanı: Dr. Öğr. Üyesi Tuğçe Yüksel

Anahtar Kelimeler: yakıt hücreli hibrit elektrikli araçlar, elektriksel güç aktarma organı modelleme, enerji yönetim sistemi, model öngörülü kontrol, kural tabanlı kontrol

Günümüzde fosil yakıtlı araçların çevre kirliliğine ve iklim problemlerine yol açması, kabiliyet anlamında bu araçlara alternatif olabilecek ve çevreyi en az düzeyde kirletecek alternatif teknolojilerin gelşitirilmesini bir ihtiyaç haline getirmiştir. Nitekim elektrikli ve hibrit araçlar, bulundurdukları enerji kaynaklarının çevreye daha az zarar vermesi nedeniyle fosil yakıtlı araçlara birer alternatif teknoloji olarak ortaya çıkmaktadır. Elektrikli araçların sıfır karbon salınımı nedeniyle sahip olduğu öneme rağmen; menzil problemleri, uzun şarj süreleri, şarj istasyon sayısının akaryakıt istasyonları kadar yaygın olmaması ve batarya ömrünün kısalığı gibi dezavantajlar, birden fazla enerji kaynağının bir arada kullanılması prensibine dayanan hibrit araçlara yönelik çalışmaların yoğunluk kazanmasına neden olmuştur. İçten yanmalı hibrit araçlar fosil yakıt kullanması nedeniyle çevre dostu değildir, bu noktada yakıt hücreli hibrit araçlar sıfır karbon salınımı, yakıt hücresinin bataryaya göre daha uzun ömürlü olması ve şarj süresinin daha kısa olması gibi avantajları sayesinde dikkat çekmektedir. Batarya ve yakıt hücresinin farklı dinamiklere sahip olması, bu kaynakların en verimli şekilde ve uyum içerisinde kullanılmasını sağlayabilecek bir enerji yönetimi stratejisinin gerekliliğini ortaya koymaktadır.

Bu tez kapsamında yakıt hücreli hibrit bir elektrikli araçtaki enerji yönetimi problemi ele alınmıştır. Öncelikle çalışmada, bir yakıt hücreli hibrit elektrikli aracın elektriksel güç aktarma sisteminin modeli Cruise-M simulasyon ortamında geliştir-

ilmiş, ortamın sunduğu kapsamlı ve gerçekçi komponentler kullanılarak enerji yönetim stratejilerinin test edilebileceği bir platform sunulmuştur. Tasarlanan sistem modeli için birinci nesil Toyota Mirai'nin özellikleri baz alınmıştır. Daha sonra, hem ortaya konan modelin referans sistemi temsil edebilirliğini sınamak, hem de bir karşılaştırma yöntemi olmak üzere bir kural tabanlı enerji yönetimi stratejisi geliştirilmiştir. Devamında, enerji yönetim problemini optimizasyon temelli olarak çözmek için model öngörülü kontrole dayanan bir enerji yönetim stratejisi tasarlanmış ve kullanılmıştır. Geliştirilen strateji, gerçek zamanlı olarak maliyet fonksiyonundaki ağırlık faktörlerini ayarlayabilmekte ve optimizasyonun başarısını artırarak kontrolör performansını iyileştirmektedir. Toyota Mirai'ye ait dinamometre testi sonuçlarında sunulan güç kaynaklarının performans çıktıları göz önünde bulundurulduğunda, tasarlanan sistem modelinin gerçekçi sonuçlar üretebildiği gözlemlenmiştir. Simulasyon sonuçlarına göre model öngörülü kontrol tabanlı enerji yönetim stratejisinin güç paylaşımı performansının kural tabanlı enerji yönetim stratejisine göre daha başarılı olduğu gözlemlenmiştir. Yöntem, kural tabanlı stratejiye kıyasla yakıt tüketimini tüm test sonuçlarının toplamında %3 azaltarak yakıt ekonomisini iyileştirmiş ve bataryanın şarj seviyesini belirli bir aralıkta tutabilmiştir. Sonuçta, ortaya konan güç aktarma modelinin farklı enerji yönetim stratejilerini çalışmak için gerçekçi bir platform olma potansiyeline sahip olduğu anlaşılmıştır. Ayrıca, model öngörülü kontrol yaklaşımında kontrolör parametrelerinin geri besleme mekanizması aracılığıyla sistemim anlık koşullarına bağlı olarak gerçek zamanlı olarak ayarlanabilmesi, bu yöntemin potansiyel olarak bu tür bir uygulamada daha da geliştirmeye açık olduğunu göstermektedir.

ACKNOWLEDGEMENTS

I would first like to express my gratitude to my advisor Dr. Tuğçe Yüksel for her guidance, patience, and unflagging support during the course of this whole study. I could not have completed this work without her unwavering support and endless patience. Whenever I have become lost, her invaluable guidance and insightful feedback have illuminated my way.

I extend my gratitude to Prof. Dr. Serhat Yeşilyurt and Doç. Dr. Ahmet Onat for accepting to participate as a jury member of the committee for my thesis defense. Their constructive critiques have greatly enriched the quality of my study and thesis.

An important part of the study was conducted using Cruise-M, therefore I would like to state my appreciation to my company, AVL List GmbH, for providing me with this opportunity.

I would also like to thank Dr. Sabri Yılmaz for supporting me with his deep expertise, wherever I was lacking the key knowledge. Also, I appreciate the support of my other colleagues, this challenging process could not have proceeded without their support and understanding.

I wish to express my heartfelt appreciation to my beloved family for their constant support, not only during this particular phase but also throughout my entire life journey. None of my achievements would have been possible without their guidance and encouragement.

To my family,
for their endless love, patience, and encouragement

TABLE OF CONTENTS

LIST OF TABLES

LIST OF FIGURES

1. Introduction

The first chapter discusses the importance of alternative energy sources in transportation and the concept of hybrid electric vehicles, followed by an exploration of the powertrain system of fuel cell hybrid electric vehicles and various topologies in use. Subsequently, the energy management problem in fuel hybrid cell electric vehicles is addressed, along with a survey on different types of energy management systems developed to solve this problem. Finally, the main focus of the study is introduced, emphasizing the potential benefits of an optimization-based energy management strategy using an advanced control method with improved robustness.

1.1 Hybrid Electric Vehicles

In today's automotive industry, the idea of environmentally friendly and sustainable transportation is gaining importance. The main reason behind this trend is the heightened awareness of the environmental damage caused by internal combustion engine (ICE) vehicles, reaching significant proportions nowadays. As is known, the burning of fossil-based fuels releases stored carbon and other greenhouse gases into the atmosphere. In 2022, it is observed that approximately 80% of the primary energy demand is met by fossil fuels [2]. Considering the world's increasing energy demand, the use of fossil fuels on the same scale will inevitably lead to climate problems. Looking at the energy demand between the sectors, transportation plays a significant role. In the United States in 2022, 27% of the total energy consumption was for transportation purposes, and also during the same year, petroleum-based fuels accounted for 90% of the energy demand in transportation [9]. Therefore, one of the most crucial sectors to address the climate crisis is the transportation. Figure 1.1 shows that light-duty vehicles including light trucks, cars, and motorcycles, have the largest share in energy usage in transportation in the U.S. At this point, in addition to electric vehicles, hybrid vehicles that use various alternative energy sources come to the forefront to reduce carbon emissions caused by transportation.

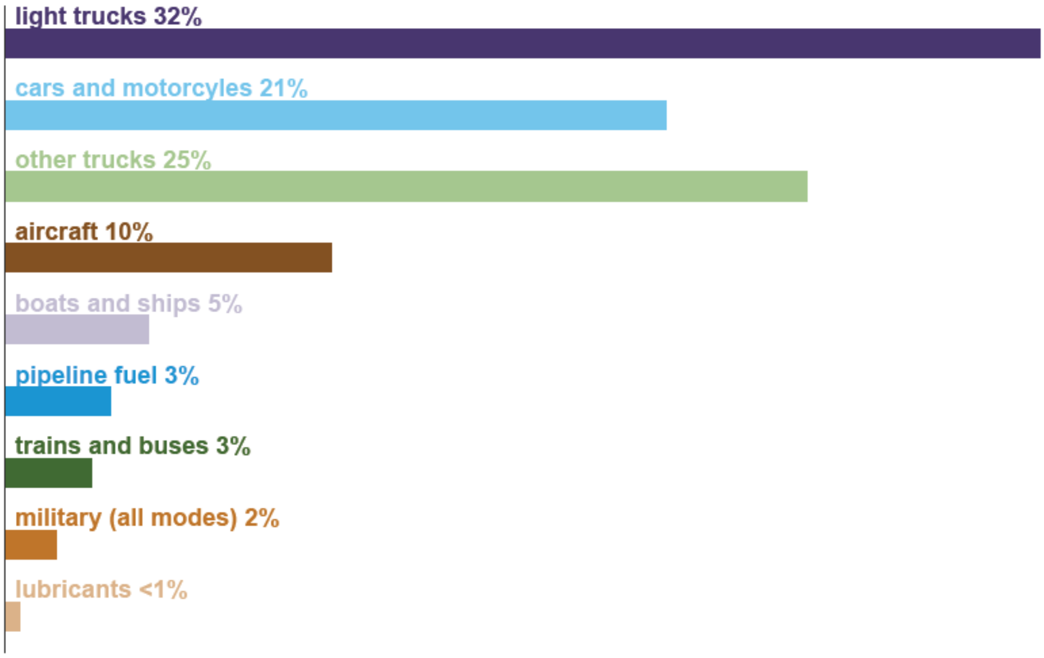

Figure 1.1 U.S. energy use in transportation by type [2]

While the history of hybrid and electric vehicles dates back to the 19th century, their widespread use in the automotive sector has increased in the late 20th and early 21st centuries [10]. Although the potential of electric vehicles to reduce carbon emissions has been increasingly recognized recently, several obstacles are preventing their dominance in transportation. To exemplify, electric vehicles do not have as a long range as internal combustion engine vehicles, and their long charging times coupled with the limited availability of charging stations, pose significant challenges to their widespread adoption. In this context, hybrid vehicles, by combining different energy sources, have the potential to overcome the disadvantages of electric vehicles. For instance, in a full hybrid electric vehicle, the battery-powered electric motor is used instead of the internal combustion engine in regions where the ICE operates at low efficiency, aiming to increase overall efficiency and reduce carbon emissions. However, the relatively smaller capacity of the battery and its inability to be charged externally in such hybrid vehicles require the majority of power demands still to be met by the internal combustion engine. On the other hand, plug-in hybrid electric vehicles (PHEVs) generally have a battery with a larger capacity that can be charged by the internal combustion engine or an external charger. The larger battery capacity allows for more efficient operation by mainly using the electric motor and reduces carbon emissions. The fact that the battery can be charged from an external grid, it enables a longer-range with the battery and further reduction in carbon emissions by relying solely on the electric motor. In range-extender configurations, the hybrid vehicle always draws the required power from the electric motor only. The internal combustion engine in such vehicles is used to charge the battery, allowing it to operate in its most efficient region. Despite the conventional hybrid electric vehicles offer various advantages through different configurations, they cannot cancel out carbon emissions due to the employment of an internal combustion engine.

When looking at alternative fuel types in transportation, hydrogen stands out due to its carbon-free nature, offering significant potential for sustainable and clean transportation. Fuel cell hybrid electric vehicles (FCHEV) utilize both fuel cells and batteries as power sources and do not generate any harmful end products during energy conversion, only releasing water and heat. Indeed, FCHEVs have drawn attention for being carbon-zero and highly efficient, leading to ongoing efforts to promote their widespread use in transportation. Various original equipment manufacturers (OEMs) currently offer FCHEV models in the market, such as the Hyundai Nexo, Honda Clarity, and Toyota Mirai among the most popular ones. FCHEVs have several advantages over internal combustion hybrid vehicles and electric vehicles. For instance, refueling hydrogen into high-pressure tanks on the vehicle takes approximately five minutes, whereas fully charging a battery can take around 20 minutes with fast chargers or up to 20 hours with a domestic plug [11][12]. Additionally, as mentioned earlier, hydrogen which is a completely carbon-free energy source, makes FCHEVs environmentally superior to internal combustion hybrid vehicles. Furthermore, the efficiency of the chemical-to-electrical energy conversion process in a fuel cell can exceed 60%, while the efficiency of converting chemical energy to kinetic energy in internal combustion engines ranges from 12% to 30% [13][14]. This is because, in a fuel cell system, chemical energy is directly converted into usable electrical energy, whereas e.g. in the Otto cycle for a spark ignition internal combustion engine, chemical energy is firstly converted to thermal energy and then to mechanical energy. Despite these advantages, several challenges hinder the widespread adoption of FCHEVs in the market. The first challenge is the high cost associated with using hydrogen as a fuel. Additionally, the limited number of hydrogen refueling stations today poses another disadvantage. Considering that the FCHEV is a relatively new concept and the aforementioned problems are expected to be overcome with the development of the fuel cell system technology, the control of power flow through different power sources in FCHEVs emerges as a fundamental problem to be addressed.

1.2 Fuel Cell Hybrid Electric Vehicle Powertrain and Topologies

FCHEVs offer a distinctive sustainable transportation solution by utilizing fuel cell technology for electrical power generation to provide propulsion. The fuel cell generates electrical power through a series of electrochemical reactions. Throughout these electrochemical reactions, hydrogen and oxygen are used as fuels, and the only byproducts released in the reaction are water and heat. This section delves into the utilization of the electrical energy converted in the fuel cell for the vehicle's propulsion, discussing the power flow on the powertrain, components within the powertrain, and various FCHEV topologies.

The powertrain of FCHEV generally consists of fundamental components present in all configurations, and each of these components plays a specific role in the overall system. A typical FCHEV powertrain comprises a fuel cell stack, an energy storage system as a secondary power source, a hydrogen storage system, and an electric drive system, apart from the mechanical system. The fuel cell stack serves as the primary energy converter, and the hydrogen storage system ensures a reliable fuel supply. Due to the slow dynamics of the fuel cell and the need for an initialization time during the startup, a battery is typically introduced as a secondary power source to provide energy to the powertrain in cases where the operation of the fuel cell system is infeasible. Beyond this, there exists a configuration known as range-extender FCHEVs, where the battery serves as the sole power source for propulsion, and the fuel cell system is used to charge the battery. In such configurations, a larger capacity battery pack is deployed. Considering dynamic power demands throughout the driving, configurations incorporating a supercapacitor in addition to the fuel cell and battery, are also in use to take advantage of the high power density of supercapacitors.

The selection and placement of different power sources in the powertrain have led to the emergence of various topologies, aiming to achieve higher efficiency and reduce operational costs. Examining the literature and industry, six different configurations are identified in FCHEVs based on the type of power source and their connection to the DC bus [3]. Each configuration has its own set of advantages and disadvantages. Increasing the diversity of power sources offers advantages in meeting dynamic power demands, enhancing operational efficiency, and increasing component durability. However, it also results in a higher powertrain complexity, complicating the control problem and increasing production costs. In FCHEVs, the regulation of output voltages through DC/DC converters is conducted by the energy management system (EMS). Increasing the number of DC/DC converters provides a higher degree of freedom for independent control of each power source, facilitating more effective utilization of them. However, using more DC/DC converters also causes increased switch losses in the powertrain and lower efficiency. Conversely, reducing the variety of power sources and the number of DC/DC converters can lower the vehicle's cost and weight but may result in underperformance of the power control, leading to inefficient operation and quicker aging of sources. In Figure 1.2, topologies are listed according to increasing complexities. T1, T2, T3, and T4 configurations have only one secondary power source, either a battery or a supercapacitor, while T5 and T6 comprise both a battery and a supercapacitor in addition to the fuel cell system.

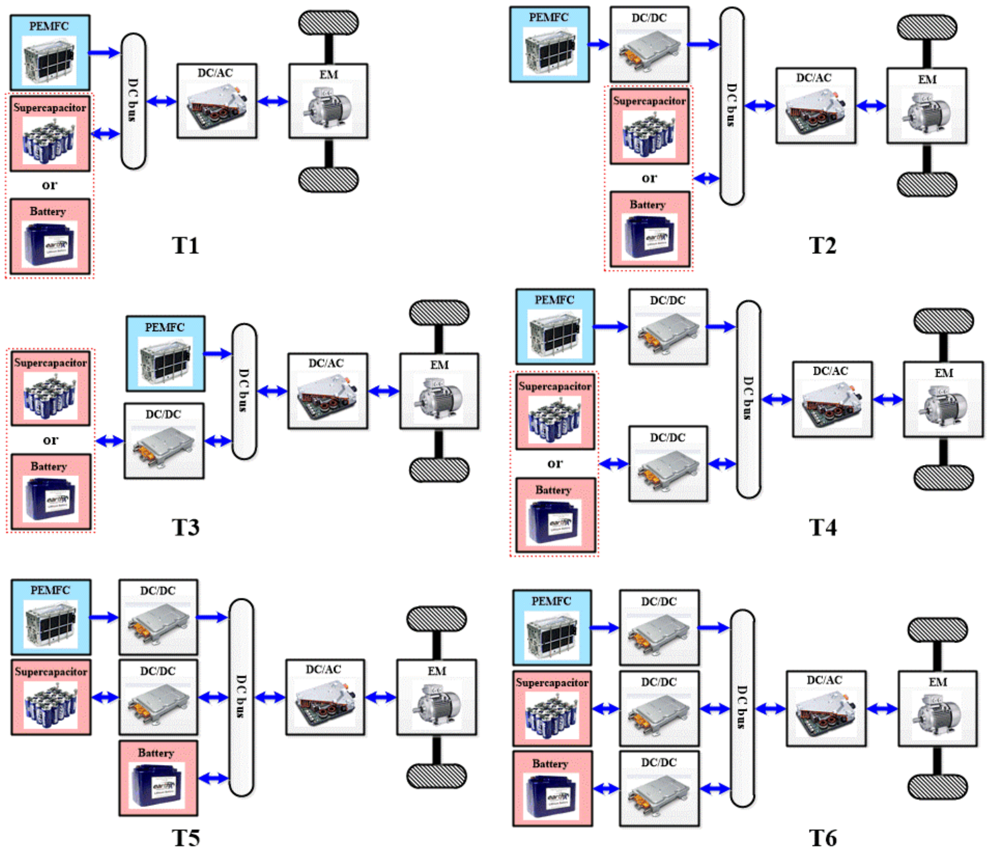

Figure 1.2 Schematic of six different topologies utilized in FCHEVs [3]

All topologies have a DC/AC converter (inverter) on the DC bus to drive the AC motor. However, in this study, the power produced on the DC bus directly powers the electric motor and the impact of this assumption is examined in the subsequent sections of the thesis. In the study, the electric motor, fuel cell stack, and battery pack operate at different voltage levels. Therefore, it is necessary to elevate the output voltages of the power sources to the operating level of the electric machine on the DC bus. Additionally, considering the limited prevalence of supercapacitor usage in the industry, the T4 configuration, utilizing a battery and two DC/DC converters, was chosen for this study.

1.3 Energy Management Strategies in Fuel Cell Hybrid Electric Vehicles

As discussed earlier, using more than one power source has necessitated the development of various energy management strategies in FCHEVs for the balanced and compatible utilization of power sources. An EMS is a framework consisting of algorithms for optimizing the usage of power sources to ensure efficient operation and high performance. In a typical EMS, the energy supply from the fuel cell for powering the electric motor is controlled, and the energy stored in the battery and/or the supercapacitor is managed at the same time throughout the driving. Under the command of a successful EMS, fuel economy is improved by maximizing the fuel cell system efficiency, battery state of charge (SOC) is kept within a desired range to prolong the battery lifetime, and also degradation of the fuel cell system is reduced by decreasing the on-off switchings and operating it smoothly without violating the physical limits.

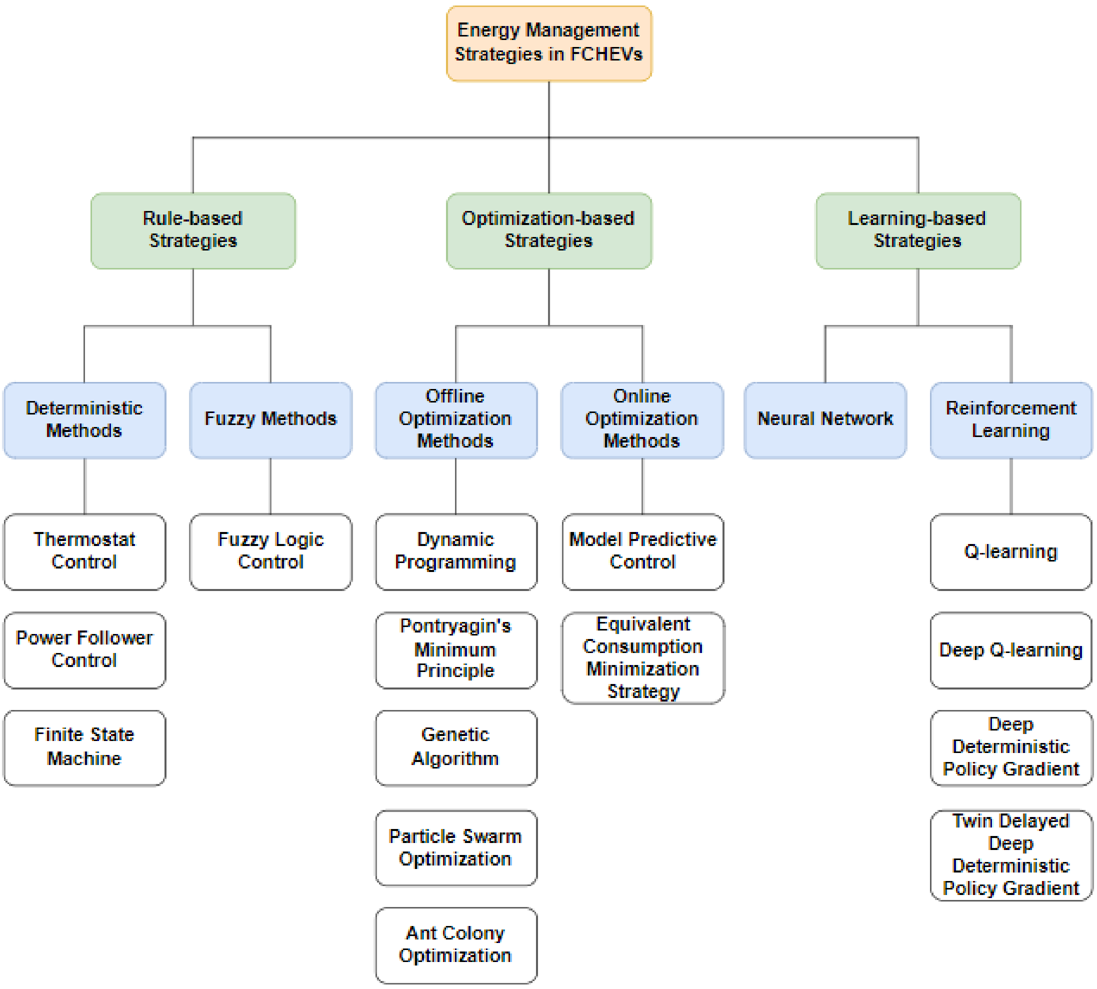

Figure 1.3 Different types of energy management strategies used in FCHEVs (adapted from [4])

Although FCHEV technology has not matured to the same extent as classical HEV and EV yet, there are several studies conducted on the energy management problem of FCHEVs in the literature. According to these studies, the EMSs are mainly categorized as rule-based, optimization-based, and learning-based [4].

Rule-based EMSs perform energy management based on a set of predefined rules, generally in the form of if-then decision-making statements to derive actions from conditions. Rule-based EMSs control the utilization of power sources in real time. In today's automotive industry, it is known that an important portion of the control applications in vehicle systems are based on rule-based algorithms, e.g. state machines, static maps, etc. since they are reliable, fast, easy to implement, and require less memory and processor power [15]. In the literature, rule-based methods are split into two categories which are deterministic techniques and fuzzy rule-based control strategies. Finite state machine [16], thermostat control [17], load-following control [18], and PID control [19] are some of the approaches that fall under the deterministic rule-based strategies. Despite their low computational requirements and simple design that enables them to be used in commercial applications, the control performance is not strong since rules cover only limited driving scenarios and they are based on the designer's expertise. Fuzzy rule-based strategies exhibit a higher level of sophistication than deterministic rule-based approaches, as they emulate a human-like decision-making process to control the power allocation between the sources [20][21]. However, since they rely on rules defined heuristically, fuzzy rule-based EMSs do not guarantee optimal power-splitting under uncertain driving conditions. In the literature, rule-based strategies are generally studied for comparison purposes with other methods and outperformed by other strategies [22][23].

Optimization-based strategies are divided into two categories which are online and offline optimization techniques. Offline optimization strategies do not produce real-time solutions but seek the global optimum solution under the assumption that the velocity data is known for the whole driving beforehand. Among these methods, dynamic programming (DP) guarantees to find the global optimum solution in a deterministic manner using the Bellman principle of optimality, however, the solution time is not feasible for online utilization due to the extensive combination of discrete states and inputs, along with the interpolation method used during the iterative process [24, 23, 25]. Pontryagin's Minimum Principle (PMP) is another typical offline approach, which searches for the optimum policy by minimizing the Hamilton function while considering the upper and lower bounds [26, 27, 28]. PMP can yield results comparable to DP, however, the requirement of co-state tuning in the Hamiltonian for different conditions emerges as a disadvantage. Although it does not guarantee to find the global optimality in all cases, it is seen that PMP has improved computational efficiency compared to DP [29]. Also in recent years, population-based meta-heuristic algorithms such as Genetic Algorithm [30, 31], Particle Swarm Optimization [32, 33], and Ant Colony Optimization [34, 35] have been used in the management of hybrid energy systems to search the optimum solution in a stochastic way. Although these methods are effective at exploring large solution spaces, global optimality is not guaranteed. Even though there are studies applying PMP in real-time by searching sub-optimal solutions [36], the offline approaches cannot be adapted to the online optimization process of EMSs because of long execution times. However, the global optimization methods are extensively used in EMS design studies e.g. component sizing and controller parameter tuning [37, 38]. They are also widely used as benchmark methods since they seek the global optimum solution obtaining the best outcomes to be compared with other methods [39, 40].

Online optimization strategies minimize a cost function in a cyclic way by searching for a local optimum solution within a sampling period. So, a time-dependent optimization problem emerges by receiving the new values of the system outputs at each time step. Hence, different from the global optimization methods, the entire optimization problem is split into sub-problems to be solved in a real-time manner. In FCHEV studies, the equivalent consumption minimization strategy (ECMS) is a well-known online optimization-based method that adjusts the power split between the energy sources by computing the equivalent fuel consumption based on the energy usage of the fuel cell and the energy storage component [41][42]. Model predictive control (MPC) is another extensively used optimal control technique in the energy management of FCHEVs that power-allocation is optimized based on the predictions of the system dynamics over a certain time horizon. MPC leverages core concepts such as states, internal model, prediction horizon, and control horizon, to formulate a predictive control system that optimizes system performance while adhering to operational constraints. By integrating real-time feedback and predictive modeling, MPC enables effective control of dynamic systems across various domains. MPC has been studied widely in the energy management of FCHEVs due to its strong performance in finding sub-optimal solutions under a constrained optimization problem [43][44][45]. However, there is a trend in literature that MPC architecture is modified to improve the optimal control performance so that the controller is enabled to respond the system states dynamically. [46] proposes a Markov-based pattern recognizer to identify the actual driving conditions and uses different cost function weights. However, fixed weights are used in the cost function. In [47], a fuzzy cognitive map is integrated into an MPC-based EMS to dynamically adjust the cost function weights according to the actual performance outcomes of the system, and it is found that the proposed MPC method outperforms constant weight-based non-linear MPC and conventional non-linear MPC using a cost function with fewer objectives.

Intelligent methods, which are based on learning techniques, have become a favorable approach in recent years due to the advantage of model-freeness. There are various techniques in the literature that involves artificial intelligence such as reinforcement learning [48, 49] and artificial neural networks [50, 51]. Q-learning appears as one of the most common methods [52, 53], among the reinforcement learning techniques. Also, there are techniques such as Deep Q-learning (DQN) [54] and Deep Deterministic Policy Gradient [55] which are evolved from Q-learning. Overall, while intelligent energy management strategies offer promising benefits owing to the complexities in systems and the strong precision capability of these methods, they also pose challenges related to data dependence, computational complexity, and generalization problems.

1.4 Thesis Objectives and Contributions

As an overview of the studies on the development of EMS for FCHEVs, rule-based strategies are incomprehensive and often used as an underperforming approach in comparative studies since they do not involve optimization, although they are the most relied method in the industry. On the other hand, offline optimization strategies can find the best results within a long execution time and even in infinite time. However, the problem with this method is that it is not feasible for the real-time energy management problem due to the realization issue stemming from the long execution time. The machine learning methods are promising due to strong precision, however, they still suffer from realization in commercial transportation applications due to their limited reliability in safety-critical systems. At this point, online optimization strategies become prominent due to their suitability for real-time applications and ability to find optimal results. However, considering the wide range of driving conditions, the formulation of the problem with a fixed cost function would not be effectively reacting to all cases such as low-speed cruising, high-speed cruising, and aggressive driving. Thus, within this study, we develop an MPC-based EMS that adjusts the weight factors of the objective function dynamically. A map-based weight selection approach is involved in the problem formulation to achieve the dynamic adjustment of the weights, which is driven by the system states.

In summary, one of the objectives of this study is to propose an online optimization-based energy management strategy using model predictive control to maximize fuel economy, prolong the lifetime of the power sources by minimizing the degradation throughout their utilization, and be able to change controller parameters according to the actual system states to improve the performance of the optimization while considering the physical limits of the controlled FCHEV powertrain system model. To realize those targets, a model must be available that can produce the performance outputs of the powertrain components. In this context, this study also aims to provide a comprehensive model of an FCHEV being able to yield almost realistic system behavior of the power sources. The main expectation in this study is that the MPC-based EMS outperforms the RB-EMS on the obtained FCHEV powertrain model, in terms of fuel consumption and feasible utilization of the power sources. To this end, the work packages are described in the following steps:

- Creating an FCHEV powertrain model based on the electrical units of Toyota Mirai, using the comprehensive components of the Cruise-M simulation platform.
- Development of a rule-based EMS as a benchmark method that can be used for evaluating the reliability of the model concerning the dynamometer results of the Mirai.
- Development of a model predictive control-based EMS to solve the multi-objective optimization problem.
- Comparison of the MPC-based EMS and the RB-EMS results by evaluating not only the fuel consumption but also success in the lifetime extension of the battery and the fuel cell.

The main contribution of this thesis is to present a realistic plant model using Cruise-M vehicle system simulation platform, which includes calibrated system and component models that can provide energy and performance outputs so that the RB- and MPC-based energy management strategies are assessed exhaustively.

1.5 Thesis Outline

The thesis consists of a total of 6 chapters. The organization is listed below:

- **Chapter 2** presents the FCHEV powertrain model created in Cruise-M and the specifications of the utilized electrical and electrochemical components in the model.

- **Chapter 3** explains the development of the RB-EMS and the evaluation of the plant model by comparing its results with the dynamometer results.
- **Chapter 4** elucidates the design of MPC-based EMS, including the theory of model predictive control and problem formulation. Additionally, this chapter discusses the simulation results of three different calibrated controllers and shares the parameter adjustments for these MPC-based EMSs.
- **Chapter 5** presents the simulation results for five different drive cycles and discusses the behavior and performance of the RB-EMS and MPC-based EMS under different driving conditions.
- Lastly in **Chapter 6**, the thesis is concluded and the general inferences about the study are shared. In addition, the future works and the recommendations are included in this chapter.

2. Electrical powertrain Model of Fuel Cell Hybrid Electric Vehicle

Solution of the energy management problem requires a deep knowledge of the system being focused on. For this reason, to be able to tackle the energy management problem, the utilized FCHEV powertrain model is analyzed in this chapter at first. The electrical powertrain system model is designed in Cruise-M, which is developed by AVL List GmbH and offers a multi-physical environment. Due to its comprehensive components, Cruise-M appeals in automotive studies as a virtual test environment in domains such as driveline, engine, aftertreatment, hydraulics, and electrics [7]. Thanks to its real-time simulation capability and compatibility with third-party software e.g. Simulink, it becomes a suitable choice for creating the FCHEV powertrain model. The powertrain model developed in Cruise-M comprises a fuel cell, a battery, and two DC/DC converters which are the components placed between the electric motor (EM) and power sources. Figure 2.1 shows the powertrain topology used in this study, which is T4 as described in the first chapter. Since the AC/DC converter and supercapacitor are not in the scope of the study, they are removed from the original architecture. Also, the schematic of the model which is developed in Cruise-M is presented in Figure 2.2.

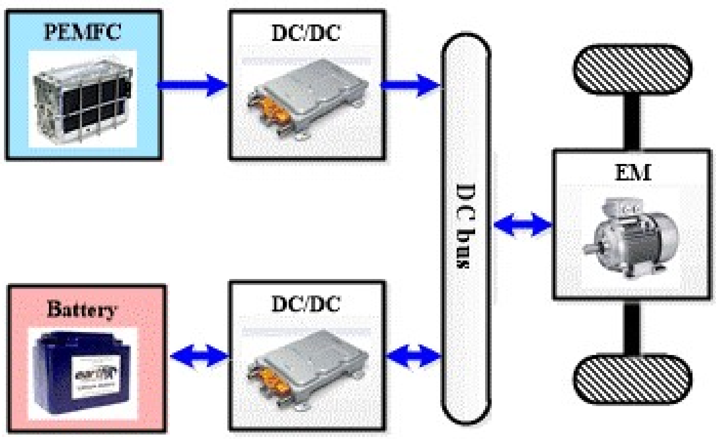

Figure 2.1 Powertrain architecture of the FCHEV in the study [3]

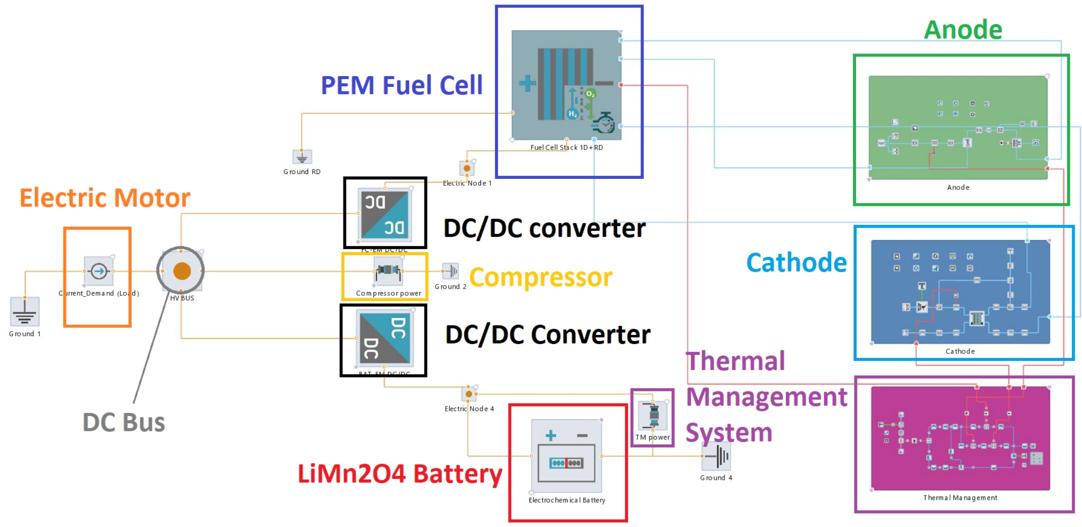

Figure 2.2 Eletrical Powertrain of the FCHEV in Cruise-M

The powertrain created in Cruise-M is based on the specifications of a first-generation Toyota Mirai. The main mission of the model is to be able to sufficiently, without significant deviations in performance outcomes, represent the results of the dynamometer test executed by Argonne Laboratory for the Toyota Mirai [56]. In direct proportion to this, only the electrical components of the powertrain are taken into consideration during the design phase. The main reason behind this is the fact that the mechanical losses in the drivetrain are not available in the dynamometer test data. Therefore, setting the reference load in terms of speed and then calculating the outputs of the power sources would cause an extension of the difference between the model results and the dynamometer test results of the Mirai. Hence, the reference being fed to the model is selected as the time-series data of the electric motor power rather than vehicle velocity. Since the efficiency information of the electric motor is not published by the testing authority, the electrical power of the motor is obtained from the mechanical power data by using fixed motor efficiencies of 90% and 85% for traction and braking respectively as in Equation 2.1.

$$P_{em_e} = \begin{cases} \frac{P_{em_m}(t)}{\eta_{em_t}}, & P_{em_m}(t) \geq 0 \\ P_{em_m}(t) \times \eta_{em_b}, & P_{em_m}(t) < 0 \end{cases} \tag{2.1}$$

where $P_{em_e}(t)$ and $P_{em_m}(t)$ are the electrical and mechanical power of the motor respectively, η_{em_t} and η_{em_b} are the motor efficiency respectively during the traction and braking. Also as mentioned earlier, no inverter is employed in the electrical powertrain model under the assumption that the EM is directly fed via the DC bus without any conversion from DC to AC. For this reason the efficiency of the inverter included in η_{em_t} and η_{em_b} in Equation 2.1.

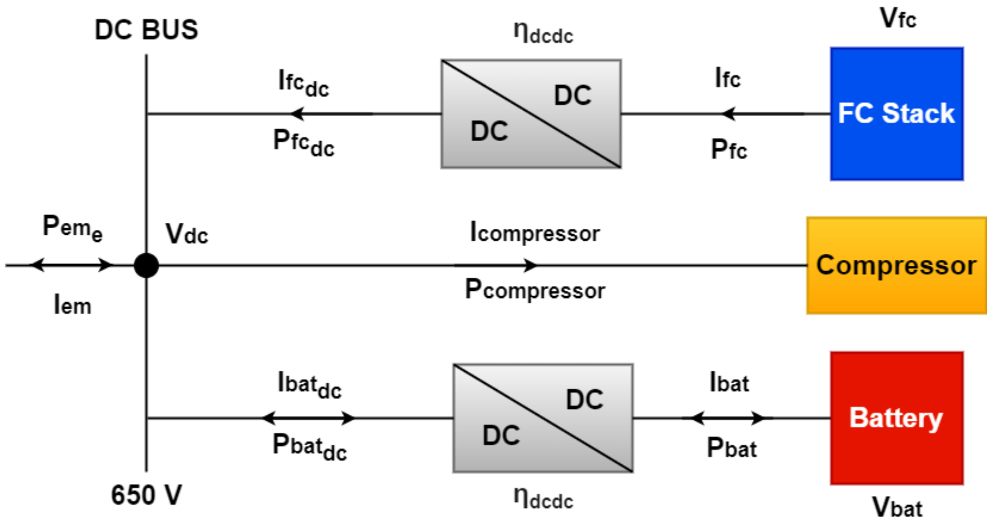

Figure 2.3 Architecture of the DC bus

The power demand is fed to the FCHEV electrical powertrain model in terms of the electrical power of the electric motor, through the DC bus shown in Figure 2.3. It is assumed in the design that the power demand is always met either by one of the power sources or both. Thus the power balance between the electrical power of the motor, the compressor power, and the power outputs of the DC/DC converters on the motor side is always satisfied as shown in Equation 2.2.

$$P_{em_e}(t) + P_{compressor}(t) = P_{fc_{dc}}(t) + P_{bat_{dc}}(t) \tag{2.2}$$

where $P_{compressor}$ is the compressor power, $P_{fc_{dc}}(t)$ and $P_{bat_{dc}}(t)$ are the power outputs of DC/DC converter's DC bus side for the fuel cell and battery respectively. After obtaining the electrical power reference, the load is applied to the electrical powertrain model in terms of current. To obtain the reference load in terms of current, the electrical motor power is divided by a constant DC bus voltage, as given in Equation 2.3

$$I_{em}(t) = \frac{P_{em_e}(t)}{V_{dc}} \tag{2.3}$$

where V_{dc} is the DC bus voltage specified in the model as the DC bus voltage of the Mirai.

The simulation starts by applying the power demand to the powertrain system in terms of current. Then the power demand is allocated between the fuel cell and the battery depending on the decisions of the EMS cyclically. The decision is executed in the model by setting the DC bus output current of the DC/DC converter between the fuel cell and the electric motor. Sequentially, the rest of the demand is always met by the battery. Since the fuel cell and battery operate at the DC bus voltage thanks to the DC/DC converters, the current equation shown in Equation 2.4 is always fulfilled in the electrical powertrain model in Cruise-M.

$$I_{em}(t) + I_{compressor}(t) = I_{fc_{dc}}(t) + I_{bat_{dc}}(t) \tag{2.4}$$

where $I_{em}(t)$, $I_{compressor}(t)$, $I_{fc_{dc}}(t)$, and $I_{bat_{dc}}(t)$ are respectively motor, compressor, fuel cell, and battery currents at the DC bus. The model also contains a thermal management subsystem that performs the thermal control of the fuel cell. In the study, since no investigation is aimed at the thermal effects, the thermal management subsystem will not be further mentioned except for the energy outcome of the cooling pump. In the plant model, the energy consumption at the thermal management system units is directly met by the battery due to the topology and included in the battery efficiency. Also other than the thermal management system, the compressor power which depends on the fuel cell power is assumed to be the total loss at the auxiliary system. Specifications of the electrical powertrain model and Toyota Mirai are presented in Table 2.1

Table 2.1 The powertrain specifications [1]

Powertrain Specification	FCHEV model	Toyota Mirai	Unit
DC bus voltage	650	650	V
Maximum motor power	114	114	kW
Motor and inverter efficiency traction	90	Not Available	%
Motor and inverter efficiency braking	85	Not Available	%
DC/DC converter efficiency	95	Not Available	%
Battery DC/DC converter type	bidirectional	bidirectional	-
Fuel cell DC/DC converter type	unidirectional	unidirectional	-
Battery efficiency	Cruise-M default	Not Available	%
Fuel cell efficiency	Cruise-M default	Not Available	%

2.1 Fuel Cell System Model

A fuel cell converts the chemical energy to thermal and electrical energy through its reactants in a redox reaction. Throughout the process, only water and heat are produced as byproducts. Unlike a battery, it does not store the chemical energy internally, the chemical energy container is fed to the cells externally. Since proton-exchange membrane fuel cell (PEMFC) is the most widely used type in automotive due to its feasibility for mobile applications and also the reference vehicle uses this type of a fuel cell, an electrochemical PEMFC model is equipped in the electrical powertrain in Cruise-M. The mobile ion of a PEMFC is H^+. As long as hydrogen is fed and the air intake is enabled, the redox reaction between hydrogen and oxygen proceeds. In the fuel cell system, several auxiliary units cooperate to perform the process in the fuel cell stack, and consequently, the dynamics of power production is relatively slow. On the other hand, there are multiple similarities between the structures of a battery and a fuel cell in terms of comprising anode, cathode, and electrolyte. During the process of converting the energy from chemical to electrical form, hydrogen molecules are fed through the anode, and air is supplied into the cathode. Then through the anode reaction, hydrogen molecules are split into their protons and electrons. At this point, the electrons reach to cathode through the external circuit, resulting in the electrical flow. The protons reaching the cathode, through the electrolyte, react with the oxygen in the air-filled-cathode, producing the water molecules. Throughout the process, the free electrons moving through the external circuit are available for utilization to meet the power demand. The energy conversion process in a PEM fuel cell is illustrated in Figure 2.4.

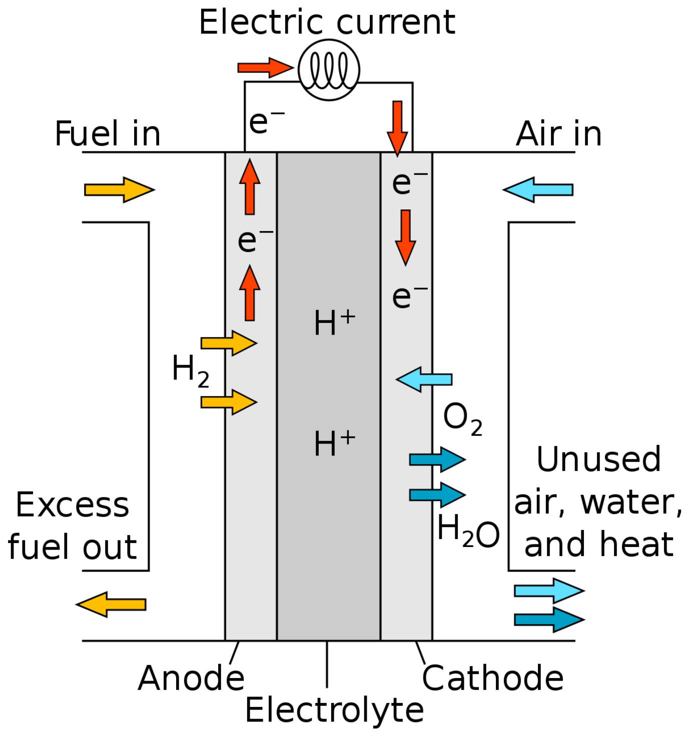

Figure 2.4 Schematic diagram of a PEM fuel cell [5]

In the selected FCHEV topology the fuel cell operates as the main power source. Cruise-M offers two different PEMFC models which are electrical and electrochemical. The electrical fuel cell is based on analytical electrochemical equations derived from the polarization curve of the PEMFC cathode side. The electrochemical fuel cell component of Cruise-M is modeled based on voltage drops, gas diffusion in the anode and cathode, temperature, catalyst layer, and the electrochemical processes in the gas diffusion layer. The electrochemical model determines the cell performance, which is voltage, for a given current density and boundary conditions such as gas state, solid temperature, water content, etc. According to the help document of Cruise-M, the electrochemical fuel cell model has been developed in collaboration with the LICeM department of the University of Ljubljana [7]. Although the electrical model could be selected due to its simplicity considering this is a control application, to study a realistic plant model, the electrochemical fuel cell model is chosen. The fuel cell models in EMS studies are generally electrical [57, 40]. This means the voltage drop during the operation of the fuel cell is mostly estimated based on the output current of the fuel cell neglecting the internal effects. Such empirical models generally do not take the temperature effect and the electrochemical factors into consideration. The electrochemical specifications of the PEMFC stack are left as the default values specified in the Cruise-M. However, the design parameters such as the number of cells in the stack and stack dimensions are set based on the Mirai specifications. Although several outputs are available in Cruise-M's electrochemical fuel cell stack, the most important outcomes are fuel consumption and efficiency regarding fuel economy.

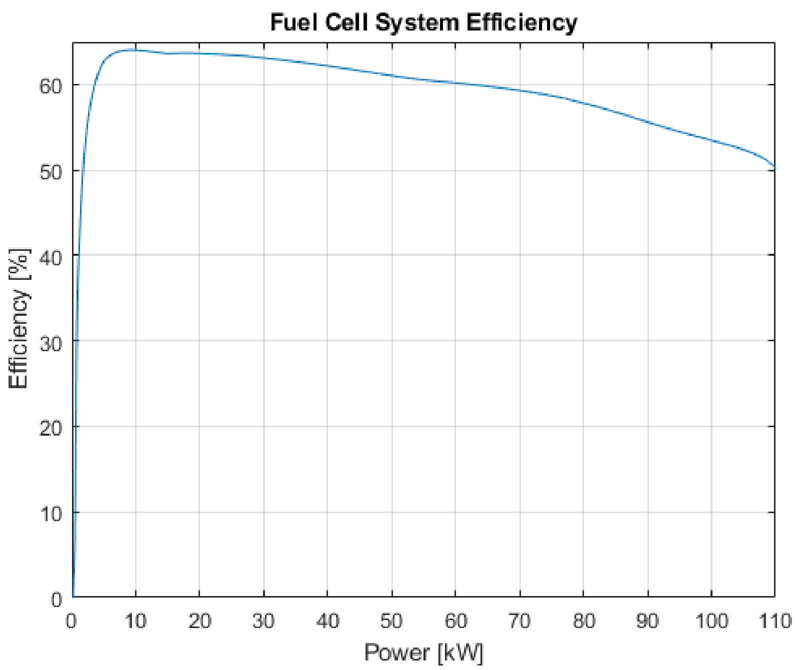

Figure 2.5 The efficiency curve obtained through the black-box testing of the fuel cell system model

A PEMFC operates at higher efficiency levels compared to an internal combustion engine, nevertheless, the system efficiency depends on the operating conditions similar to an ICE. Fuel cell system efficiency is generally expressed as an output to the fuel cell power. Like the system efficiency curve in Figure 2.5, the efficiency of the fuel cell system generally deteriorates when it operates at below or higher than certain power levels. According to the component test executed at a resolution of 1000W on Cruise-M to obtain the efficiency curve of the fuel cell, the maximum efficiency value is reached approximately at 8kW. The efficiency characteristics of the studied PEMFC system is presented in Figure 2.5. Specifications of the fuel cell stack model and the Mirai's fuel cell are given in Table 2.2.

Table 2.2 The fuel cell specifications [1]

Fuel Cell Specification	FCHEV model	Toyota Mirai	Unit
Number of cells in a stack	370	370	-
Expected nominal stack power	114	114	kW
Operating voltage	280-370	Not Available	V
System efficiency	Cruise-M default	Not Available	%

2.2 Battery Model

A battery, just like a fuel cell, involves a redox reaction that converts chemical energy to electrical energy. It consists of an anode, a cathode, an electrolyte, and a separator. Although a fuel cell and a battery are structurally similar, in terms of energy conversion mechanisms they are different. The reaction is reversible in a Li-ion battery where the fuel cell's is irreversible. Also in a Li-ion battery, the movement of Li ions releases electrons. The direction of the reaction dictates whether this is discharge or charge. During the charging, the load that is fed from the electric motor to the battery during regeneration gives rise to the voltage difference between the terminals of the battery. The difference causes a non-spontaneous reaction on the cathode, and the cathode material gives out Li ions and electrons. While the Li ions move toward the anode from the cathode through the electrolyte, the free electrons move in the same direction as the Li ions, but through the external circuit. On the other hand during discharging, a spontaneous reaction occurs at the anode, causing the Li ions and free electrons to move from the anode to the cathode. The free electrons move through the external circuit supplying electrical power for the load. This process is illustrated in Figure 2.6.

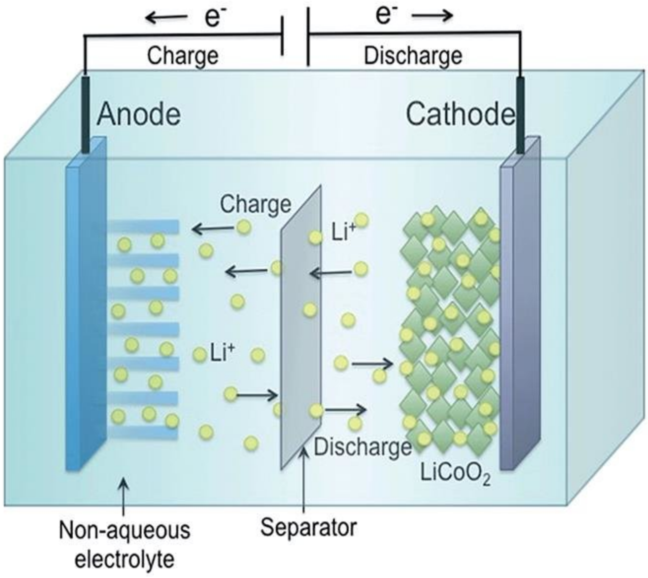

Figure 2.6 Schematic of a Li-ion battery [6]

The FCHEV powertrain utilizes the battery as a secondary power supplier in the studied topology. This indicates that the power demand is mostly met by the fuel cell. However, due to the relatively slow dynamics of fuel cells, the battery comes into action in cases of peak power demands where the fuel cell is not capable of providing a transient response to track the demand. In addition, the battery supplies power to operate the fuel cell system at higher efficiency levels. Since the power demand from the driver is always met as mentioned earlier, the power allocation must be performed harmoniously so that the physical limits of the battery are not exceeded and it is not utilized close to the limits for an unacceptably long time duration.

The first-generation Mirai uses a nickel-metal hydride battery [1]. However, the battery equipped on the electrical powertrain model is an electrochemical battery component available in Cruise-M and involves $LiMn_2O_4$ chemistry. The matching of the cathode chemistries could not be achieved, because NiMH is not available in Cruise-M. It is known that $LiMn_2O_4$ batteries can go up to high current rates [58]. Hence, the selected cathode chemistry is suitable for this kind of application under the requirement that the power demand from the driver shall always be satisfied. In addition, most of the modern FCHEV designs in the industry such as the second-generation Toyota Mirai, Hyundai Nexo, and Honda Clarity employ a Li-ion battery as an energy storage system [59, 60, 61].

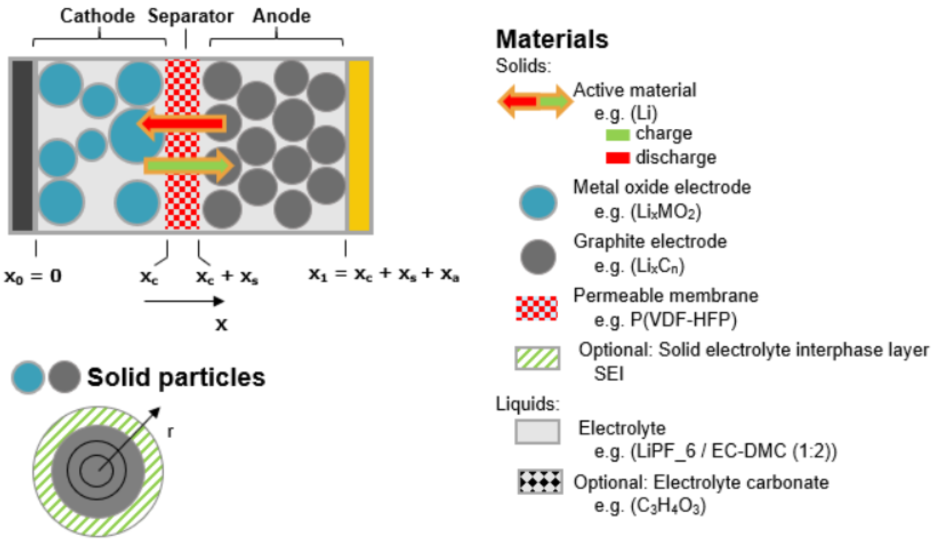

Figure 2.7 Schematic of a Li-ion battery cell and the three-dimensional geometry approach used for the simplified 1D+1D model [7]

As depicted in Figure 2.7, the electrochemical battery model within the Cruise-M framework comprises three distinct functional layers: a metal oxide cathode, a separator, and a graphite layer anode. During discharge, lithium ions, previously stored within the anode, undergo extracalation from the active material and migrate through the liquid electrolyte across the separator towards the metal oxide layer. Upon reaching the metal oxide layer, facilitated by the presence of electrons, lithium ions undergo intercalation into the structure of the metal oxide. The electrons, derived from the extracalation process within the graphite layer, are conveyed through an external current pathway from the anode to the cathode. Conversely, during the charging phase, the entire sequence of events reverses, with the metal oxide layer assuming the role of ion donor, thereby liberating lithium ions and electrons from its solid structure. This modeling framework adopts a 1D+1D methodology, which is inspired by the seminal work of Doyle et al. [62] concerning the transport phenomena of both current and ions within porous electrodes immersed in concentrated solutions. To simulate all the aforementioned processes, the 1D+1D approach consists of several governing equations such as transient mass balance equation, steady potential equations, energy balance equation, transient 1D particle model, current density equation, half-cell model, double layer model, collector dynamics, and aging models. Further information is presented in the help documentation of Cruise-M. The electrochemical battery available in Cruise-M is used in the study as it is, however some main parameters are specified based on the high-voltage battery of the Mirai. Specifications of the Li-ion battery model and the reference battery are given on Table 2.3.

Table 2.3 The battery specifications [1]

Battery Specification	FCHEV model	Toyota Mirai	Unit
Cathode chemistry	$LiMn_2O_4$	NiMH	-
Number of cells in battery pack	60s1p	Not Available	-
Operating voltage	240	244.8	V
Maximum pulse power (10s)	27.5	25.5	kW
Capacity	6.5	6.5	Ah

2.3 DC/DC Converter Model

In this study, the fuel cell operates at 280-370 V, the battery at around 240 V, and the electric motor at 650 V. Since the powertrain units operate at different voltage levels, they require a DC/DC converter that regulates the output voltage of the units to set them to the same voltage level. In the studied powertrain, a unidirectional DC/DC converter and a bidirectional DC/DC converter are placed respectively between the fuel cell and DC bus, and the battery and DC bus. By the converters, the output voltages of all the components in the powertrain are boosted to the voltage level of the electric motor. Since the mission of the model is to provide a platform to evaluate EMSs in terms of fuel economy and power outputs, only the efficiency impact of the DC/DC converter is taken into account in the study. Considering a modern DC/DC converter in such an automotive application, the efficiency of the DC/DC converter model is assumed to be 95%.

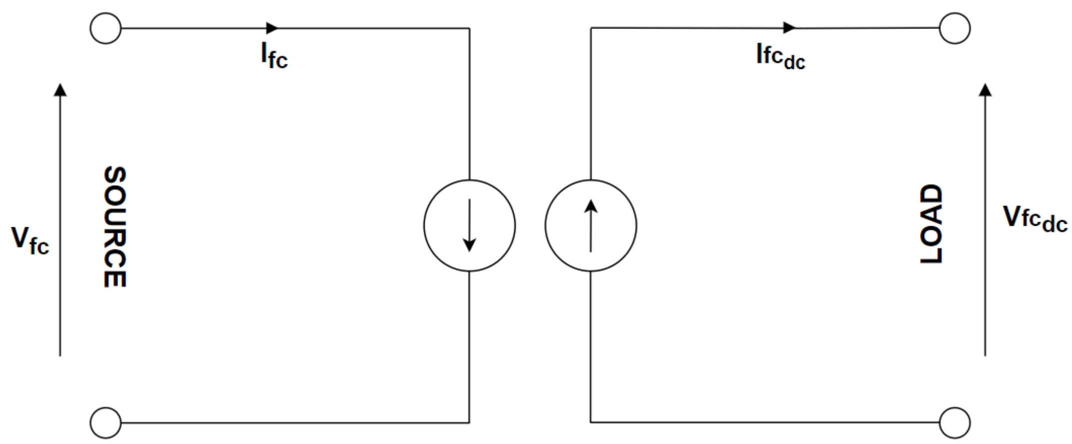

Figure 2.8 DC/DC converter circuit model used for the fuel cell

Two different DC/DC converter models are used in Cruise-M for the fuel cell and the battery. The converter used for boosting the fuel cell voltage consists of two ideal current sources as shown in Figure 2.8. The current source at the load side is driven by the EMS so that the power share of the fuel cell at the DC bus is requested from the power source. While the current source at the load side feeds the motor, the current source at the source side regulates the current requested from the fuel cell. By demanding power from the load side of the converter in terms of current, the input power of the converter which is the source power is determined considering the efficiency. The power balance is redressed between the input and the output of the converter as in Equation 2.5 and Equation 2.6 so that the allocated power share of the source is generated and the corresponding current output of the fuel cell stack is determined.

$$P_{fc}(t) = \frac{P_{fc_{dc}}(t)}{\eta_{dcdc}} \tag{2.5}$$

$$I_{fc}(t) = \frac{I_{fc_{dc}}(t) \times V_{fc_{dc}}}{V_{fc}(t) \times \eta_{dcdc}} \tag{2.6}$$

In the equations, $P_{fc_{dc}}(t)$ is the power share of the fuel cell at the DC bus, P_{fc} is the power that must be supplied by the fuel cell to balance the input and output powers of the converter considering the efficiency, η_{dcdc} is the converter efficiency, $I_{fc_{dc}}(t)$ is the current reference which is controlled by EMS and flows from the DC/DC converter to the electric motor, $I_{fc}(t)$ is the fuel cell current, and $V_{fc_{dc}}$ is the voltage level at the DC bus which is fixed to the voltage of the electric motor. It is assumed that the electric motor operates at a constant voltage of the DC bus voltage specified by the manufacturer. Sequentially, the power allocated to the fuel cell directly determines the battery's power share as given in Equation 2.7. Since the equation also represents the power balance at the DC bus where the voltages are equalized through Equation 2.8, the balance is also valid in terms of currents at the DC bus as in Equation 2.9.

$$P_{bat_{dc}}(t) = P_{em}(t) + P_{compressor}(t) - P_{fc_{dc}}(t) \tag{2.7}$$

$$V_{fc_{dc}} = V_{bat_{dc}} = V_{compressor} = V_{em} \tag{2.8}$$

$$I_{bat_{dc}}(t) = I_{em}(t) + I_{compressor}(t) - I_{fc_{dc}}(t) \tag{2.9}$$

where $P_{bat_{dc}}(t)$ is the power allocated to the battery at the DC bus, $P_{em}(t)$ is the power demand, $P_{compressor}(t)$ is the power of the compressor that is assumed to be operated at the DC bus voltage, $I_{bat_{dc}}(t)$ is the DC bus side current of the battery's DC/DC converter, and $I_{em}(t)$ is the load in terms of current. Similar to the fuel cell, the battery voltage is boosted by a DC/DC converter as stated earlier. The DC/DC converter model in Cruise-M consists of an ideal voltage source at the load side and an ideal current source at the source side as shown in Figure 2.9. Since the power can flow in both directions depending on whether it is a regenerative braking phase or not, the DC/DC converter of the battery is bidirectional.

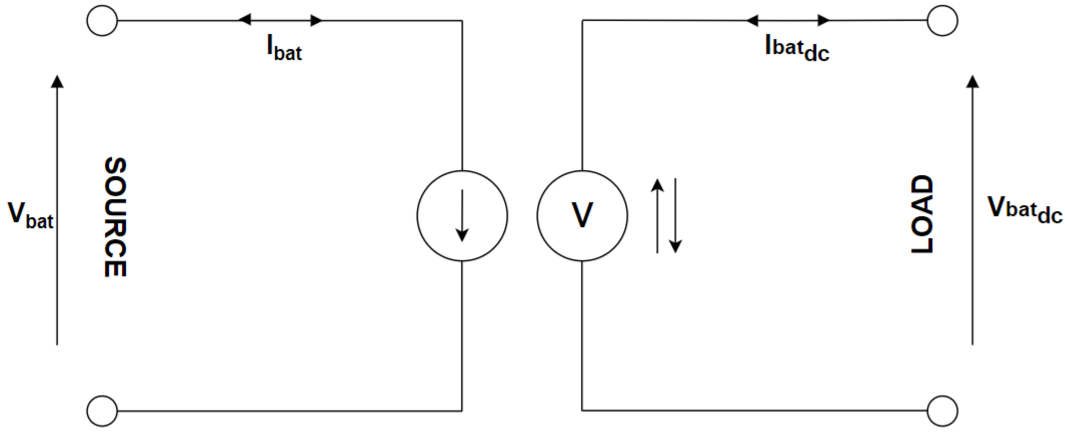

Figure 2.9 DC/DC converter circuit model used for the battery

Unlike the converter model used for the fuel cell, the battery power is dependently controlled by regulating the current source at the source side based on the current share of the battery at the DC bus, which is represented by $I_{bat_{dc}}$ in the figure. By boosting the battery voltage to the DC bus voltage through the ideal voltage source fixed to the motor voltage, the battery's discharge current is determined using the Equation 2.11 so that the power balance in Equation 2.10 is fulfilled.

$$P_{bat}(t) = \frac{P_{bat_{dc}}(t)}{\eta_{dcdc}} \tag{2.10}$$

$$I_{bat}(t) = \frac{I_{bat_{dc}}(t) \times V_{bat_{dc}}}{V_{bat}(t) \times \eta_{dcdc}} \tag{2.11}$$

where $P_{bat}(t)$ is the battery power that must be generated to fulfill the power balance between the input and output considering the efficiency and I_{bat} is the input or output current of the battery. On the other hand, the same operation terms for the battery are determined during charging, by arranging the place of efficiency term in Equation 2.12 and Equation 2.13.

$$P_{bat}(t) = P_{bat_{dc}}(t) \times \eta_{dcdc} \tag{2.12}$$

$$I_{bat}(t) = \frac{I_{bat_{dc}}(t) \times V_{bat_{dc}} \times \eta_{dcdc}}{V_{bat}(t)} \tag{2.13}$$

3. Rule-Based Energy Management Strategy

In an FCHEV energy management application, while meeting the power demand from the driver is the main requirement, energy management strategies are also expected to achieve a satisfactory fuel economy by operating the fuel cell close to the maximum efficiency point and also to keep SOC between certain limits for the sake of the battery. However, the efficiency of the fuel cell depends on its utilization, and it is not always possible to work close to the maximum efficiency point. Considering these two goals, there are various cases to happen during the operation of the power sources to meet the power demand. Firstly, when the power demand is low enough so that it can be fully met by the battery, the fuel cell would be kept closed to reduce consumption. When the power demand increases, the fuel cell may start to work and the power-splitting is performed between the sources so that the fuel cell can get closer to the maximum efficiency point. For even higher magnitudes of power demand, it may exceed the battery power limits, and in this case, the fuel cell is forced to operate inefficiently at high power levels because the highest priority task is to meet the power demand and the battery already reached at its maximum limit. Synchronously, SOC of the battery must be considered during the operation of the fuel cell, because drastic changes in SOC shorten the useful life of the battery, and also state of power (SOP) of the battery depends highly on the SOC. A certain amount of the energy is recuperated during the regenerative braking, however, to keep SOC within the desired range and achieve a better fuel economy, the amount of energy supplied by the battery can also be recovered by charging it using the fuel cell in the high-efficiency region. Since the battery is incapable of reaching as high output power as the fuel cell due to the power limits, the larger portion of the power demand is mostly met by the fuel cell in case of high power requests. In such a high power request, charging the battery by the fuel cell causes an increase in its output power and decreases the efficiency. Therefore, charging the battery would not be a priority until the power request decreases to a suitable level to charge the battery at a high-efficiency point. Consequently, the energy management problem involves a wide variety of cases. Under such a high diversity of situations that may occur during operation, the EMS should perform the power distribution between the sources by considering fuel economy, SOC level, and system capabilities, thus providing a solution to the mentioned problem.

In automotive control applications, the rule-based approach is widely used due to its higher interpretability, lower complexity, and less utilization of resources in terms of processor load and memory usage [63]. Also, rule-based algorithms are reliable since they strictly obey the defined rules and operate the system only in the allowed regions. To accomplish the above-mentioned goals, we developed a rule-based EMS since it is one of the most relied and utilized methods in today's automotive application software. This chapter introduces the rule-based algorithm first, then discusses its similarities and differences to a real EMS by comparing the results with the dynamometer test measurements of the Toyota Mirai.

3.1 Rule-Based Energy Management Strategy Design

A rule-based strategy makes the control decisions based on a set of pre-defined conditions or rules. Rule-based methods are known as the most commonly used approach in automotive software. The two main types of rule-based methods which are fuzzy rules and deterministic rules are used in control applications, however, no optimization is involved in either method [64]. In FCHEVs, the operating state of the powertrain is determined by checking pre-defined conditions obtained by the states of the powertrain. Based on the signal measurements from the powertrain system, the power limits of the sources must be determined first and foremost, because the fuel cell and the battery have physical limits depending on the design specifications and characteristics. Then considering the fuel economy and SOC level, the most suitable operating state is selected by the rule-based EMS based on the requested power from the driver and the determined limits of the sources.

In our RB-EMS which is a state-based deterministic method, the mode decisions are made depending on the power demand, the SOC level, and actual power limits of the sources. The method of the RB-EMS to split the power between the fuel cell and the battery has three main steps which are calculating the power limits, deciding the mode by checking the pre-defined conditions, and determining the output power of the sources at each mode. The architecture of the designed EMS is shown in Figure 3.1.

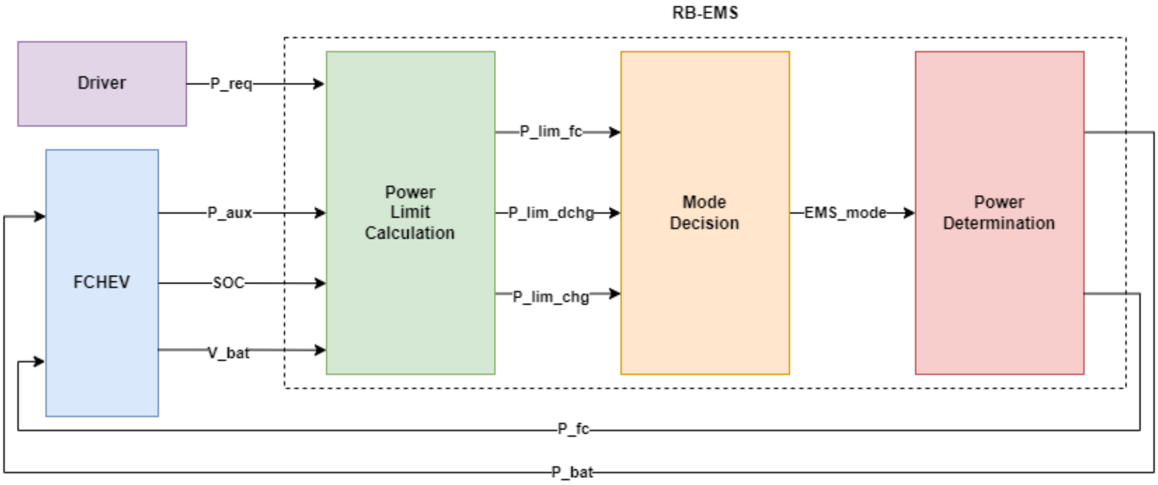

Figure 3.1 Architecture of the RB-EMS

The RB-EMS has five different modes which are braking, battery-only, fuel cell-only with battery charging, fuel cell-only without battery charging, and boost mode that both sources supply the power simultaneously. Several sets of conditions are defined to enter and exit each mode in the algorithm as in Figure 3.2.

The **regenerative braking mode** is deployed during the deceleration where the motor power has the negative sign. At this interval, the motor power is utilized to charge the battery considering its power and voltage limits. If the recuperation power exceeds the battery limits, then braking power is assumed to be consumed in the friction brakes to prevent any hazardous case from occurring in the battery. However, such a situation has not been faced during the simulations under the drive cycles selected for the study.

The **battery-only mode** is entered in two cases. Only the battery meets the power demand, if SOC is sufficiently high and the power demand does not exceed the output power limit of the battery. In this case, the fuel cell is shut down and it hands over the power-supplying task completely to the battery. Alternatively, when the fuel cell is already turned off and the power demand is less than the output power limit of the battery, the power demand is met by only the battery even if the SOC is lower than the threshold value mentioned in the previous case. Hereby, only the battery is used at the beginning phase of the acceleration. The purpose of this decision is to reduce the on-off switchings of the fuel cell to prolong its remaining useful life. Generally, the battery-only mode is enabled at low-speed driving conditions or initial phase of the acceleration.

The **fuel cell-only (with charging the battery) mode** is another mode such that the fuel cell charges the battery and meets the power demand at the same time. It is entered only when the SOC is lower than a certain threshold, and the total power required for charging the battery and meeting the power demand is within the power limits of the fuel cell.

The **fuel cell-only (without charging the battery) mode** is executed if the SOC is lower than a certain threshold and the power demand exceeds the power limits of the fuel cell. In this case, the power demand cannot be met completely so as not to harm the battery. The mode is potentially executed in case of demanding very peak power from the sources when the SOC is critically low and the fuel cell cannot meet such a rapidly increasing power demand because of its slow dynamics. In such a case, there is no option other than saturating the power demand to not harm the physical limits of the battery. However, the tests did not reveal any instances of the described situation.

Lastly, the **boost mode** is entered if the vehicle is traveling and any of the conditions aforementioned cannot be satisfied. In such a case, both the fuel cell and the battery meet the power demand. The distribution of the power demand between the fuel cell and the battery is carried out using a low-pass filter approach. The power demand from the driver is fed to the fuel cell after processing the load signal through a low-pass filter. The calibration of the filter's time constant is tuned in a way that the load-following policy of the EMS sufficiently smoothens transients of the fuel cell power, but also responds quickly to keep battery's share at reasonably values e.g. it does not work at the maximum limit continuously for a long time duration.

The algorithm of the developed rule-based EMS is shown in Figure 3.2. The flow of the state-machine based EMS algorithm is from up to down for the mode selection, then left to right to execute the power assignments to the power sources. It starts by checking the availability of the modes, in an order of braking, battery-only, fuel cell-only with battery charging, fuel cell-only without battery charging, and boost mode. If any of the first four modes are unavailable to enter, then the boost mode is selected as default. Once a mode is selected, it stays in this mode for a one-time step, therefore the algorithm decides cyclically without allowing multi-transitions in one step. During the execution of the mode, the power assignments are done based on pre-defined rules. Then the next time-step starts by checking the exit conditions of the actual state. Throughout the simulation, it keeps executing the state until the exit condition is fulfilled. The algorithm repeats these three main steps. The RB-EMS is implemented in Matlab Simulink, also using Stateflow's graphical language environment.

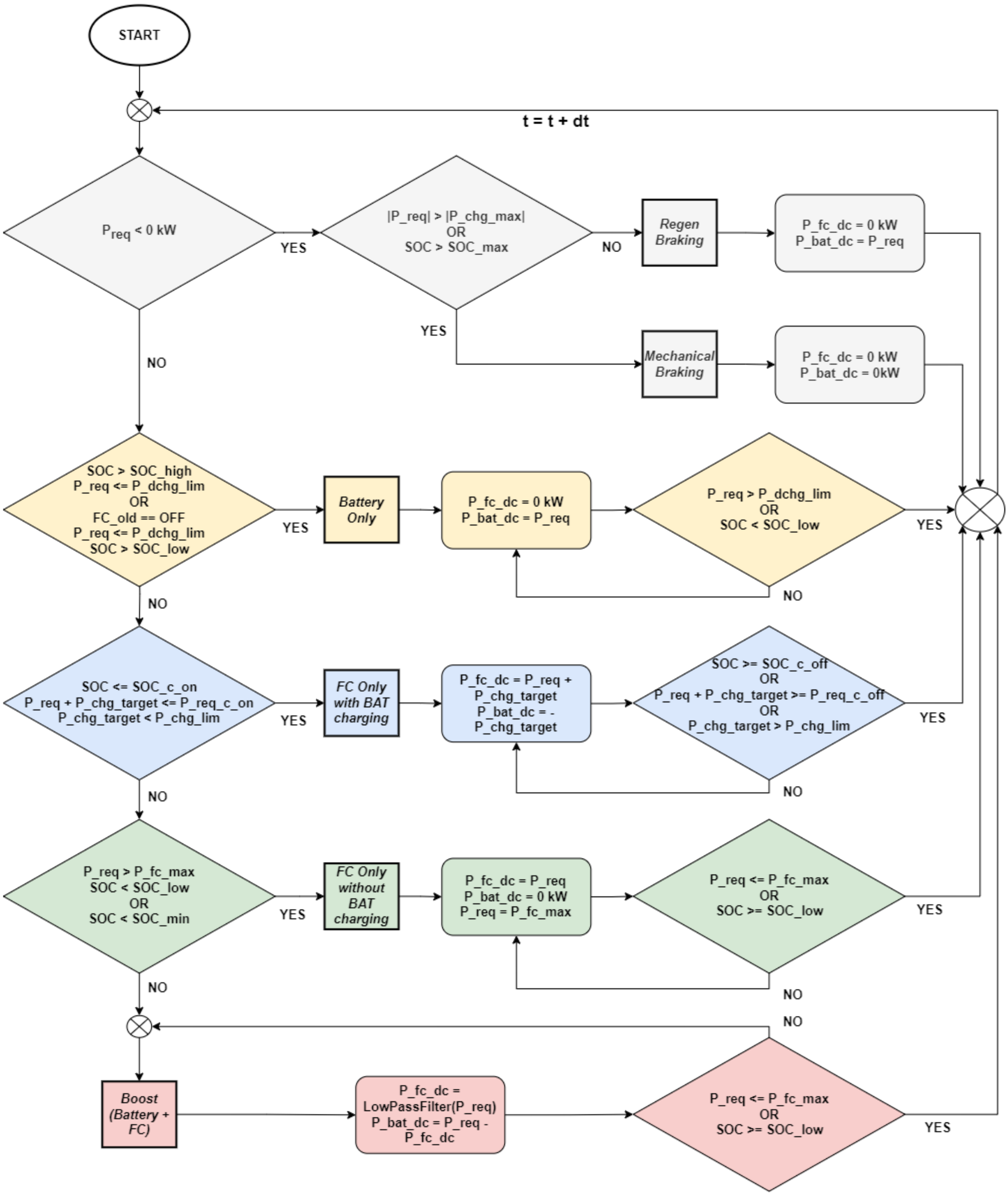

Figure 3.2 Algorithm of the RB-EMS

As mentioned before, the power limits of the fuel cell and the battery must be checked by the EMS at each time step for using them in feasible regions. We base our model on Toyota Mirai, therefore for the fuel cell we employ a static power limit specified by the OEM, which is 114kW [1].

Although the maximum power limit of the battery model is specified as $\pm 30kW$ based on the dynamometer results [56], it requires dynamical handling on the power management since batteries have potential safety issues during the operation and their performance fades at long durations of utilization at close to the power limits. Possible problems with the studied battery can be examined separately for discharging and charging. As the battery supplies power, the output power decreases due to the voltage drop because of the internal losses of the battery regarding ohmic drop, activation polarization, and concentration polarization. Therefore undervoltage is a potential problem creating a necessity of limiting the battery output power while the voltage drops below a certain level. Another undesired situation during the discharging is the undercharge. As the battery energizes the load, the charge decreases, even resulting in critically low levels of SOC. Additionally, since the open circuit voltage of the battery drops as the SOC decreases, the power capability of the battery will decrease if the charge level cannot be kept above a certain value. Because of this phenomenon, the magnitude of the discharge power must be limited when the SOC is critically low, to prevent the undercharge issue. Similar to the discharge problems, overcharging and overvoltage are the other two critical cases that need to be prevented by the energy management strategy. As the battery is charged by the fuel cell, if the magnitude of the power input exceeds the physical limits of the battery, then it causes a drastic increase in the battery voltage and harms the battery due to high temperatures. Similar to overvoltage, if the amount of energy for charging the battery is not controlled and the voltage increases undesirably, then it causes several safety issues e.g. critically high temperatures due to the thermal runaway. In summary, all of the problems aforementioned can cause an excess of the design limits of the battery, and reduce its lifespan.

As mentioned in the second chapter, the battery model in Cruise-M is based on several equations implying the electrochemical reactions and it is sensitive to safety issues such as overdischarging, overcharging, overvoltage, and undervoltage. In such states, the simulation fails due to the instabilities in the internal dynamics of the battery model. To prevent these dangerous situations that may occur in the battery, the EMS determines the maximum and minimum power limits via predefined calibratable maps by using interpolation based on the SOC level and operating voltage of the battery. In this way, the battery power will not be allowed to exceed the limits during discharging or charging, as defined in Equation 3.1 and Equation 3.2. In the study, it is assumed that the battery power and current have negative signs during charging.

$$0kW \leq \ P_{batd_k} \leq P_{batd_k}^{lim^*} \leq P_{batd}^{max} \tag{3.1}$$

$$P_{batc}^{max} \leq P_{batc_k} \leq P_{batc_k}^{lim^*} \leq 0kW \tag{3.2}$$

where P_{batd_k} and P_{batc_k} represent the battery power during discharging and charging respectively, P_{batd}^{max} and P_{batc}^{max} are the design limits for battery power, and $P_{batd_k}^{lim^*}$ and

$P_{batc_k}^{lim^*}$ are the final values of power limits which are determined by the EMS. The limits are updated each time step for the new values of the SOC and battery voltage as described in the following part of the section. Moreover, the final values of the battery's discharge and charging power limits are obtained in two steps: determining the maximum power magnitude and limiting the allowable rate of change in a one-time step. The preliminary values of discharging and charging power limits are determined as given in Equation 3.3 and Equation 3.4 respectively.

$$P_{batd_{k+1}}^{lim} = f_1(SOC_k) - f_2(V_{batk}) \tag{3.3}$$

$$P_{batc_{k+1}}^{lim} = f_3(SOC_k) - f_4(V_{bat_k}) \tag{3.4}$$

where V_{bat_k} is the operating voltage of the battery, $P_{batd_k}^{lim}$ and $P_{batc_k}^{lim}$ are the preliminarily determined power limits respectively for discharging and charging, f_1, f_2, f_3 and f_4 represent the mapping between the given states of the system and power limiting values respectively for discharging and charging. Here $f_1 : [0,100] \to [0,30]$, $f_2 : [200,280] \to [30,-30]$, $f_3 : [0,100] \to [-30,0]$, $f_4 : [200,280] \to [30,-30]$. Also, $0\% \leq SOC_k \leq 100\%$, $200V \leq V_{batk} \leq 280V$, $0kW \leq P_{batd_k}^{lim} \leq 30kW$, and $-30kW \leq P_{batc_k}^{lim} \leq 0kW$.

As an outcome of the calibration values defined in the look-up tables represented by f_1, f_2, f_3, and f_4, as the SOC decreases, the discharging power limit of the battery is reduced and the charging power limit is increased synchronously. Similarly, the discharging power limit of the battery is lowered as the voltage drops, and the charging power limit is increased. Considering the application, when the battery voltage drops dangerously, the battery output power is reduced by increasing the fuel cell's share in the power allocation, and the battery voltage is allowed for recovery. In the opposite case, when the battery voltage increases dangerously to critical levels, the fuel cell's share in the power splitting is decreased, and the battery is forced to discharge until the voltage drops to a safe level. A similar manipulation is applied using the functions f_1 and f_3 considering the SOC to prevent overcharging and overdischarging.

In the topology of the studied FCHEV model, since power shares of both the fuel cell and battery are determined by controlling the fuel cell output power, sharp changes in the battery power limitations can cause deviations in the fuel cell's power output, because the change in the battery power is added or subtracted from the fuel cell's share. Due to the fast dynamics of the battery, the recovery of the battery from overvoltage or undervoltage happens instantaneously depending on the battery's share of power which is limited in Equation 3.3 and Equation 3.4, which may cause dramatical increases or decreases in the fuel cell's power output when the power balance in Equation 2.2 is considered. This fluctuation effect is not the case for SOC recovery, since the SOC does not change as instantaneously as the battery voltage. To reduce the fluctuations in the fuel cell's output power due to the voltage manipulation via f_2 and f_4, a rate limitation is applied to the dynamical limit calculation given in Equation 3.3 and Equation 3.4. Thanks to the rate limitation applied to the battery power limits, once the fuel cell power is increased or decreased due to the change in power limits of the battery, the battery power limit returns to the normal value with a limited rate of change even if the voltage returns to the nominal value. Thus, the fuel cell power does not sharply return to the value where it was operating before the voltage rise or drop. In summary, the main idea of the rate limitation is to avoid jumping frequently between the dangerous and safe levels of the voltage and prevent fluctuations in fuel cell power. The rate of change limit is determined for discharging and charging in Equation 3.5 and Equation 3.6 respectively.

$$\Delta P^{lim}_{batd_{k+1}} = g_1(V_{bat_k}) \tag{3.5}$$

$$\Delta P^{lim}_{batc_{k+1}} = g_2(V_{bat_k}) \tag{3.6}$$

where $\Delta P^{lim}_{batd_k}$ and $\Delta P^{lim}_{batc_k}$ are the rate of change limits of the battery power limits, and g_1 and g_2 represent the mapping between the actual battery voltage and rate of change limits of battery power, respectively for discharging and charging. Here $g_1 : [200, 280] \to [0, 30]$, $g_2 : [200, 280] \to [-30, 0]$, $0kW \leq \Delta P^{lim}_{batd_k} \leq 30kW$ and $-30kW \leq \Delta P^{lim}_{batc_k} \leq 0kW$. After applying the rate limitation to the preliminary power limit values calculated using Equation 3.3 and Equation 3.4, the final values of the battery power limits are determined using Equation 3.7 and Equation 3.8 for discharging and charging respectively.

$$P^{lim^*}_{batd_{k+1}} = \begin{cases} P^{lim}_{batd_{k+1}}, & P^{lim}_{batd_{k+1}} - P^{lim}_{batd_k} < 0 \\ P^{lim}_{batd_{k+1}}, & P^{lim}_{batd_{k+1}} - P^{lim}_{batd_k} \leq \Delta P^{lim}_{batd_{k+1}} \geq 0 \\ P^{lim}_{batd_k} + \Delta P^{lim}_{batd_{k+1}}, & P^{lim}_{batd_{k+1}} - P^{lim}_{batd_k} > \Delta P^{lim}_{batd_{k+1}} \geq 0 \end{cases} \tag{3.7}$$

$$P^{lim^*}_{batc_{k+1}} = \begin{cases} P^{lim}_{batc_{k+1}}, & P^{lim}_{batc_{k+1}} - P^{lim}_{batc_k} > 0 \\ P^{lim}_{batc_{k+1}}, & P^{lim}_{batc_{k+1}} - P^{lim}_{batc_k} \geq \Delta P^{lim}_{batc_{k+1}} \leq 0 \\ P^{lim}_{batc_k} + \Delta P^{lim}_{batc_{k+1}}, & P^{lim}_{batc_{k+1}} - P^{lim}_{batc_k} < \Delta P^{lim}_{batc_{k+1}} \leq 0 \end{cases} \tag{3.8}$$

where $0kW \leq P^{lim^*}_{batd_k} \leq 30kW$ and $-30kW \leq P^{lim^*}_{batc_k} \leq 0kW$.

The threshold variables for the power limitation are given in Table 3.1. In the algorithm, P_fc_max is the maximum power limit of the fuel cell, P_dchg_max is the maximum discharging power of the battery, and P_chg_max is the maximum power for charging the battery. These are the static design limits of the sources. As mentioned above, P_chg_lim and P_dchg_lim are the maximum and minimum allowable power limits which indicates the SOP of the battery. P_chg_target is the target power to charge the battery, SOC_max and SOC_min are the highest and lowest possible SOC levels that SOC is allowed. Also, additional threshold values which are SOC_high, SOC_low, SOC_chg_on, and SOC_chg_off are defined to be checked in enter and exit conditions during the mode decision process.

Table 3.1 Parameters of the RB-EMS

Algorithm Reference	Thesis Reference	Value	Unit
P_fc_max	-	114	kW
P_dchg_max	P_{batd}^{max}	30	kW
P_chg_max	P_{batc}^{max}	-30	kW
P_dchg_lim	$\mathrm{P}_{batd}^{lim^*}$	from EMS	kW
P_chg_lim	$\mathrm{P}_{batc}^{lim^*}$	from EMS	kW
P_req_c_on	-	70	kW
P_req_c_off	-	75	kW
P_chg_target	$\mathrm{P}_{batc}^{target}$	from EMS	kW
SOC_max	-	80	%
SOC_min	-	30	%
SOC_high	-	60.5	%
SOC_low	-	57.5	%
SOC_c_on	-	59.5	%
SOC_c_off	-	61.5	%

Table 3.2 Calibration values for the RB-EMS

Map	Dimension	Map Data				Dependency	Unit
f_1	Breakpoint	0	50	60	100	SOC	%
	Value	0	15	30	30	Battery Power	kW
f_2	Breakpoint	200	220	240	280	Output Voltage	V
	Value	30	15	0	-30	Battery Power	kW
f_3	Breakpoint	0	60	65	100	SOC	%
	Value	-30	-5	0	0	Battery Power	kW
f_4	Breakpoint	200	240	260	280	Output Voltage	V
	Value	30	0	-15	-30	Battery Power	kW
g_1	Breakpoint	200	240	260	280	Output Voltage	V
	Value	0	10	30	30	Battery Power	kW
g_2	Breakpoint	200	220	240	280	Output Voltage	V
	Value	-30	-30	-10	0	Battery Power	kW

3.2 Validation of the RB-EMS

Since one of the main purposes of the study is to design EMSs that can act realistically by making feasible decisions, the simulation tests are conducted in five different drive cycles to validate the reliability and the representativeness in terms of similarities and differences compared to the dynamometer results of the Toyota Mirai conducted by the Argonne Laboratory [56]. The RB-EMS strategy does not aim to mimic the behavior of RB-EMS of the Toyota Mirai by making the same decisions. However, the dynamometer results are examined during the design phase of the RB-EMS to ensure that the EMS can sufficiently represent the dynamometer results in terms of staying within the physical limits and plausible utilization of the power sources. Therefore, although the pattern of the real EMS for allocating the power between the sources is not expected to be reproduced, it is expected to be performed similarly to the real EMS in terms of fuel consumption and trends in the power source utilization. It should also be noted that we designed an FCHEV model based on only the available parameters of the Toyota Mirai. Therefore, differences between the model and the real vehicle must also be taken into consideration in the EMS decisions and results. Various factors such as the efficiency of the electric motor, fuel cell, battery, and DC/DC converters might cause differences in the results.

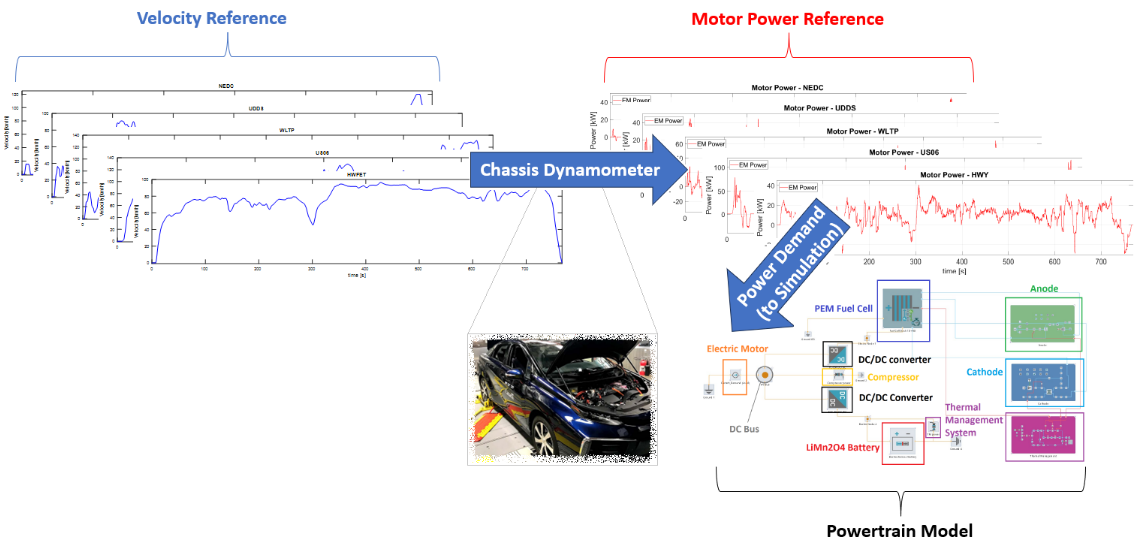

Figure 3.3 Validation procedure and feeding the motor power data to the powertrain model [8]

The validation procedure of the model and the EMS through the simulation test is shown in Figure 3.3. As discussed in the second chapter, the electrical powertrain model receives the driver's command only in terms of power demand of the electric motor since the chassis and drivetrain are excluded from the model. The main purpose of this design decision is to eliminate the modelling errors due to unknown factors in the chassis and drivetrain of the vehicle, and be able to make a fair evaluation between the power source outcomes of the designed energy management strategies and the Mirai's EMS. During the simulation test, the powertrain model in Cruise-M is fed by the motor power data which is collected through the dynamometer test conducted by the testing authority. The motor power data is the outcome of the driver's acceleration and braking pedal commands to control vehicle's velocity while performing a drive cycle. All the simulation tests conducted in this study are based on this procedure. Various drive cycles and the power demand outcomes, and also the power outcomes of the sources, used in this study are presented by Argonne Lab [8].

The Worldwide Harmonised Light Vehicles Test Procedure (WLTP) drive cycle was chosen for testing the model under the control of the RB-EMS, since it represents various driving characteristics with four different phases which are low, medium, high, and extra high in terms of average speeds. Also, it contains an important variety of driving patterns, in terms of acceleration, braking, and start-stops. The results under the New European Driving Cycle (NEDC), Urban Dynamometer Driving Schedule (UDDS), US06 cycle, and Highway Fuel Economy Driving Schedule (HWFET) are also available in the appendix for further investigation of the RB-EMS's and the Mirai's behaviors. The evaluation is made according to the fuel cell power, battery power, compressor power, and SOC results given in Figure 3.4, Figure 3.5, Figure 3.6, and Figure 3.7 respectively. In addition to the graphical results, the numerical results are shown in Table 3.2 at the end of the section. Moreover, to further investigate the representativeness of the plant model, hydrogen consumption and compressor energy results are obtained by feeding the fuel cell power data of the dynamometer test to our fuel cell system model. These model results are also reported in the tables along with the dynamometer results. The overall resemblance of the model is reported in terms of mean absolute error. It is a measure of the error between the dynamometer results and the plant model under the control of the RB-EMS. To present the convergence of the error in real-time, the mean absolute error is calculated with varying sample size as in Equation 3.9.

$$MAE = \sum_{k=1}^{n} \frac{|y_k - x_k|}{k} \tag{3.9}$$

where k represents the index of the actual sample, n is the total number of measurements, y_k and x_k are respectively the dynamometer result and RB-EMS result samples for the index k.

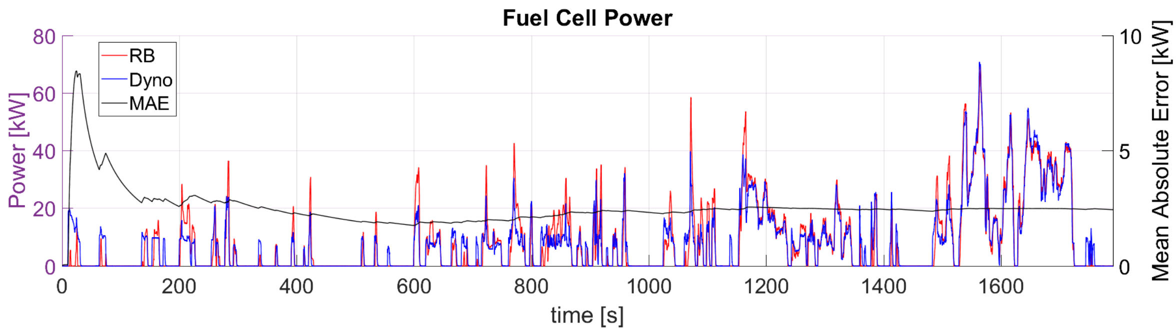

Figure 3.4 Fuel cell power results of the RB-EMS and the dynamometer test under WLTP cycle

Firstly, it is seen in the Figure 3.4 that the output trends of the fuel cell have shown a similarity. Moreover, although it is not aimed, the power patterns of the fuel cell overlap for most of the cycle. There is no available information about the RB-EMS algorithm of the Mirai, nevertheless, the results might be interpreted that the fuel cell on-off strategy of the EMSs performs similarly, since the points where that fuel cell starts the operation and is shut down are relatively close. However, once the fuel cell starts the power supply, there are deviations between the magnitudes of the output powers, which may be because of the difference in the power assignments between the RB-EMS and the EMS of the Mirai. According to the graphical results, it can be expected to yield a higher fuel consumption result in the proposed RB-EMS, however, the efficiency data is unknown for the dynamometer result. Also, our strategy switched the fuel cell between on-off states 55 times, while the total number of on-off cycles is 54 in the dynamometer test result. Generally, the fuel cell output of our method has shown a representative performance in terms of the trends, however, there are differences in power allocation decisions between the strategies.

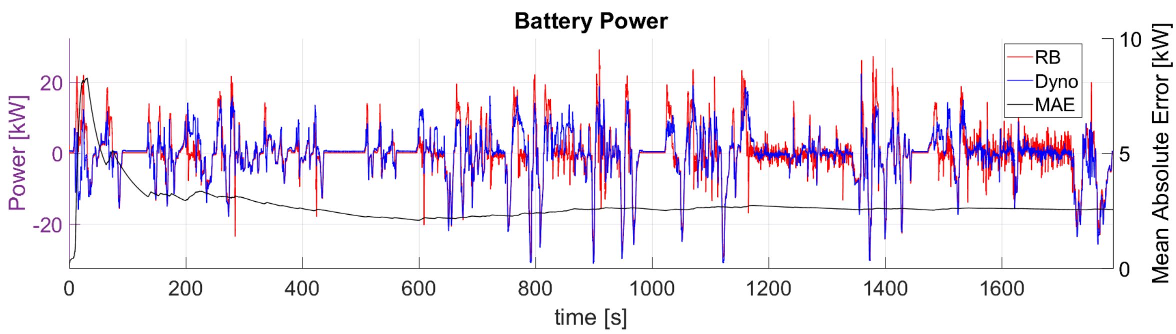

Figure 3.5 Battery power results of the RB-EMS and the dynamometer test under WLTP cycle

As a result of using the fuel cell in higher power regions compared to the dynamometer result, the battery power results have shown a difference in the peak values of the power which can be seen in Figure 3.5. Our strategy kept the battery output power lower than the experimental result. Since the battery limits are important as discussed earlier, there is no unrealistic behavior seen in the result e.g. unacceptable magnitudes, long durations with discontinuous power supply at high regions, etc. Especially in the high and extra high parts of the WLTP, from 1200th s to the end of the cycle, our strategy and the Mirai tended to use the fuel cell for meeting the big portion of the power demand, except the deceleration and acceleration phases around 1400th and 1500th seconds and the braking phase at the end of the cycle. This is expected for the RB-EMS since it runs the boost mode at such high-speed driving conditions. In this mode, low-pass-filtered power demand is fed to the fuel cell as the power reference. Therefore in steady-state, e.g. flat regions at high speeds, the fuel cell is expected to meet power demand almost completely.

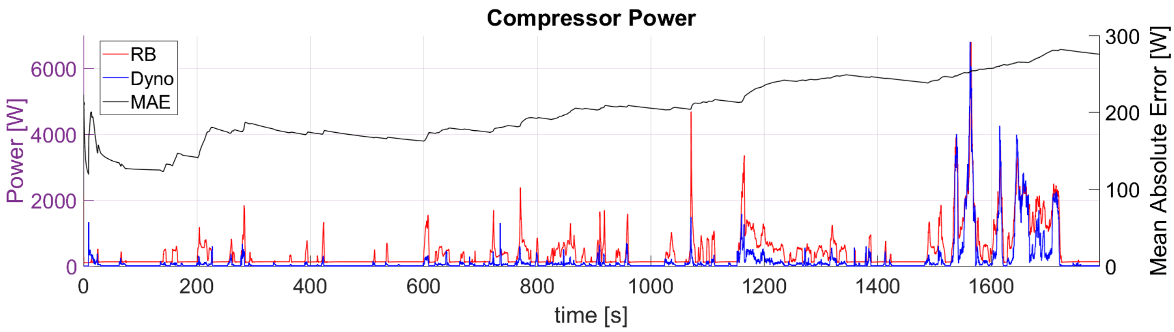

Figure 3.6 Compressor power results of the RB-EMS and the dynamometer test under WLTP cycle

According to the WLTP result, our compressor model consumed a higher amount of energy which can be expected since the fuel cell supplied higher amounts of power compared to the Mirai result. However, when the magnitudes of the output powers overlapped at 1560th s, the compressor powers almost the same, which is 6797kW and 6790kW for our model and the Mirai respectively. Also unlike the Mirai's compressor, the compressor model always operates at a constant power of approximately 125W, even if the fuel cell does not deliver power.

An important difference between the EMS behaviors was observed in SOC results at the beginning of the WLTP, which can be seen in Figure 3.7. While the EMS of the Mirai started charging the battery although the SOC is above the target value (60%), our strategy allowed the SOC to decrease by utilizing the battery. It is expected in our algorithm because when the SOC is above the target value, it allows the battery to supply the power within the limits to not consume hydrogen. However, from 600th s to the end of the cycle, the SOC pattern is relatively close, and any undesirable result, e.g. moving away from the target value, undesired charging, discharging, etc., has not been observed in our strategy.

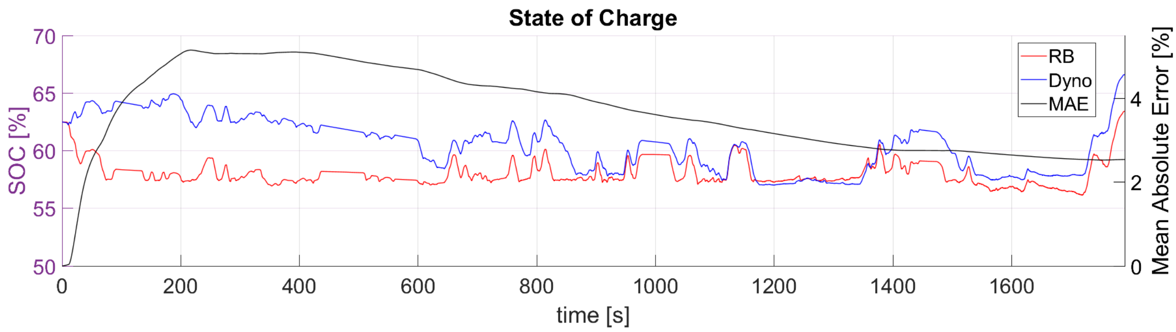

Figure 3.7 SOC results of the RB-EMS and the dynamometer test under WLTP cycle

According to the similarity in the numerical results in Table 3.3, our model and the RB-EMS could sufficiently represent the dynamometer results of the Toyota Mirai in terms of the criteria given in the table. Based on that, the reliability of the model and the RB-EMS is presented under the WLTP drive cycle. Although there are deviations in the total amount of energy of the fuel cell and the battery, the results have not shown any unacceptable deviations compared to the experimental data. Since the aim was not to mimic the actions of the Toyota Mirai, differences in the power allocation were observed between our strategy and the EMS of the Toyota Mirai. Other than the EMS decisions, there are possibly a certain amount of deviations due to the modeling differences. Since the efficiency data for the powertrain components is not shared by the authority, it is not possible to conduct a more representative FCHEV model. In any case, no deviations that we would suspect were observed in the FCHEV model.

Table 3.3 Toyota Mirai dynamometer test and RB-EMS results under WLTP cycle, (*model result)

Result	Dynamometer	RB	Unit
EM Energy Net	3167.9		Wh
Hydrogen Consumption	196.4	185.2	g
	182.3*		
FC Energy	3888.9	3953.6	Wh
Compressor Energy	24	213.3	Wh
	207.4*		
FC Power Change Accumulation	3555.0	3504.6	kW
SOC Initial	62.5	62.5	%
SOC Final	66.60	63.42	%
BAT Energy Output	954.7	1042.3	Wh
BAT Energy Input	-1143.7	-1175.5	Wh
BAT Energy Total (absolute)	2098.4	2217.8	Wh
BAT Energy Net	-189.0	-80.6	Wh

4. Model Predictive Controller-Based Optimal Energy Management Strategy

Energy management in HEVs is a research topic that involves a multi-objective optimization problem and requires the fulfillment of several criteria simultaneously. The main target is to be able to meet the power demand from the driver by considering the physical limits of the power sources. In a HEV, either one of the power sources or both can be utilized to meet the power demand, however, the decisions taken by the EMS to meet the power demand are crucial due to the impacts on the power sources in terms of energy consumption and stress. The major objectives are to minimize fuel consumption and keep the SOC level at a certain range synchronously, while the power demand is always met. Specifically, fuel economy can be improved by lowering the utilization of the fuel cell and operating it in the high-efficiency region. However, such decisions may increase the battery's share of the power demand to meet the large proportions and force the battery to operate close to the limits. This will cause the SOC level to dangerously fluctuate and even reach critically low levels, which may also cause safety issues. Under such infeasible control actions the battery degradation is accelerated. On the contrary, using the fuel cell to meet the power demand and keep SOC in a narrow range would cause undesired operations, such as operating the fuel cell system in inefficient regions, frequent cyclings, reaching very high power levels, and delivering the power transients with large deviations exceeding its physical limits. In such cases, the fuel cell ages quickly and fuel consumption increases due to the weak control decisions for the power allocation.

As mentioned also in the previous chapter, utilizing different types of power sources, e.g. a fuel cell and battery, creates a trade-off and involves a multi-objective optimization problem in energy management. To solve the problem, rule-based, optimization-based, and intelligent (learning-based) EMSs have been developed in several studies. In this study, to solve the multi-objective power allocation problem in real-time under the constraints due to the physical limits of the sources, a Model Predictive Control-based EMS is developed which adjusts its parameters based on the user-defined calibratable maps. The calibration of the maps is performed to design three different types of controller characteristics which are smooth, aggressive, and balanced. This chapter discusses the MPC-based EMS in the scope of its design and integration into the problem and compares these three different characteristics. Additionally, a further evaluation of the MPC-based EMS is presented in the last part of the chapter by comparing its results with the dynamometer results.

4.1 The Concept of Model Predictive Control

MPC is an optimal control method that minimizes a cost function for a finite horizon by predicting the states of a system over a specified horizon. It solves the optimization problem iteratively in a deterministic way. It requires the existence of a model to predict the states of the controlled system, therefore it is a model-dependent control method. To accurately determine the future response of a state in real-time, its actual value has to be measured or estimated at each time step. Main advantages of MPC are listed as follows:

- The optimal control signal is determined by considering not only the current states but also their future responses
- Since it executes the internal dynamics of the system, a strong performance is achieved depending on the representativeness of the predictive model
- The control actions are obtained considering the system's limits
- Although it is a model-dependent method, the predictive model does not have to be very accurate, it performs harmoniously with estimators and empirical models
- It can solve non-linear problems directly without requiring linearization

On the other hand, MPC has some disadvantages. Some of them are listed as follows:

- Dynamics of the system has to be known
- It creates a heavy computational load
- It requires an important effort during the design phase because of the complexity of the method and system modeling.

Before discussing the application of MPC in the energy management problem, some key components related to the concept must also be mentioned.

State $x(t)$ of a dynamical system is a set of variables representing the dynamics of the system. They can either be derived using mathematical expressions or, if available, directly measured as an output of the system. Response of the system at $t \geq t_0$ can be calculated if the initial value of the state x_0 and control inputs at $t \geq t_0$ are known.

An **internal model** is a set of equations being used for determining the future response of the states using the obtained control signal. The internal model is embedded in the controller and must adequately represent the behavior of the controlled plant. It enables the states to be manipulated by the control signal. Since the states are directly or indirectly involved in the cost function and their limits have to be considered, the controller performance directly depends on its accuracy.

Cost function L is a function that defines the objectives of the optimization. Then the optimization is performed by minimizing the cost function. A cost function is a mapping between its inputs, outputs, and cost which is the measure of success for optimization. It can be in different forms e.g. linear, quadratic, and exponential depending on the structure of the relationship between the variables. The selection of the form depends on the nature of the controlled system and the choice of the designer. In control systems, the main purpose of the control action is to minimize the error between the output and the reference. The error is involved in the cost function and does not have to be scalar, unlike a PID controller. In the cost function, the errors are defined in a vector form, hereby, MPC is able to minimize all of the error terms contained in the cost function synchronously.

Prediction horizon H_p is a finite time interval that obtains the number of future responses to be considered in the control actions.

Control horizon H_k is another finite time interval obtaining the number of control outputs applied during manipulation of the future outputs over the prediction horizon.

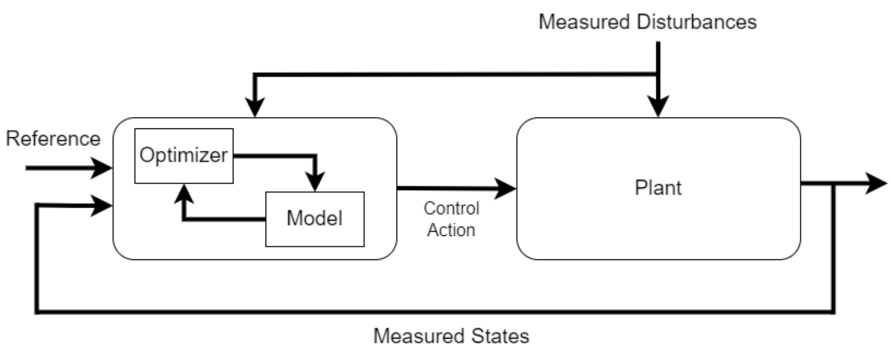

Figure 4.1 Operation of model predictive control

The determination process of the optimal control action is illustrated in Figure 4.1. MPC receives the states by the measurements from the plant at each time step. As stated earlier, if they are not measurable, the states can be estimated. Then, over the prediction horizon H_p, MPC determines a control sequence with the number of elements specified by the control horizon H_c to minimize the cost function L. The control sequence is determined to manipulate the states also considering their future responses. However, only the first element of the sequence is applied to the plant. The steps are repeated at each time step by measuring or estimating the updated values of the states.

4.2 Problem Formulation and Controller Design

In the energy management problem of an FCHEV, the fuel cell is aimed to be operated at the efficient region, while the SOC must cruise within a defined interval in a controlled manner. The main problem is to determine when and how the sources are utilized. This decision must be taken considering multiple criteria because the battery and the fuel cell have different dynamics and characteristics. Due to its way of producing power as discussed earlier, a fuel cell can provide output power for longer time durations continuously unlike a battery. On the other hand, a fuel cell has slower dynamics compared to a battery. A battery cannot provide high magnitudes of power as continuously as a fuel cell, however, it can deliver peak powers in a short time to meet the power demand varying with high change rates. Considering the physical system, the solution requires the controller to know the physical limits of both the fuel cell and the battery e.g. maximum power, the discharge limits, etc.

The fuel cell model utilized in this study performs the most efficient power generation at around 8 kW. By extension, considering a power demand in a range of 0 to 5 kW, if the SOC level is not critically below the target value, the decision is obviously to keep the fuel cell closed. In this way, the fuel consumption is minimized and the SOC still tends to go within the defined interval. However, under fast-changing driving conditions, the power demand always varies in a wide range, so the fulfillment of multi-objectives is not obvious in all conditions. For instance, when the power demand rises to the maximum power of the battery, shutting down the fuel cell will cause the battery to operate at its limits, a sharp decrease in SOC even to move away outside of the desired range, and a shortened battery life. On the other hand, if SOC reference is tracked with a minimum error, it would cause frequent on-off switchings of the fuel cell and force it to operate in infeasible conditions where the fuel cell degrades fast. In the same case, when the SOC is overshooting, due to the minimization of the SOC error at any cost, the EMS could decide to suspend the fuel cell to decrease the SOC back to the target value, however it would not be acceptable for a power demand exceeding the limits of the battery. Therefore defining the objectives properly is very critical in the application. Considering the design limits of the sources, the optimum solution has to be found within a large space. Based on the system analysis, defining the requirements that a successful EMS must fulfill is the initial part of the design. They are listed as follows:

- Efficiency of the fuel cell system shall be maximized to improve the fuel economy.
- SOC shall be kept within a desired range around a certain target level to prolong the battery life.
- The fuel cell shall be operated smoothly by minimizing the deviations in the transient of the power, and the on-off switchings shall be reduced to not cause further degradation of the fuel cell.
- The control action shall comply with the design limits of the power sources during the operation to not harm them or accelerate the degradation process.

To formulate those requirements in the energy management problem, a specific quadratic cost function as in Equation 4.1 is defined to be minimized by the MPC algorithm over the prediction horizon:

$$\begin{aligned} L = \sum_{k=1}^{H_p} (1-s_k) \times [w_{eff} \times (\eta_{max} - \eta_k)^2 + w_{soc_k} \times (SOC_{target} - SOC_k)^2] \\ + s_k \times P_{fc_k}^2 \end{aligned} \tag{4.1}$$

where H_p is the prediction horizon, η_{max} is the maximum efficiency value of the fuel cell system corresponding to 8kW of output power, η_k is the actual efficiency of the fuel cell system, SOC_{target} is the target value of the SOC which is set to 60% based on the specifications of the Toyota Mirai presented by the Argonne Laboratory [56], SOC_k is the actual state of charge of the battery, P_{fc_k} is the output power of the fuel cell stack. The SOC and efficiency costs are, respectively, the square of the difference between SOC_{target} and SOC_k, and between η_{max} and η_k. The weights of the efficiency and SOC costs are represented by w_{eff} and w_{soc_k} respectively. Moreover, the term s_k which is a boolean variable is involved in the cost function to minimize the on-off cycles of the fuel cell system by forcing P_{fc_k} to be 0 at certain conditions. Determination of s_k will be presented later in the section. Equation 4.1 implies that, once the fuel cell starts running as the term

s is deactivated (0), the control decisions are taken to minimize the SOC and the efficiency costs synchronously. In this case, the fuel cell's on-off strategy does not have any impact on the decisions, and the optimization problem is solved considering only the trade-off between the efficiency cost and the SOC cost.

Note that the weight of the SOC cost is not constant, unlike the weight of the efficiency cost. It is determined based on the actual states of the battery in real-time, which are the output power and the SOC. The reason behind that, with the fixed values of the SOC cost weight, the controller is not able to perform robustly under different driving conditions. When the weights are specified as static values adjusted based on a specific drive cycle, potentially, the overfitting issue is faced, and generalization of the problem cannot be achieved. More specifically, when w_{eff} and w_{soc} were adjusted according to NEDC, the SOC could not be kept in a certain range under the US06 drive cycle even though it was achieved under the NEDC. Considering the NEDC cycle has a smoother driving pattern compared to the US06 in terms of the aggressiveness of the vehicle accelerations, the decelerations, and the magnitudes of the power demand, a smaller value of the SOC term would be sufficient to force the controller to minimize the SOC cost. However under the US06, with such a low value of the SOC cost weight, the SOC cost does not sufficiently increase to dominate the efficiency cost over the total cost, and it cannot force the controller to take corrective action for minimizing the SOC error. As a result that, the SOC error keeps increasing as the SOC drops away from the target value. Consequently, using the weights tuned for a smooth cycle, the controller's performance in minimization of the SOC error weakens in an aggressive drive cycle. In the opposite case, when the SOC weight is adjusted according to an aggressive drive cycle e.g. US06, in a non-aggressive cycle e.g. NEDC the fuel cell power rapidly varies since the controller is hypersensitive to SOC cost because of the high value of the weight. Considering the aggressiveness that varies even within a driving cycle, the constant weights would not be sufficient to achieve the same optimal control performance under opposite conditions, which is related to the robustness of the controller. To overcome this problem, the SOC term is determined in real-time via look-up tables using interpolation. The values calibrated in the maps are tuned by trials and errors. Equation 4.2 presents the determination of the weight for the SOC term based on the SOC and the battery power.

$$w_{soc_{k+1}} = h_1(SOC_k) + h_2(P_{bat_k}) \times \alpha_k - h_3(P_{bat_k}) \times (1 - \alpha_k) \tag{4.2}$$

where $h_1 : [0, 100] \rightarrow [0, m]$, $h_2 : [0, 30] \rightarrow [0, n]$ and $h_3 : [-30, 0] \rightarrow [0, p]$. Here, depending on the SOC and the battery power P_{bat}, the weight of the SOC term w_{soc} is dynamically adjusted to raise or lose the importance of the SOC cost over the cost function. The calibration is done in a way that w_{soc} keeps increasing as the SOC error or battery power increases. Firstly, when the SOC cost is not sufficiently large to dominate the efficiency cost over the cost function in Equation 4.1 even if the SOC error is undesirably high, h_1 increases thanks to the calibrated values in the map depending on the SOC. After the weight reaches a certain point, the controller becomes adequately sensitive to the SOC error to take corrective action against the SOC drops. In the opposite case, when the SOC approaches the target value, then h_1 decreases and efficiency cost is allowed to have more importance than the SOC cost by decreasing the SOC cost weight. The second map, h_2, which depends on the battery power, is introduced to the calculation of w_{soc} to prevent the battery from being utilized close to the maximum power during discharging. The third map, h_3, is used to avoid charging the battery close to the maximum input power of -30kW. It has a counter-effect to h_1 and h_2, so lowers the w_{soc}. To make this decision, the variable α is involved in the equation to indicate if the battery is charging or discharging as in Equation 4.3.

$$\alpha_k = \begin{cases} 1 & P_{bat_k} \geq 0 \\ 0 & P_{bat_k} < 0 \end{cases} \tag{4.3}$$

Consequently, the importance of the SOC tracking error, allowance to reach the maximum magnitude of discharging power, and allowance to reach the maximum magnitude of discharging power are controlled by h_1, h_2, and h_3 respectively. The breakpoints for these maps, which are defined in Equation 4.2 with maximum values of m, n, and p, are calibrated so that three different types of controllers are obtained, which are smooth, aggressive, and balanced.

As mentioned earlier, the term s_k determines if the fuel cell will run or shut down. When s_k is 1, the fuel cell is switched off. To make this decision, a hysteresis control strategy is used with a map-based approach depending on the actual power demand and the SOC level. If decided, the on-off strategy penalizes the square of fuel cell power to force it to be zero, as in the cost function given in Equation 4.1. The decision of s_k term is expressed with a piecewise function as in Equation 4.4.

$$s_{k+1} = \begin{cases} 0, & s_k = 0 \, and \, P_{em_k} \geq P_{on}(SOC_k) \\ 1, & s_k = 1 \, and \, P_{em_k} \leq P_{off}(SOC_k) \\ 0, & s_k = 0 \, and \, P_{em_k} < P_{on}(SOC_k) \\ 1, & s_k = 1 \, and \, P_{em_k} > P_{off}(SOC_k) \end{cases} \tag{4.4}$$

where $P_{on} > P_{off}$ and $s_0 = 1$.

Here, the hysteresis involves s a dependency of its previous value on top of the other dependencies, P_{em_k} and SOC_k. If its previous value is 1, in other words the fuel cell is off, s_k stays at this value until the power demand reaches the upper threshold value P_{on}. Once the threshold is reached, then the switch variable s is set to 0 and starts the fuel cell's operation until the power demand decreases to the lower threshold value P_{off}. Note that here the thresholds P_{on} and P_{off} depend on the SOC_k to consider the SOC level in the fuel cell's activation/deactivation strategy. As the SOC level decreases, P_{on} is lowered to not further decrease the SOC, and vice versa. The bidirectional movement of the on-off threshold points depending on the SOC over the power demand horizon, and the hysteresis-based approach for the fuel cell on-off strategy is illustrated in Figure 4.2. The calibration of the maps for the

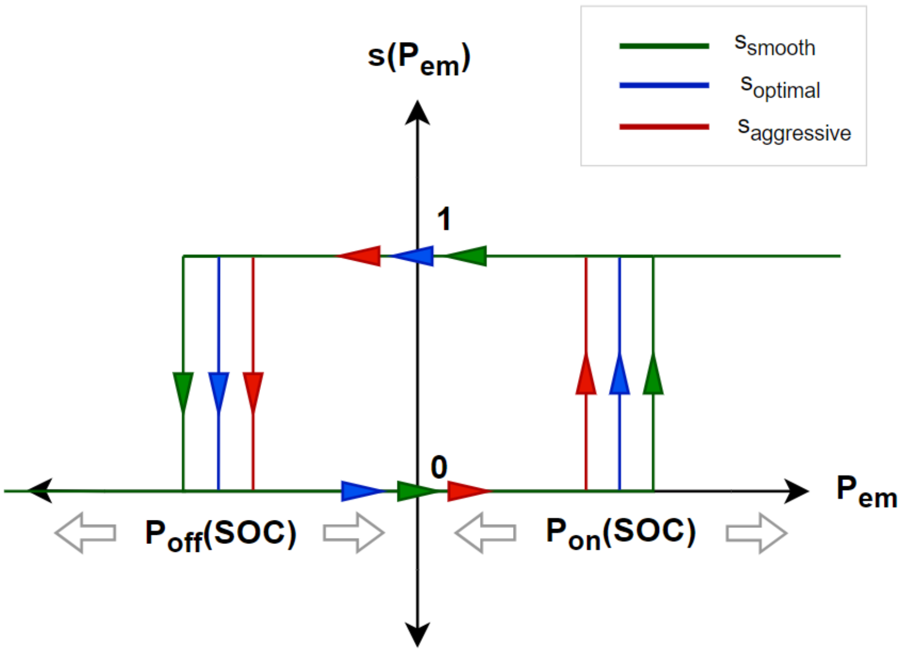

Figure 4.2 The strategy for calculating the fuel cell's on-off switching term

SOC cost term and the fuel cell enabling/disabling thresholds of the fuel cell were performed separately for the three different characteristics. Firstly, the objectives of the calibration for the smooth configuration are listed as the following requirements:

- Once the fuel cell is closed, the EMS shall suspend the fuel cell at lower levels of the power demand to not frequently initialize and shut down the fuel cell.
- Once the fuel cell starts operation, even if the power demand is relatively low, it shall be able to keep the power supply at the efficient region to charge the battery when the SOC level is considerably low.
- The EMS shall perform the power allocation in a way that the spikes and deviations in the power transient of the fuel cell are minimized, fuel cell system

efficiency is maximized, and the SOC is allowed to decrease to improve the fuel economy.

On the other hand, the aggressive configuration of the MPC is calibrated according to the requirements below:

- The fuel cell shall be able to run at relatively low power demands, to stand ready for meeting potential dramatically increasing power demands in order to prevent loading the battery to the limits.
- The fuel cell shall be shut down at a relatively higher value of power demand compared to smooth, to reduce the fuel consumption.
- The EMS shall perform the power allocation in a way that the SOC is not allowed to decrease relatively much below the target value to increase the available power in the battery for potential peak requests.
- The EMS shall keep the battery power away from the design limits by increasing the fuel cell's share of power demand and decreasing its response time.

The balanced configuration, which is the last configuration, is calibrated based on the following objectives described within the following requirements.

- The fuel cell shall be able to start operation at adequately low power demands to reduce the battery load, and at sufficiently high values to prevent the fuel cell from inefficient operation at low power demands.
- The fuel cell shall be turned off at a relatively higher value of power demand compared to the smooth configuration and a lower value than the aggressive configuration, to balance the importance of SOC control and fuel economy.
- The EMS shall be able to utilize the fuel cell aggressively under high magnitudes of power demands, and smoothly at low magnitudes.
- The EMS shall allow the SOC to circumspectively decrease in order to increase fuel cell system efficiency.

The calibration process for all types is done empirically by trial and error. For the balanced configuration, w_{eff}, $_1$, h_2, h_3, and the switching points P_{on}, P_{off} are calibrated to the values where the behavior of the controller obtained between the smooth and aggressive configurations in a balanced way. Table 4.1 presents the calibration values used in the MPC-based EMS.

As mentioned earlier, MPC is an online optimal control method that finds the optimal control action by predicting the future outputs of a plant through an internal

Table 4.1 Calibration values for the MPC-based EMS

Configuration	Map	Dimension	Map Data						Dependency	Unit
Smooth	h_1	Breakpoint	0	50	52.5	60	65	100	SOC	%
		Value	50	40	17.5	5	7.5	15	Weight Value	-
	h_2	Breakpoint	0	10	15	20	28	30	Battery Power	kW
		Value	0	10	20	30	40	50	Weight Value	-
	h_3	Breakpoint	-30	-28	-20	-15	-10	0	Battery Power	kW
		Value	50	40	30	20	10	0	Weight Value	-
	P_{on}	Breakpoint	0	50	52.5	60	65	100	SOC	%
		Value	-2.5	2.5	6	7.5	10	15	Power Demand	kW
	P_{off}	Breakpoint	0	50	52.5	60	65	100	SOC	%
		Value	-5	0	4	6	7.5	10	Power Demand	kW
Aggressive	h_1	Breakpoint	0	50	52.5	60	65	100	SOC	%
		Value	200	90	35	7.5	15	30	Weight Value	-
	h_2	Breakpoint	0	10	15	20	28	30	Battery Power	kW
		Value	0	20	40	60	100	200	Weight Value	-
	h_3	Breakpoint	-30	-28	-20	-15	-10	0	Battery Power	kW
		Value	200	100	60	40	20	0	Weight Value	-
	P_{on}	Breakpoint	0	50	52.5	60	65	100	SOC	%
		Value	-10	-2.5	0	3	5	10	Power Demand	kW
	P_{off}	Breakpoint	0	50	52.5	60	65	100	SOC	%
		Value	-15	-7.5	-2.5	0	2.5	7.5	Power Demand	kW
Balanced	h_1	Breakpoint	0	50	52.5	60	65	100	SOC	%
		Value	120	60	25	6	7.5	15	Weight Value	-
	h_2	Breakpoint	0	10	15	20	28	30	Battery Power	kW
		Value	0	15	30	40	60	120	Weight Value	-
	h_3	Breakpoint	-30	-28	-20	-15	-10	0	Battery Power	kW
		Value	120	60	40	30	15	0	Weight Value	-
	P_{on}	Breakpoint	0	50	52.5	60	65	100	SOC	%
		Value	-2.5	0	3	5	7.5	12.5	Power Demand	kW
	P_{off}	Breakpoint	0	50	52.5	60	65	100	SOC	%
		Value	-7.5	-2.5	0	2.5	5	10	Power Demand	kW

model representing the dynamics of the controlled plant. It takes input and output constraints into account throughout the optimization process. Since MPC is a model-dependent method, the controller's success directly depends on the internal model's accuracy. It solves the optimization problem periodically with the specified sampling time and finds the control outputs minimizing the cost function.

The design phase of the controller starts by constructing the architecture of the MPC in the application. In Figure 4.3, interactions between the FCHEV and the controller are shown in a block diagram. As indicated in the diagram, the controller is implemented using the CasADi tool and runs in the Simulink environment while the plant designed in Cruise-M interacts with the controller throughout the simulation cyclically. In the application, the states received by the MPC are the SOC and the fuel cell power at the DC bus, represented by x_1 and x_2 respectively. Although the SOC cannot be directly measured in practice, the electrochemical battery model in Cruise-M serves it as a measurable signal. The control signal, u is the reference change in the fuel cell power in a one-time step. Aiming to track the reference

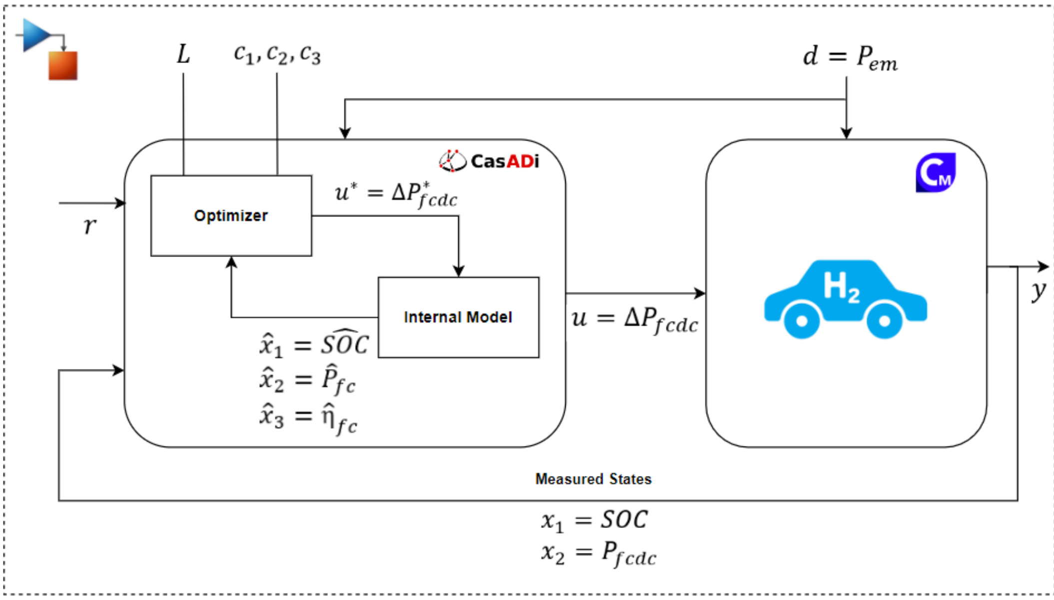

Figure 4.3 The control system and interaction between the MPC-based EMS and the plant

signal r, the controller determines the optimal control signal sequence through the iterations between the internal model and the optimizer using a solver minimizing the cost function L. Based on the system dynamics of the internal model, using the acquired power demand P_{em} and the determined optimal control sequence $u^\star$, future values of SOC are calculated which is represented by $S\hat{O}C$ in the figure. Here, via the internal model, the fuel cell power at the DC bus, $\hat{P}_{fc_{dc}}$, is directly calculated by integrating the determined optimum incrementation or decrementation sequence of the fuel cell power over the prediction horizon. However, only the first sample of the sequence is applied to the FCHEV plant model in Cruise-M. Since the fuel cell system efficiency, η_{fc}, can directly be estimated using the fuel cell power, there is no need to receive the actual fuel cell system efficiency from the plant, even though it is available in the electrochemical fuel cell system model. The system constraints c_1, c_2 and c_3 are always satisfied throughout the determination process of the control actions. After applying the control input, the power source outputs, y, are produced by the plant, including the SOC and fuel cell system efficiency.

The internal model embedded in the MPC must represent the system behavior through the states being manipulated in the process. In the study, the states are the SOC and the efficiency of the fuel cell system. Although MPC is model-dependent, it does not require a comprehensive internal model to represent the states of the system, thus a simple system model is used to not increase the complexity. At each time step, the control signal sequence is updated based on the new measurements. This feedback mechanism enables MPC to adapt to changing system dynamics and reject prediction errors due to modeling errors or uncertainties. So the MPC controller tolerates modeling errors and performs a robust control. But in any case, MPC performance is expected to be improved as the modeling errors are eliminated.

The powertrain of the studied FCHEV is non-linear because of the battery and fuel cell dynamics. Equation 4.5 and Equation 4.6 present dynamics of a non-linear system.

$$\dot{x}(t) = f(t, x(t), u(t)) \tag{4.5}$$

$$y(t) = h(t, x(t), u(t)) \tag{4.6}$$

Considering the non-linear system dynamics given above, the internal model or the predictive model of the problem can be reconstructed in a discrete form as follows:

$$x_{k+1} = f(k, x_k, u_k, w_k) \tag{4.7}$$

$$x_k = [P_{fcdc_{k-1}}, SOC_k] \tag{4.8}$$

$$u_k = \Delta P_{fcdc_k} = P_{fcdc_k} - P_{fcdc_{k-1}} \tag{4.9}$$

$$d_k = P_{em_k} \tag{4.10}$$

Here, P_{fcdc_k} and SOC_k are the measured states of the components, which are the fuel cell power at the DC bus and the SOC of the electrochemical battery. The control signal u_k is the reference change in the fuel cell's DC bus power, which is represented by ΔP_{fcdc_k}. Also P_{em_k} is the power load from the electric motor.

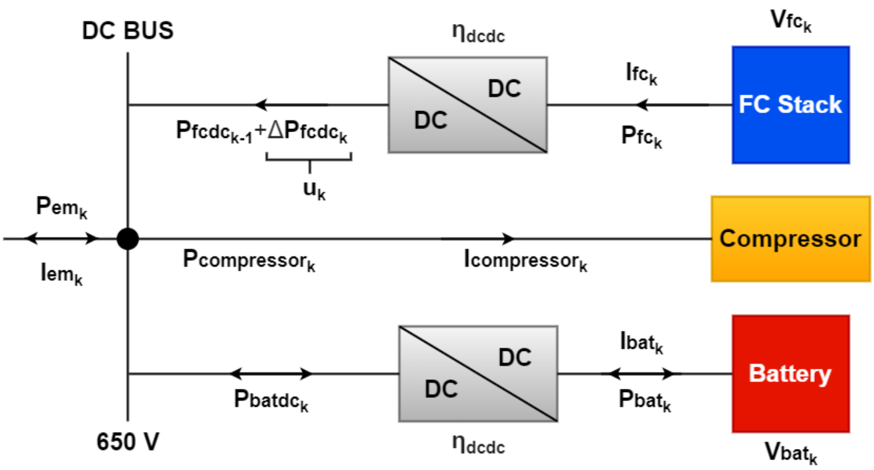

Figure 4.4 Power balance between the sources and the DC bus

Two main outputs aimed to be served by the internal model are SOC_k and the fuel cell efficiency η_{fc_k}. At first, the set of equations used for predicting the SOC will be presented. To be able to control the SOC, its dynamics must be available in the internal model. Hence, Equation 4.11 and Equation 4.12 are used for SOC estimation based on the Coulomb Counting method.

$$\dot{SOC}_{k+1} = \frac{-I_{bat_k}}{C_{bat} \times 3600} \times \Delta T \tag{4.11}$$

$$SOC_{k+1} = SOC_k + \dot{SOC}_{k+1} \tag{4.12}$$

Here, $\dot{SOC}_k$ is the SOC change in one time-step, I_{batk} is the battery current, and C_{bat} is the battery capacity. To derive the battery current for SOC estimation, the power balance at the DC bus is used which holds for the architecture given in Figure 4.4. Equation 4.13 implies the power balance at the DC bus between the control signal ΔP_{fcdc_k}, the previous value of the fuel cell power at the DC bus $P_{fcdc_{k-1}}$, the load P_{em_k} and the previous value of the SOC.

$$P_{batdc_k} = -(P_{fcdc_{k-1}} + \Delta P_{fcdc_k}) + P_{em_k} + P_{compressor_k} \tag{4.13}$$

$$P_{bat_k} = \begin{cases} \frac{P_{bat_{dc}}}{\eta_{dcdc}} , & \alpha_k = 1 \\ P_{bat_{dc}} \times \eta_{dcdc} , & \alpha_k = 0 \end{cases} \tag{4.14}$$

$$I_{bat_k} = \frac{E_{ocv}(SOC_k) - \sqrt{E_{ocv}^2(SOC_k) - 4R_{bat}^{\alpha_k}(SOC_k)P_{bat_k}}}{2R_{bat}^{\alpha_k}(SOC_k)} \tag{4.15}$$

$$V_{bat_k} = E_{ocv}(SOC_k) - R_{bat}^{\alpha_k}(SOC_k) \times I_{bat_k} \tag{4.16}$$

In the given equations above, once the battery's power share at the DC bus, P_{batdc_k}, is obtained using Equation 4.13, the battery current, I_{bat_k}, is derived using Equation 4.15 considering the converter efficiency as shown in Equation 4.14. Here α_k indicates if the battery is discharging or charging as defined earlier in Equation 4.3. Also the battery voltage, V_{bat_k} is estimated by using Equation 4.16. The equations are based on an equivalent circuit model approach as illustrated in Figure 4.5.

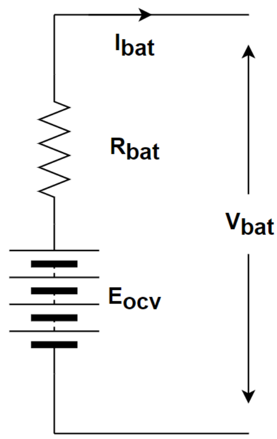

Figure 4.5 Equivalent circuit of the internal resistance model for the studied battery pack

For the studied battery, the relations between the SOC and open circuit voltage E_{bat_k}, and internal resistance $R^{\alpha}_{bat_k}$ are graphically expressed in Figure 4.6. Due to these internal variables being used for SOC estimation are not available in the form of mathematical expressions since the studied battery is a black-box electrochemical model, they are obtained via black-box testing at a constant current of 1C rate, 6.5A. The temperature effect is neglected during the tests by setting the battery temperature to fixed $25°C$, and these variables are assumed to depend only on SOC. Note that these variables are available as outputs for the electrochemical battery in Cruise-M, and the internal resistance is assumed to be the variable that refers to the entire voltage drop as used in equivalent circuit models, although no further information is available in Cruise-M for this output. Consequently, Figure 4.6 respectively presents the open circuit voltage, and internal resistances during discharging and charging against SOC.

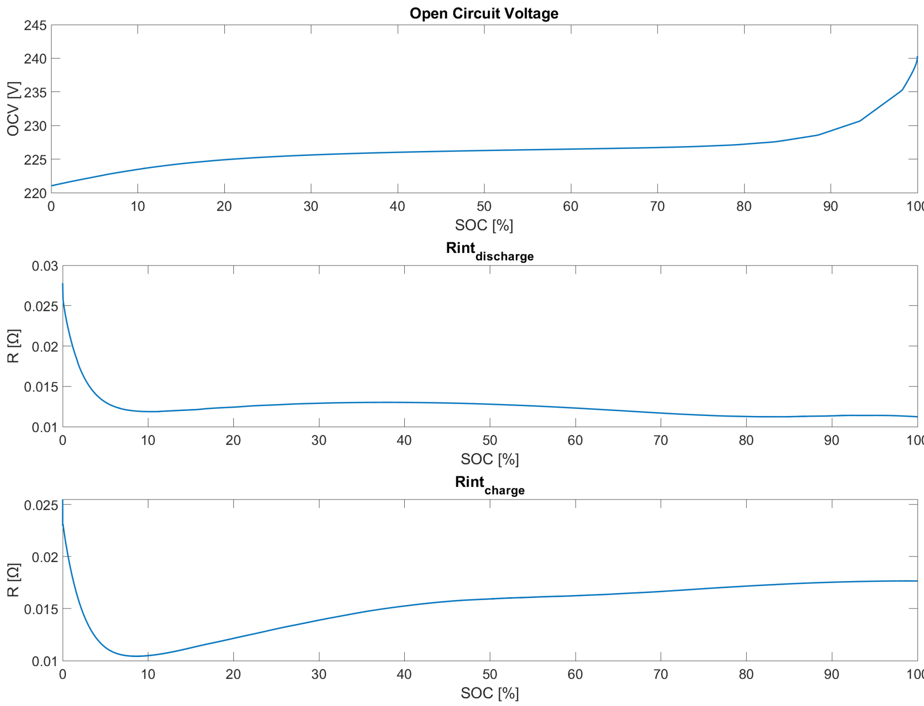

Figure 4.6 Battery open circuit voltage and internal resistances during discharging and charging

Synchronously, as the second main output of the internal model, the fuel cell system efficiency is determined against the fuel cell power using the efficiency curve of the fuel cell system presented in Equation 2.4. The fuel cell power is directly determined based on its power share at the DC bus and the converter efficiency as in Equation 4.17.

$$P_{fc_k} = \frac{P_{fcdc_{k-1}} + \Delta P_{fcdc_k}}{\eta_{dcdc}} \tag{4.17}$$

The set of calculations aforementioned are executed over the prediction horizon. The future response of the states is predicted by using the given set of equations via the internal model. In this way, the future values of the cost function are predicted, and the optimal control action is determined based on not only the current state values but also their future responses.

Another important framework of the problem formulation is to involve constraints in the MPC controller to limit certain states of the system considering the physical limits of the powertrain components. To this end, four different constraints are introduced into the MPC that define the limits for the fuel cell current, the battery current, the rate of change of the fuel cell current, and the state of charge which are given in Equation 4.18, Equation 4.19, Equation 4.20, and Equation 4.21 respectively.

$$c_1 : \Delta P_{fc}^{min} \leq \Delta P_{fc_k} \leq \Delta P_{fc}^{max} \tag{4.18}$$

$$c_2 : P_{fc}^{min} \leq P_{fc_k} \leq P_{fc}^{max} \tag{4.19}$$

$$c_3 : P_{bat}^{min} \leq P_{bat_k} \leq P_{bat}^{max} \tag{4.20}$$

$$c_4 : SOC_{min} \leq SOC_k \leq SOC_{max} \tag{4.21}$$

The constraints for the fuel cell and battery power magnitudes are set to the design limits, which are either specified by the manufacturer or extracted from the dynamometer results. Additionally, the rate of change of the fuel cell current is limited to achieve a smooth operation and to not create a transient load exceeding the fuel cell's reaction capabilities. On the other hand, it must be adequately fast considering the power capabilities of the powertrain of the Mirai [1]. Since these are the design limits, the constraints are set to the same for the three MPC types to make a fair comparison. The limit values of the constrained variables are specified s in Table 4.2.

Table 4.2 Constraint values defined in the MPC-based EMS

Constraint	Value	Unit
P$_{fc}^{max}$	114	kW
ΔP_{fc}^{max}	1.1	kW
ΔP_{fc}^{min}	-1.9	kW
P$_{bat}^{max}$	30	kW
P$_{bat}^{min}$	-30	kW
SOC$_{max}$	80	%
SOC$_{min}$	30	%

In the application, the controller parameters are tuned so that a balanced performance of the controller is achieved in terms of controller performance and computational burden. The prediction horizon is specified as 10s, and the control horizon is tuned as 2s. The sampling time of the controller is specified as 100ms which is the simulation's step size. These values are selected empirically based on trials and errors in the simulation. The controller parameters have an important impact on the performance of MPC. It is seen that, as the sampling time decreases, the controller becomes more robust, so the disturbance rejection performance is improved. However, the computation load becomes heavier. Theoretically, the performance of the MPC is improved as the prediction horizon increases, however, it is seen that increasing the prediction horizon also significantly increases the execution time. The control horizon is specified as 2s, so that it not only provides a sufficient degree of freedom for the determination of the control sequence but also does not exceed the prediction horizon and does not increase the computational burden.

Finally, as mentioned earlier, the MPC is implemented using the CasADi open-source software tool for numerical optimizations. With the help of the symbolic framework of CasADi, any non-linear optimization problem can be studied comprehensively using it [65]. Although it is available also for other languages such as C++ and Python, the application in the study is performed in the Matlab-Simulink environment, and the MPC is implemented using CasADi's symbolic syntax. After implementing the MPC in Matlab scripts using the CasADi environment, the source code is generated and integrated into the Simulink. As an advantage of it, the MPC controller code does not require compilation every time the simulation starts, and the simulation speed is increased. To solve the non-linear problem, the *ipopt* algorithm is used, which is available in the CasADi environment. *ipopt* utilizes the nonlinear interior point method and can be used in any optimization problem e.g. linear, non-linear, convex, non-convex [66].

4.3 Evaluation of the MPC-based EMS with Smooth, Aggressive and Balanced Configurations

As mentioned in the previous section, dynamic weight selection of the SOC term and the fuel cell on-off strategy are performed based on certain thresholds determined through the maps via interpolation. Calibration of the maps has a crucial impact on the controller's characteristics since the importance of the cost terms depends on the values defined in the maps. We perform the simulation under five different drive cycles which are NEDC, UDDS, WLTP, US06, and HWFET. Considering the variety of driving characteristics in these drive cycles, tuning the map breakpoints and output values based on a certain drive cycle would bring an overfitting problem. In this case, selecting the optimal values through the calibration process is necessary to ensure that the EMS performs in a balanced way under different driving conditions. For this purpose, three different configurations of the MPC were created to select the more balanced calibration values based on different drive cycles.

Calibration of the maps for each of the smooth and aggressive configurations was performed empirically by evaluating the results under one drive cycle per type. Since NEDC has non-aggressive characteristics due to the low average speed and non-aggressive accelerations/decelerations, the smooth configuration was calibrated based on it. On the other hand, US06 was used for calibrating the aggressive configuration since it contains drastic accelerations and decelerations, and a higher value of the average speed among the five drive cycles. The designed controller requires calibration only for selecting the SOC cost weight and the on-off switch thresholds for the fuel cell.

Firstly, the calibration is performed in a way that a smoother and more efficient operation of the fuel cell is achieved with the price of heavier battery utilization. This is reasonable when the non-aggressive power demand of the NEDC shown in Figure 4.7 is considered.

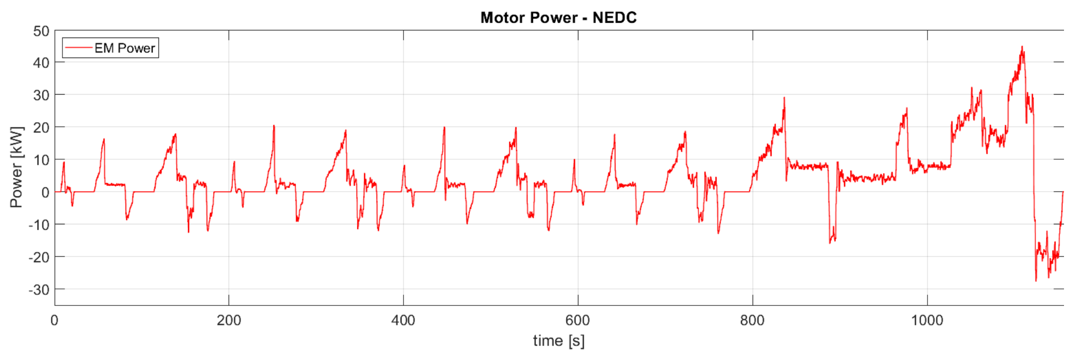

Figure 4.7 Power demand of the electric motor in NEDC cycle

As can be seen in the power demand in Figure 4.7, NEDC overall requires lower magnitudes of power demand from the sources. For this reason, we do not expect to use the fuel cell to meet the demand for lower amounts of power requests, to reduce fuel consumption, and to prevent low-efficient operation. To achieve that, the calibration of the map used for calculating the fuel cell's switch-on point is set to a higher value than the aggressive configuration, so that the fuel cell is enabled when the power demand exceeds a relatively higher value. As a result of that, the power will be supplied by the battery at low magnitudes, and the utilization will cause a decrease in SOC. At this point, the switch-off point of the fuel cell is set to a higher value for recovering the SOC by utilizing the fuel cell in a high-efficiency region. Also mostly, NEDC does not contain peak power requests that may cause the battery to operate at critically high power magnitudes close to the design limits.

Afterward, the second configuration, aggressive, is calibrated by considering the sharply increasing and higher magnitudes of the power demand in US06 cycle.

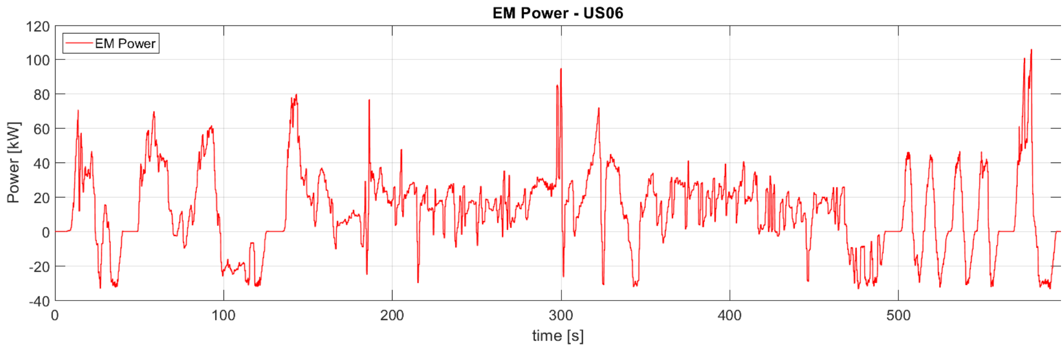

Figure 4.8 Power demand of the electric motor in US06 cycle

When the power demand increases drastically in US06, the battery meets a big portion of the demand due to the slower dynamics of the fuel cell. On top of that, if the decision to enable the fuel cell takes an unacceptably long time, the battery will suffer from critically high amounts of requests. To prevent such an undesired action, the switch-on point of the fuel cell is set to a lower magnitude of power demand compared to the smooth configuration. It will compulsorily cause fluctuations in the fuel cell's output power and increase in fuel consumption due to inefficient operation of it, however ensures that the battery will not utilized at critically high power levels for long times.

Finally, with a combination of different portions of the five drive cycles, another drive cycle is created to contain all of the characteristics in terms of aggressiveness. By trial and error, the maps were calibrated aiming to achieve an EMS behavior performing a tendency between the smooth and aggressive characteristics.

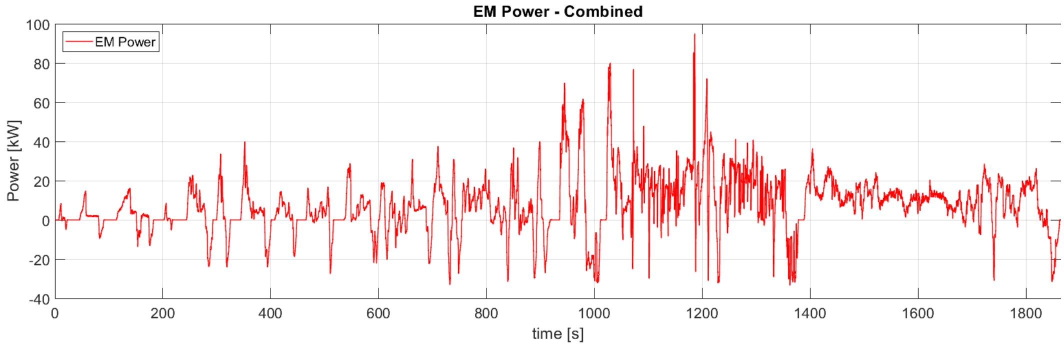

Figure 4.9 Power demand of the electric motor in the combined drive cycle

After the calibration, the three different EMSs were evaluated under five different drive cycles in an order of NEDC, UDDS, WLTP, US06, and HWFET. Only the NEDC and US06 performances of three MPCs are evaluated in this section since these two cycles are the best options to asses the EMSs under the boundary driving conditions as the smoothest and the most aggressive ones.

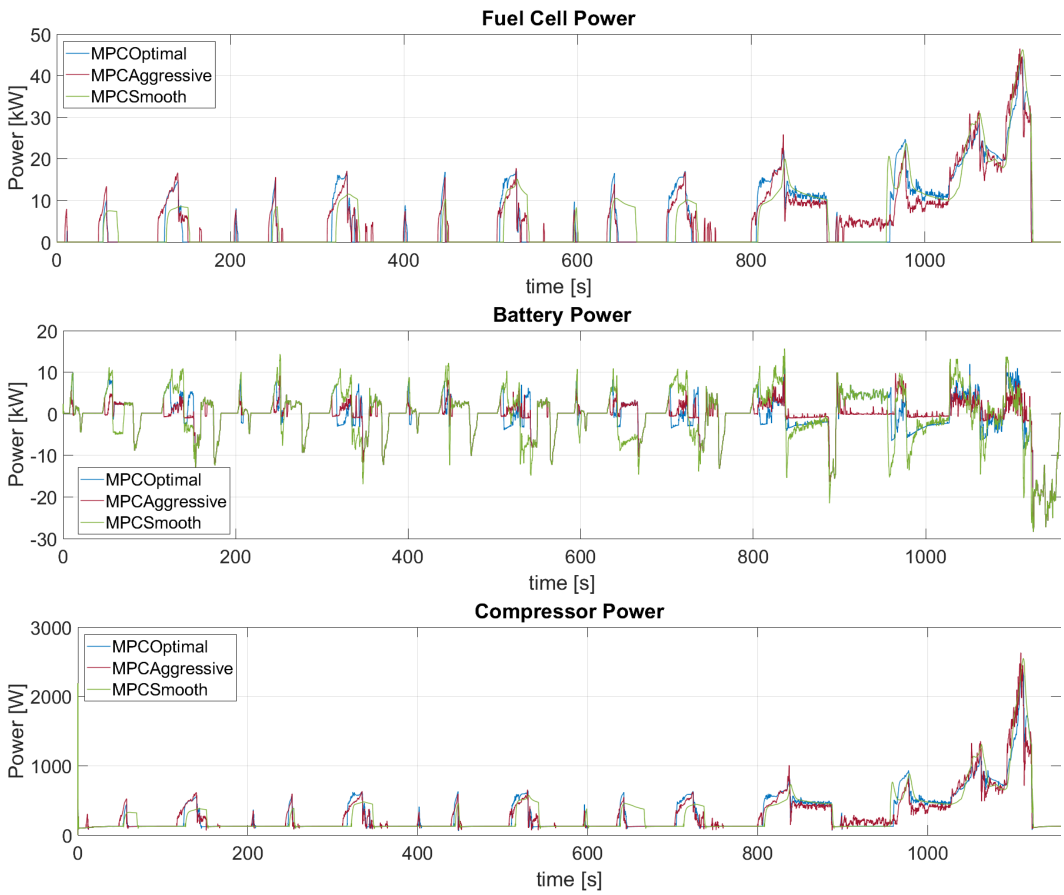

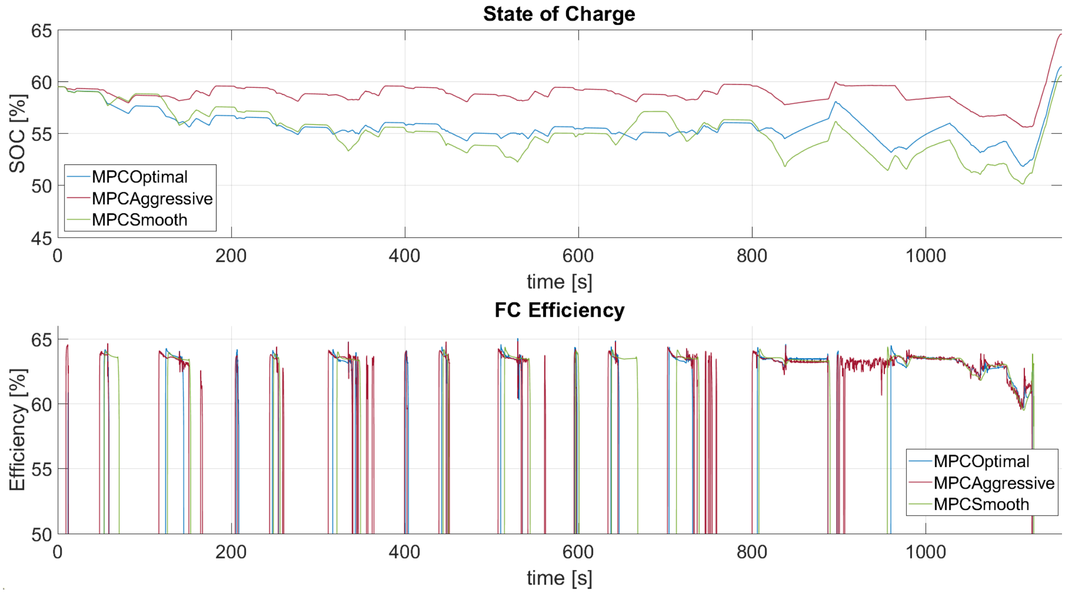

Figure 4.10 Performance of smooth, aggressive, and balanced configurations of MPC-based MPC under NEDC cycle

According to the results shown in Figure 4.10, the smooth configuration behaved in a strategy that the fuel cell does not frequently cyclings, performs in the efficient region with a smaller dependency on the power demand, and with smoother transients. The fuel cell was suspended at the low power demands. This allowed to reduction in the on-off switchings of the fuel cell and decreased the fuel consumption. However, since the share of battery in the power allocation is increased, the EMS allowed the SOC to decrease compared to other configurations, and a relatively more oscillatory SOC result was obtained. Nevertheless, the SOC could be kept still in a certain range. On the other hand, the aggressive configuration overreacted against the deviations in SOC. By the calibration of the on-off switch points of the fuel cell, the EMS tended to start the operation of the fuel cell at relatively lower amounts of power demands and shut it down quickly since the power demand in NEDC generally decreases below the switch-off point of the fuel cell after passing the switch-on point for the aggressive configuration. Also, during the fuel cell's operation, since the SOC cost is unnecessarily high because of the calibration of the map used for calculating the weight of the SOC cost, the fuel cell power oscillated throughout the driving to minimize the SOC error. Lastly, it is observed in the same results that balanced calibration of the MPC-based EMS shows a tendency between the smooth and aggressive ones. The fuel cell is operated relatively more aggressively than the smooth configuration, and more smoothly than the aggressive type. It kept the SOC in a region between that in the other two configurations.

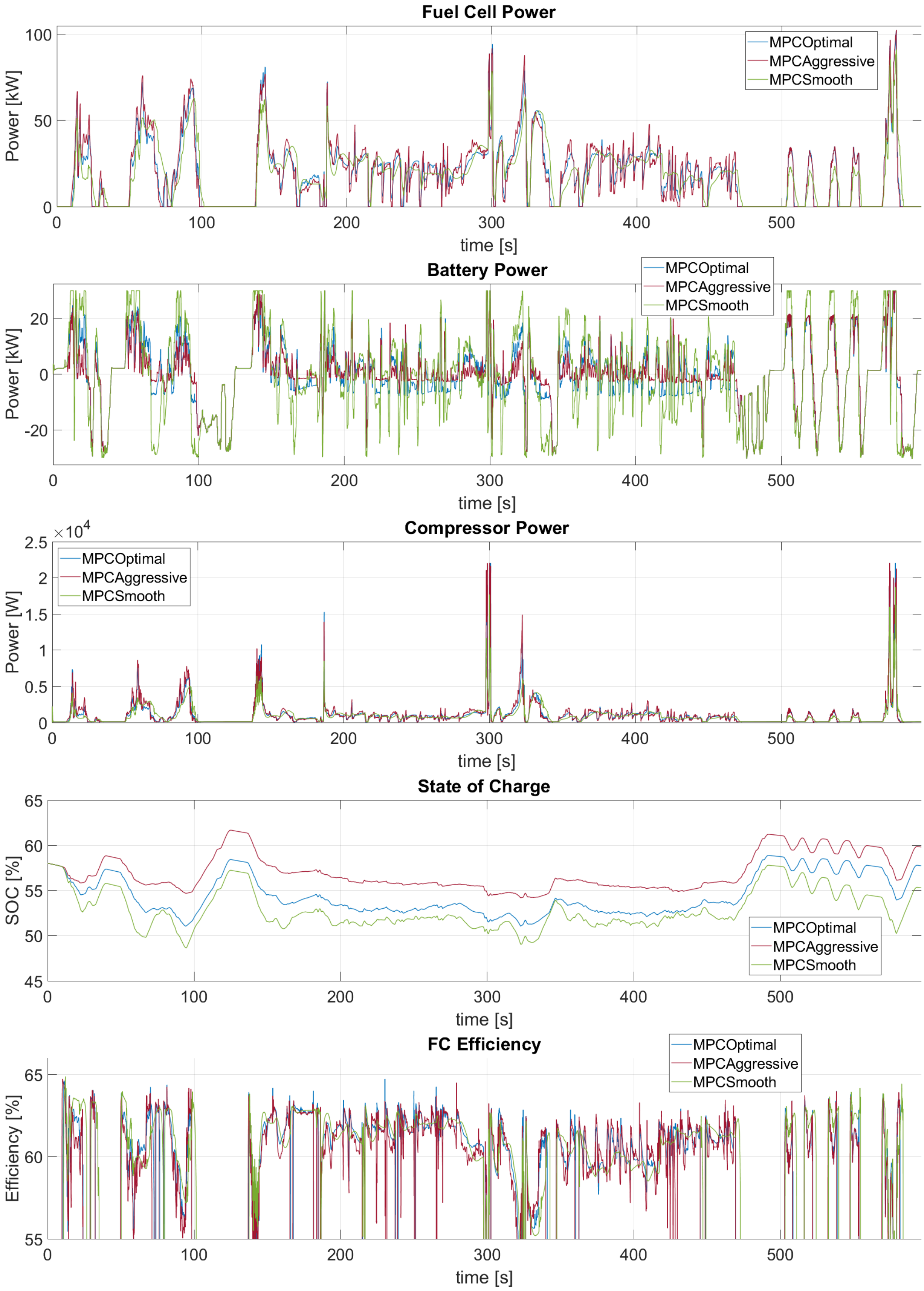

Figure 4.11 Performance of smooth, aggressive, and balanced configurations of MPC-based MPC under US06 cycle

As an aggressive drive cycle, US06 necessitates giving more importance to the SOC cost to not harm the battery so that the fuel cell meets the big share of the power demand. To this end, the aggressive configuration of the MPC-based EMSs reacted to the power demands by starting to operate under the lower amounts of power demands. It lowered the battery's power share and tried to prevent utilizing it at maximum power. During the limited power supply of the fuel cell because of the slower dynamics, even if the battery power is forced to reach the maximum value to fulfill the power demand, the aggressive configuration increases the share of the fuel cell more quickly than the others and decreases the battery's output power. On the other hand, the smooth configuration still gives more importance to the efficiency cost, although the SOC error increases as the battery supplies high amounts of power for a long time. Due to the unnecessarily higher efficiency cost, the fuel cell performs smoother and tends to operate closer to the efficient region compared to the other configurations. Although a more efficient operation is observed, the battery was utilized at its maximum limit for unacceptable long durations, which will accelerate the battery degradation or even cause to safety issues. Lastly, although the balanced configuration tends to utilize the battery more than the aggressive type, the output power results are acceptable and it sufficiently keeps the battery output power away from the maximum limit. Similar to the NEDC results, the balanced configuration of the MPC-based EMS behaved in a way between the smooth and the aggressive configurations. It is observed that the tendency is closer to the aggressive one in terms of power outputs, however, the course of the SOC is closer to the smooth configuration result.

Table 4.3 Performance of smooth, aggressive, and balanced configurations of the MPC-based EMS under NEDC cycle, (*model result)

<table>
<tr><th>Result</th><th>Dynamometer</th><th>MPC-s</th><th>MPC-a</th><th>MPC-o</th><th>Unit</th></tr>
<tr><td>EM Energy Net</td><td colspan="4">1262.4</td><td>Wh</td></tr>
<tr><td rowspan="2">Hydrogen Consumption</td><td>79.6</td><td rowspan="2">73.9</td><td rowspan="2">75.7</td><td rowspan="2">74.4</td><td rowspan="2">g</td></tr>
<tr><td>74.8*</td></tr>
<tr><td>Average FC System Efficiency</td><td>Not Available</td><td>63.4</td><td>63.2</td><td>63.1</td><td>%</td></tr>
<tr><td>FC Energy</td><td>1624.7</td><td>1613.3</td><td>1654.4</td><td>1625.1</td><td>Wh</td></tr>
<tr><td rowspan="2">Compressor Energy</td><td>24</td><td rowspan="2">92.6</td><td rowspan="2">91.2*</td><td rowspan="2">92.1</td><td rowspan="2">Wh</td></tr>
<tr><td>91.2</td></tr>
<tr><td>FC Power Change Accumulation</td><td>1134.0</td><td>393.8</td><td>1199.5</td><td>768.7</td><td>kW</td></tr>
<tr><td>SOC Initial</td><td>59.5</td><td>59.5</td><td>59.5</td><td>59.5</td><td>%</td></tr>
<tr><td>SOC Final</td><td>64.18</td><td>60.61</td><td>64.57</td><td>61.42</td><td>%</td></tr>
<tr><td>BAT Energy Output</td><td>402.8</td><td>617.5</td><td>304.2</td><td>469.7</td><td>Wh</td></tr>
<tr><td>BAT Energy Input</td><td>-536.9</td><td>-731.2</td><td>744.7</td><td>-572.7</td><td>Wh</td></tr>
<tr><td>BAT Energy Total (absolute)</td><td>939.7</td><td>1348.7</td><td>1048.9</td><td>1042.4</td><td>Wh</td></tr>
<tr><td>BAT Energy Net</td><td>-134.1</td><td>-113.7</td><td>-136.3</td><td>-102.9</td><td>Wh</td></tr>
</table>

Table 4.4 Performance of smooth, aggressive, and balanced configurations of the MPC-based EMS under US06 cycle, (*model result)

Result	Dynamometer	MPC-s	MPC-a	MPC-o	Unit
EM Energy Net	2851.9				Wh
Hydrogen Consumption	161.2 157.3*	144.3	146.2	145.0	g
Average FC System Efficiency	Not Available	60.91	60.53	60.74	%
FC Energy	3247.2	3034.7	3066.9	3049.1	Wh
Compressor Energy	115.1 216.6*	155.8	182.6	173.8	Wh
FC Power Change Accumulation	5578.0	4462.1	3857.2	1071.4	kW
SOC Initial	58	58	58	58	%
SOC Final	60.79	55.29	59.80	57.73	%
BAT Energy Output	498.0	955.8	515.3	673.3	Wh
BAT Energy Input	-631.7	-1086.9	-638.6	-784.7	Wh
BAT Energy Total (absolute)	1129.7	2042.8	1153.9	1458.0	Wh
BAT Energy Net	-133.7	-131.0	-123.2	-111.6	Wh

In the last part of the section, the balanced configuration of the MPC-based EMS is assessed by comparing the results with dynamometer results under WLTP drive cycle. WLTP is selected due to its high wide range of driving characteristics in terms of power requirements as explained in the third chapter.

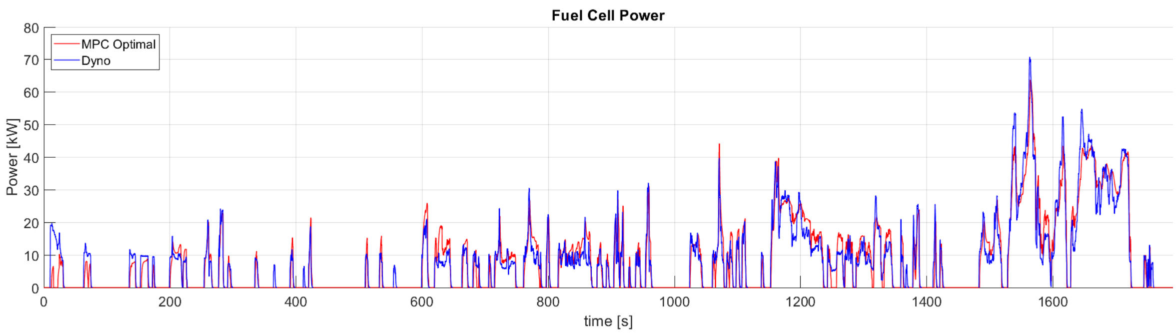

Figure 4.12 Fuel cell power results of the MPC-based EMS and the dynamometer test under WLTP cycle

As presented in Figure 4.12, the fuel cell power results of the balanced configuration of MPC-based EMS follows a similar trend with the dynamometer test results in terms of on-off switchings of the fuel cell. Yet, the MPC-based EMS more frequently cycled the fuel cell in the beginning phase, and between 1000th and 1400th seconds. On the other hand, the Mirai EMS performed a higher number of switchings between

300th and 600th seconds, and at the ending, where the MPC-based EMS mostly suspended the fuel cell. In total, the number of switchings obtained by these strategies is equal for WLTP drive cycle. On the other hand, the peak magnitudes of fuel cell power are generally higher for the MPC-based EMS compared to the Mirai, except from the beginning until 200th second and from 1400th to the end of the cycle. The difference at the beginning can be due to the SOC level overshooting 60%. However, the deviation in the last phase can be related to the fuel economy purpose of the MPC-based EMS, although the SOC level is below the target. The SOC is still in the desired range, nevertheless, the fuel cell's power share could be increased and SOC error can be reduced by re-adjusting the maps used for calculating the SOC cost term, if SOC error compensation is wanted to be improved.

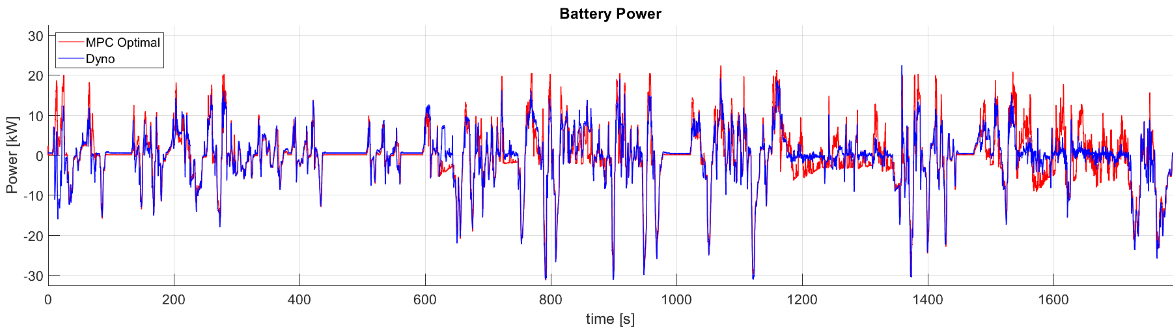

Figure 4.13 Battery power results of the MPC-based EMS and the dynamometer test under WLTP cycle

According to the battery power results shown in Figure 4.13, especially after 1200th second the MPC-based EMS more heavily utilized the battery by repeatedly discharging and charging it. This is a result of the efficiency term effect and the on-off strategy of the MPC-based EMS. Since SOC sails below the target, the EMS tends to charge the battery without moving much away from the efficient region of the fuel cell system. Throughout the driving, considering the dynamometer result, it can be said that the MPC-based EMS achieves a realistic power allocation in terms of the battery power magnitudes, since the maximum and minimum values of the battery power are quite close for both methods.

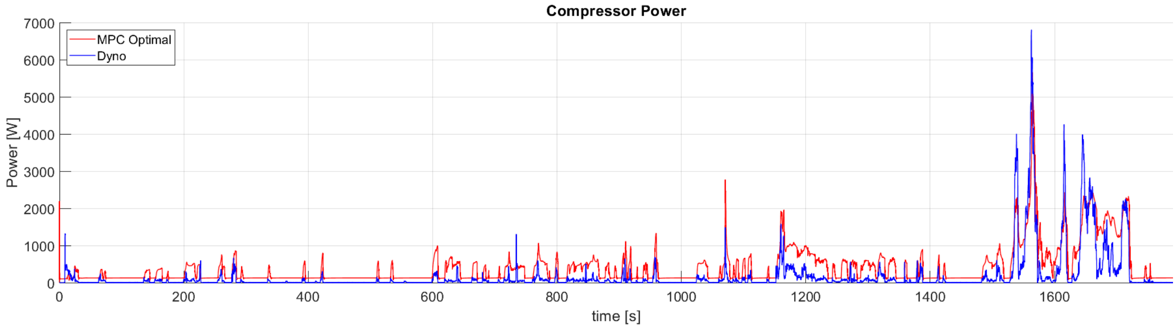

Figure 4.14 Compressor power results of the MPC-based EMS and the dynamometer test under WLTP cycle

As discussed in the second chapter where the compressor results are evaluated, more amount of energy is lost in the compressor model of the plant compared to the Mirai's. This serious deviation between the compressor results does not originate from the EMS decisions, it is due to differences between the compressor model and the real system. In general, due to the higher power request of the compressor model as shown in Figure 4.14, a larger amount of power is requested from the power sources in the FCHEV plant model.

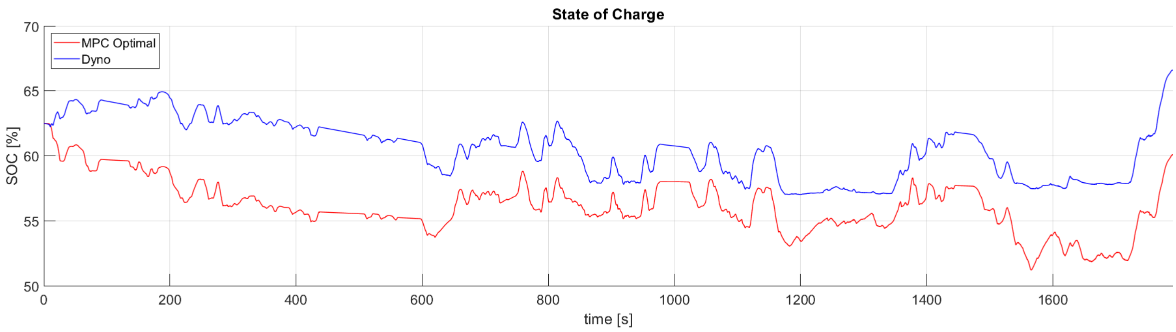

Figure 4.15 SOC results of the MPC-based EMS and the dynamometer test under WLTP cycle

According to the SOC results presented in Figure 4.15, the MPC-based EMS allows the SOC to decrease and sail below the target in order to improve the fuel economy under dictation of the efficiency cost and decisions to suspend the fuel cell. Nevertheless, the SOC is still driven within an acceptable range without decreasing to critically low values e.g. less than 50%. Also, this offset enables the SOC to settle the target value at the end of the cycle, after the hard regenerative braking phase at the end of the cycle.

5. Simulation Results and Evaluation

In this chapter, the developed EMSs are evaluated through the simulation tests, and the results are presented. The performance of the designed EMSs which are RB-EMS and MPC-based EMS are assessed under various drive cycles. Also, the dynamometer test results of a Toyota Mirai under the same drive cycles are shown there to evaluate the differences and similarities between the designed energy management strategies and the real results. The comparison is important to show the representativeness of the FCHEV model and the reliability of the simulation results.

5.1 Simulation Results

This chapter presents the simulation results for the RB-EMS and the MPC-based EMS. The output data of the power sources is generated through the simulations conducted under five different drive cycles which are NEDC, UDDS, WLTP, US06, and HWFET. In addition to the designed EMSs, the dynamometer test results are shown which are presented by the authority. The evaluation criteria of fuel economy are selected as hydrogen consumption and average fuel cell system efficiency. Apart from the evaluation of fuel economy, the feasibility of utilization of the power sources is assessed by considering the physical limits and the potential effects on the degradation of the power sources. For this purpose, various criteria are evaluated such as the power change accumulation of the fuel cell, the final value of the SOC, and the total energy transferred through the battery. The outputs of the components are presented in the figures for each drive cycle, followed by the numerical results in the tables for each drive cycle.

5.1.1 NEDC

NEDC has a total duration of 1160s. Its driving pattern starts at low speeds in an urban characteristic and keeps this attitude for a big part of the cycle. Towards the end, the velocity reference inclines to higher speeds representing highway driving which requires higher amounts of power from the sources. However, NEDC generally exhibits a less aggressive driving pattern compared to the other four cycles.

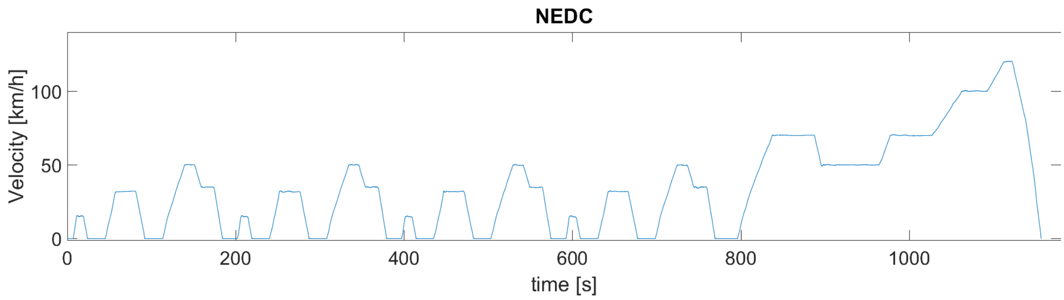

Figure 5.1 NEDC

The results in Figure 5.2 show that, during the first 800 seconds which is the urban segment, among the methods the MPC-based EMS mainly used the battery instead of the fuel cell at low power demands. As a consequence of that, the SOC coursed around a lower level than the others, but still in a controlled manner without having critically low or high values. Generally, the SOC curves are similar for the RB-EMS and the Mirai EMS. At the end of the cycle, due to the hard regenerative braking, all results show an increase in SOC. Yet, the MPC-based EMS reached a value closer to 60% of the target SOC compared to the RB-EMS and the Mirai EMS. Both the RB- and MPC-based EMSs could use the fuel cell in the efficient region. Since the average efficiency data for the fuel cell system is not available in the dynamometer test results, no evaluation could be done for the Mirai EMS. The MPC-based EMS achieved slightly a higher average value for the fuel cell system efficiency compared to the RB-EMS result. The trends in the fuel cell power are partly close for all methods, nevertheless, RB-EMS slightly more utilized the fuel cell than the others. Considering the transients of the fuel cell power, all the methods perform relatively more aggressive actions after 800th s, where is the highway segment. However, the sharpness of the changes in the fuel cell output power is close in all results, showing that the RB-EMS and MPC-based EMS does not create any unrealistic change through our FCHEV model in NEDC. The results show that the smoothest operation of the fuel cell is performed by the MPC-based EMS, followed by the RB-EMS. This reliability is important because requesting power from the fuel cell with strong deviations and pushing it to the limits would cause an acceleration in its degradation. As is seen at 200th, 400th, and 600th s, although the MPC-based EMS and the Mirai EMS tended to utilize the fuel cell for the requests pulsing, while the RB-EMS decided to suspend the fuel cell at such demands. As a result, the number of on-off switchings of the fuel cell is higher for the MPC-based EMS and the Mirai EMS compared to the RB-EMS. This could be prevented by calibrating the MPC-based EMS in a way that it enables the fuel cell at a higher amount of power demand, however during the design phase it was observed that such a calibration causes a delayed transient response of the fuel cell. This resulted in the utilization of the battery at higher power values in the peak requests, as will be discussed in US06 results. However, once the fuel cell is initialized, the MPC-based EMS tends to charge the battery by using the fuel cell. For relatively lower power demands as in between the seconds 800th and 1030th, the MPC-based EMS charged the battery, but still, the fuel cell did not move away from the efficient region. For the same interval, the RB-EMS tended similarly by requesting lower amounts of charging power from the fuel cell, while the EMS of Toyota Mirai did not charge the battery. According to the battery power results shown in Figure 5.2, all the methods operated the battery with different tendencies. However, it is utilized far from its limits by all three EMSs. Lastly, according to the compressor power results, a remarkable difference is observed between our FCHEV model and the compressor of the Toyota Mirai. However, when we applied the fuel cell power data from the dynamometer test to our fuel cell system model, all methods produced similar compressor power outputs.

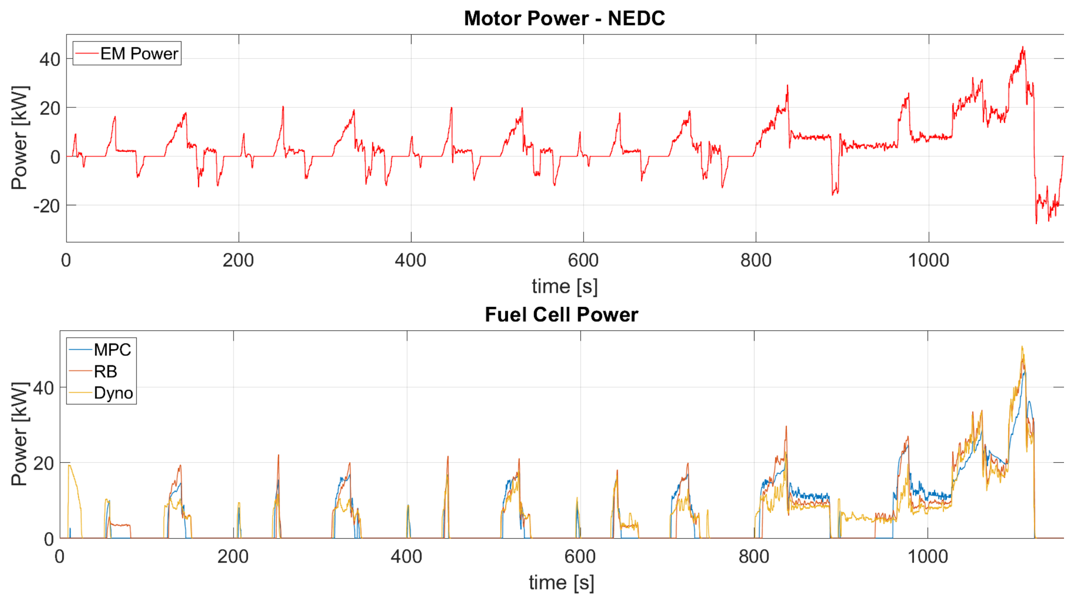

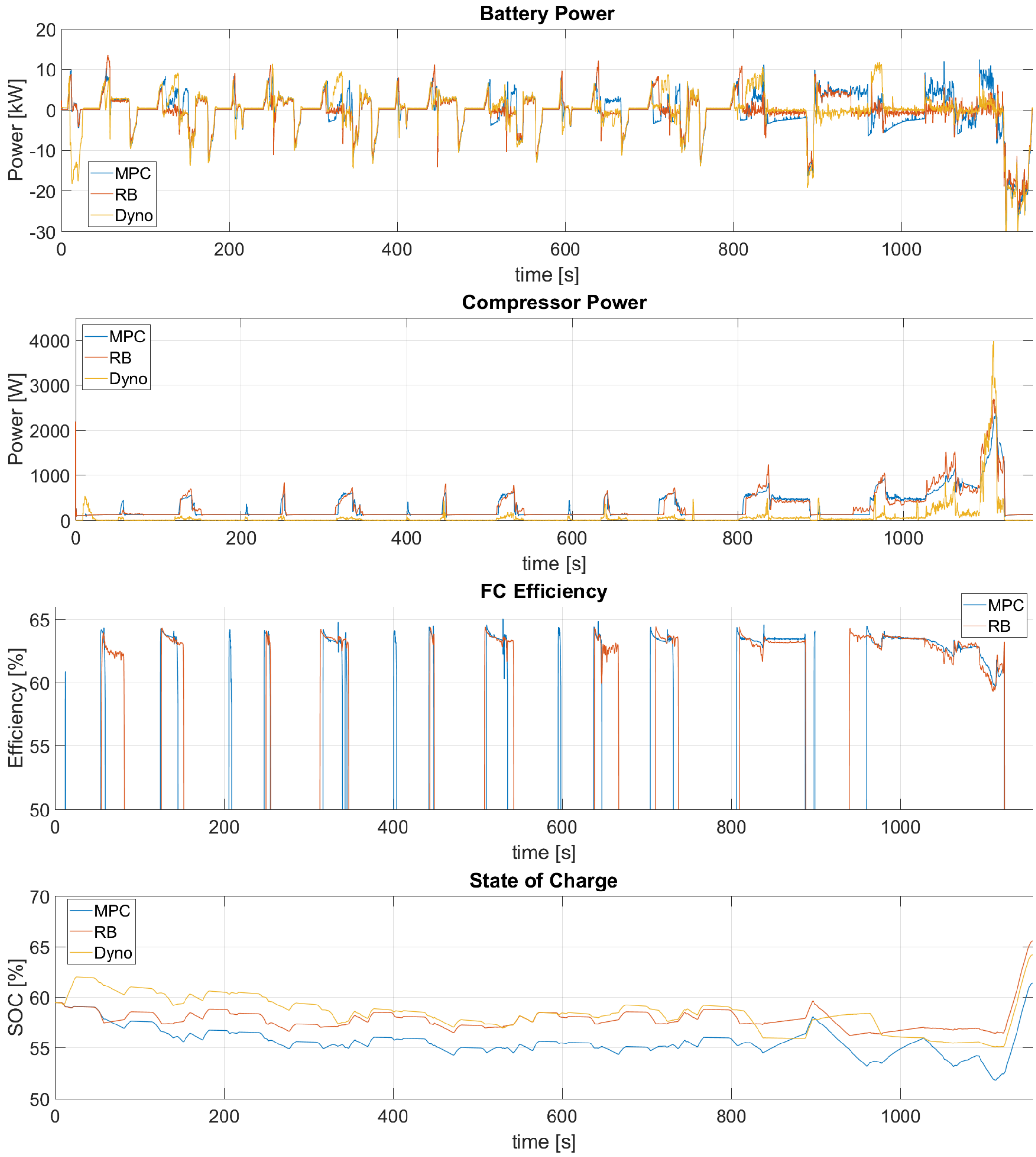

Figure 5.2 Comparision of the system outputs for the RB-EMS, MPC-based EMS, and dynamometer results under NEDC

The most important outcomes related to fuel economy are hydrogen consumption and fuel cell efficiency. On the other hand, the fuel cell power change accumulation and magnitudes of the battery power output, SOC final value, and energy outcomes are significant measurements that may be considered related to the degradation of the power sources. As reported in Table 5.1 for NEDC, the MPC-based EMS could decrease fuel consumption by 3.63% and 0.54% compared to the RB-EMS and Mirai EMS results respectively. Also, the average efficiency of the MPC-based EMS is 0.1% higher than the RB-EMS, showing that both of the methods utilized the fuel cell efficiently. In general, it is observed that a better fuel economy is achieved by the MPC-based EMS in NEDC, followed by the Mirai EMS and the RB-EMS. Although NEDC is not an aggressive cycle that pushes the sources to their limits, the MPC-based EMS utilized the fuel cell significantly more smoothly, especially compared to the dynamometer results. In NEDC, the battery power outputs are far from the limits as discussed earlier, however, less amount of energy flowed on the battery in the RB-EMS results, followed by the Mirai EMS and, with a slightly higher value, the MPC-based EMS. Lastly, the MPC-based EMS could finish the NEDC with a final SOC value closer to 60% of the target value, while the others overshot the target with a larger difference.

Table 5.1 Power source outputs for the dynamometer test, RB-EMS, and MPC-based EMS under NEDC

Result	Dynamometer	RB	MPC	Unit
EM Energy Net	1262.4			Wh
Hydrogen Consumption	79.6	77.2	74.4	g
	74.8*			
Average FC System Efficiency	Not Available	63.00	63.10	%
FC Energy	1624.7	1682.2	1625.1	Wh
Compressor Energy	24.0	93.9	92.1	Wh
	91.2*			
FC Power Change Accumulation	1134.0	872.8	768.7	kW
SOC Initial	59.5	59.5	59.5	%
SOC Final	64.18	65.57	61.42	%
BAT Energy Output	402.8	338.1	469.7	Wh
BAT Energy Input	-536.9	-459.8	-572.7	Wh
BAT Energy Total (absolute)	939.7	797.9	1042.4	Wh
BAT Energy Net	-134.1	-121.9	-102.9	Wh

5.1.2 UDDS

Although UDDS contains several start-stop phases and is typically used for city driving test scenarios, its phases with occasional and rapid accelerations cause more dramatically changing power requests from the sources compared to NEDC.

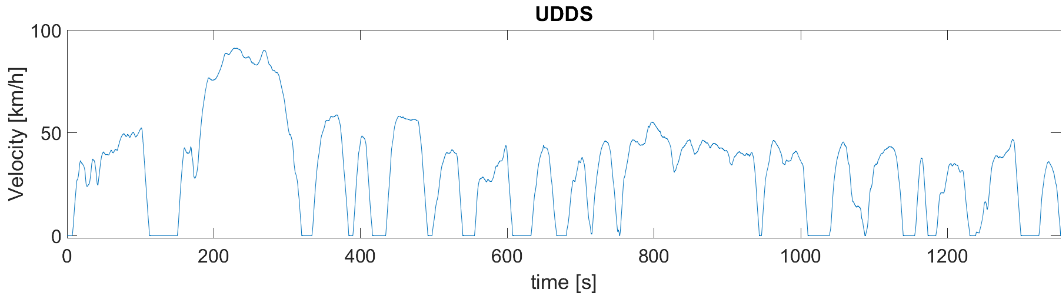

Figure 5.3 UDDS cycle

Under this scenario, the results in Figure 5.4 show that the SOC deviates under UDDS due to frequent accelerations and decelerations throughout the driving, for all EMSs compared to their behaviors in NEDC. Among the three methods, the MPC-based EMS allows the SOC to fluctuate at a lower level, while the RB-EMS tends to decrease at the beginning and stay there, and the Mirai EMS charges the battery on average the driving. Comparing the SOC final values, the RB-EMS achieves a closer value to the target than the others. The final value is lower than the target for the MPC-based EMS, while it exceeds the target value with the same magnitude as in the Mirai EMS result. According to the results in Figure 5.4, between the seconds 175th-270th, and 430th-455th, the MPC-based EMS and the Mirai EMS tend to utilize the battery in higher power demands compared to the RB-EMS result. This tendency allowed the MPC-based EMS and the Mirai EMS to operate the fuel cell in a more efficient region compared to the RB-EMS. On the other hand, the RB-EMS keeps the SOC more steady by sacrificing the fuel economy, because it uses the fuel cell to supply the peak power requests where the fuel cell would operate less efficiently. It is not observed for the MPC-based EMS that the fuel cell operated below 5kW which is an inefficient region. The number of on-off switchings of the fuel cell is higher than the dynamometer result for the MPC-based EMS, but the highest number of the switchings is achieved by the RB-EMS. The rate of change in the fuel cell power is the lowest for the MPC-based EMS, which asserts a prolonged life of the fuel cell due to the smooth operation. In this sense, the smoothness of the RB-EMS and the Mirai EMS results are closer to each other and higher than the MPC-based EMSs. Although the magnitudes of peak power outputs of the battery are higher for the RB-EMS among the methods, the total utilization of the battery is the lowest for this strategy. Also according to the results, the fuel cell is operated more efficiently by the MPC-based EMS than the RB-EMS. Lastly, similar to the NEDC results, a notable difference is observed in the compressor power outputs of our FCHEV and the Mirai.

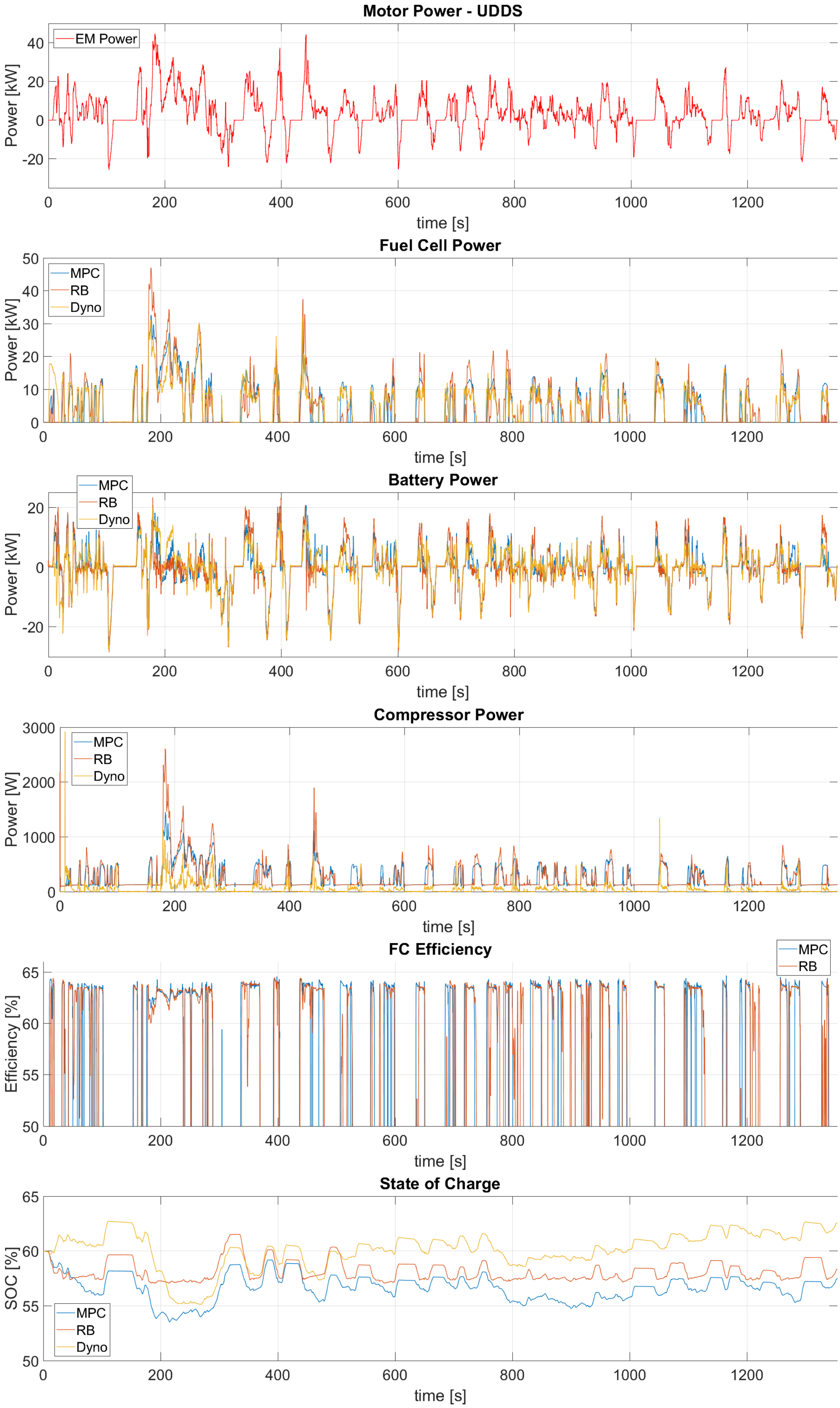

Figure 5.4 Comparision of the system outputs for the RB-EMS, MPC-based EMS, and dynamometer results under UDDS cycle

As seen in Table 5.2, the MPC-based EMS provides the best results in terms of fuel economy, with a hydrogen consumption and efficiency value of 72.9g and 63.29% respectively, followed by the RB-EMS with 74.2g and 62.41%. As mentioned earlier, the efficiency data is not available for the dynamometer test, however, the fuel consumption specified by the authority and the model result is higher than both the others. The values are 80.5g and 77.2g respectively. The RB-EMS completed the drive cycle with the closest value of the SOC to the target, with a final SOC value of 58.32 %, followed by the Mirai EMS and the MPC-based EMS with 62.55% and 57.46% respectively. Considering the feasibility of the fuel cell's operation, the best result in the power change accumulation is achieved by the MPC-based EMS with 1803kW compared to the RB-EMS and the Mirai EMS with 2170.1kW and 2199kW. Both the fuel cell and battery utilization of the Mirai EMS in terms of energy is decreased by both the MPC-based and the RB-EMS. However, the battery output result of the RB-EMS is more spiky than the others but still does not reach the limits. According to the model results, close values are produced in UDDS for compressor energy.

Table 5.2 Power source outputs for the dynamometer test, RB-EMS, and MPC-based EMS under UDDS cycle

Result	Dynamometer	RB	MPC	Unit
EM Energy Net	1228.6			Wh
Hydrogen Consumption	80.5	74.2	72.9	g
	77.2*			
Average FC System Efficiency	Not Available	62.41	63.29	%
FC Energy	1677.2	1623.4	1602.9	Wh
Compressor Energy	18.2	94.2	93.7	Wh
	94.7*			
FC Power Change Accumulation	2199.0	2170.1	1803.0	kW
SOC Initial	60	60	60	%
SOC Final	62.55	58.32	57.46	%
BAT Energy Output	693.2	723.3	723.1	Wh
BAT Energy Input	-819.5	-741.6	-783.6	Wh
BAT Energy Total (absolute)	1512.8	1464.9	1506.6	Wh
BAT Energy Net	-126.2	-18.3	-60.3	Wh

5.1.3 WLTP

WLTP is another selected drive cycle to evaluate the performance of the designed EMSs. It incorporates urban, rural, and highway patterns. The drive cycle begins with the low-speed segment that continues for 600 seconds, then followed by medium until 1000th s. After the 1000th s the high region starts, and the cycle ends with the extra-high segment which starts shortly before the 1500th s. The number of start-stop phases in WLTP is smaller than NEDC and UDDS, yet, it contains frequent accelerations and decelerations. As a result, change in the power demand reaches higher magnitudes in a short time at both positive and negative. For the high and extra-high sectors, a continuous power supply is requested from the sources until the end of the cycle.

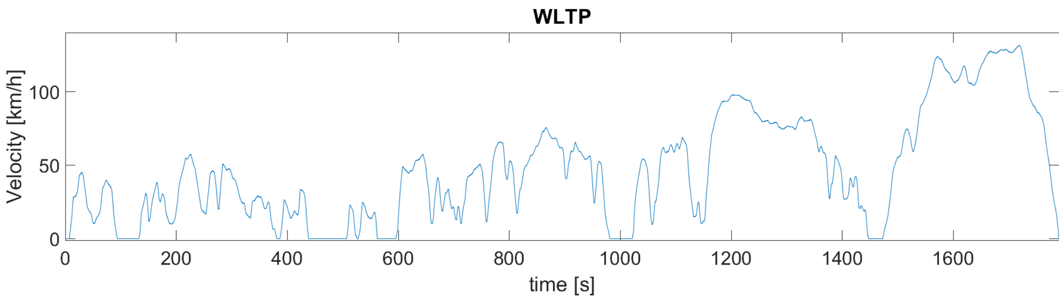

Figure 5.5 WLTP cycle

According to the results in Figure 5.6, among the three EMSs, the Mirai EMS tends to charge the battery in the low phase of the cycle, whereas the RB-EMS and MPC-based EMS allow the SOC to decrease. Although the MPC-based EMS still allows the SOC to decrease in high and extra-high phases, the RB-EMS and Mirai EMS keep the SOC for the same interval. For these phases, they behave similarly in terms of SOC control. By allowance to decrease the SOC in this interval, the MPC-based EMS can operate the fuel cell relatively at higher efficiency levels, while the SOC still changes in an acceptable range. To recover the lost energy during this interval, the MPC-based EMS operated at higher power values around the 1600s, which is reasonable since the battery can be charged by efficient utilization of the fuel cell. The closeness of the SOC final values to the target is more satisfactory for the MPC-based EMS, which is followed by the RB-EMS. The Mirai EMS outcomes a slightly higher final SOC value than the others due to the hard regenerative braking at the end. Generally, the pattern of fuel cell power is close for each result, however, the fuel cell is operated more efficiently by the MPC-based EMS than the RB-EMS. This is because of the higher magnitudes of the fuel cell power produced by the RB-EMS. Although the total energy outcome of the battery is the highest one in the MPC-based EMS among the EMSs, the magnitudes of battery power output are smaller than the RB-EMS and dynamometer results. This is a result of the battery power penalty term in the cost function of the MPC-based EMS. Moreover, the fuel cell's output power deviations are minimized by the MPC-based EMS, which is beneficial for the sake of the fuel cell in terms of degradation. This is a result of the efficiency term since it forces the fuel cell to operate at the maximum efficiency point. A significant amount of deviation is observed in the compressor energy outputs between the FCHEV model and the Mirai. However, the model results of the three EMSs are close to each other.

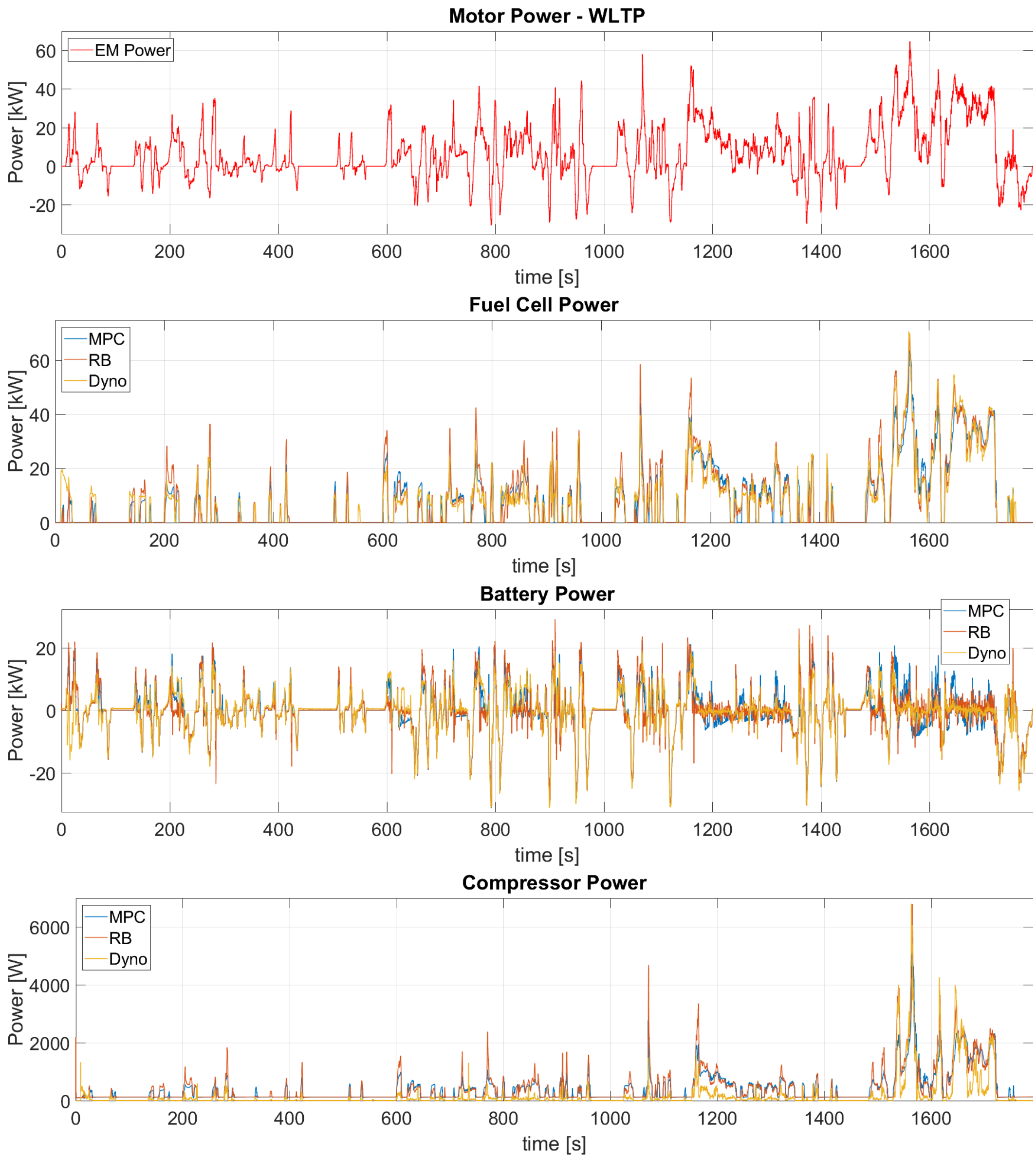

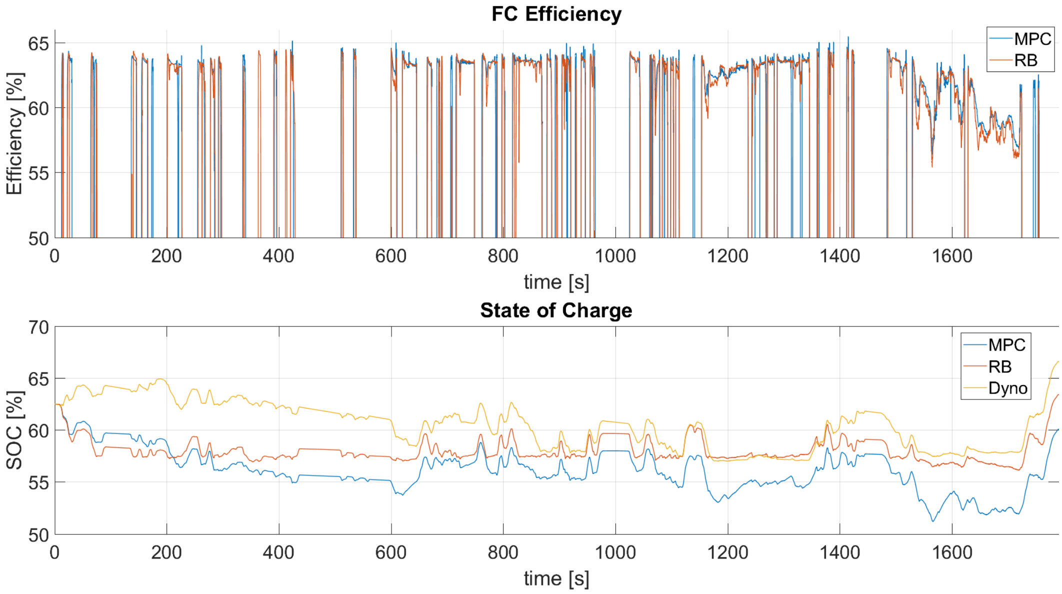

Figure 5.6 Comparision of the system outputs for the RB-EMS, MPC-based EMS, and dynamometer results under WLTP cycle

WLTP is attractive for comparing the performance of EMSs under different conditions as it incorporates three different driving patterns which are the urban, rural, and the highway. According to the numerical results in Table 5.3, the best fuel economy is achieved by the MPC-based EMS with 181.5g which is 2.00%, 7.59%, and 0.45% lower than the results of the RB-EMS, the dynamometer test, and the model results of the Mirai EMS respectively. Moreover, the MPC-based EMS reaches the highest average efficiency value which is 62.52%, 0.5% higher than the RB-EMS's average. The utilization of the fuel cell in terms of energy is very close for the MPC-based EMS and the Mirai EMS. The RB-EMS utilized the fuel cell to convert a slightly higher amount of energy. Similar to NEDC and UDDS, the fuel cell produces a smoother output power for the MPC-based EMS. In this sense, the total amount of deviations at the fuel cell power in the specified unit is close for the RB-EMS and the Mirai EMS. The fuel cell's power change accumulation is respectively 615.1kW and 665.5kW lower than the RB-EMS and the dynamometer results. As discussed earlier, although the MPC-based EMS utilizes the battery more than the RB-EMS and the Mirai EMS in ascending order, the magnitudes of power output samples are less than the other methods. A better final value of the SOC is obtained by the MPC-based EMS with 60.09%, where it is 63.42% and 66.60% for the RB-EMS and the Mirai EMS respectively. According to the compressor energy results, the same order with fuel cell utilization is achieved for compressor utilization, which can be expected since the compressor power depends on the fuel cell power.

Table 5.3 Power source outputs for the dynamometer test, RB-EMS, and MPC-based EMS under WLTP cycle

Result	Dynamometer	RB	MPC	Unit
EM Energy Net	3167.9			Wh
Hydrogen Consumption	196.4	185.2	181.5	g
	182.3*			
Average FC System Efficiency	Not Available	62.02	62.52	%
FC Energy	3888.9	3953.6	3898.9	Wh
Compressor Energy	24	213.3	202.8	Wh
	207.4*			
FC Power Change Accumulation	3555.0	3504.6	2889.5	kW
SOC Initial	62.5	62.5	62.5	%
SOC Final	66.60	63.42	60.09	%
BAT Energy Output	954.7	1042.3	1108.3	Wh
BAT Energy Input	-1143.7	-1175.3	-1232.8	Wh
BAT Energy Total (absolute)	2098.4	2217.6	2341.1	Wh
BAT Energy Net	-189.0	-80.6	-124.3	Wh

5.1.4 US06

US06 is considered to have the most aggressive driving characteristics compared to other drive cycles used in this study. It is an appropriate choice for testing the FCHEV to evaluate how the EMSs behave in the face of instantaneous peak power demand with high magnitudes. Throughout the cycle, the maximum magnitudes of power demand are well above those of other cycles, challenging EMSs to operate in regions not tested in other cycles. In this cycle, the power demand drastically increases to very high levels even above 110kW in a short time, and the success of the power allocation is tested by pushing the sources to their limits. For this reason, the agility of the fuel cell in such power requests will directly affect the magnitudes of the battery power.

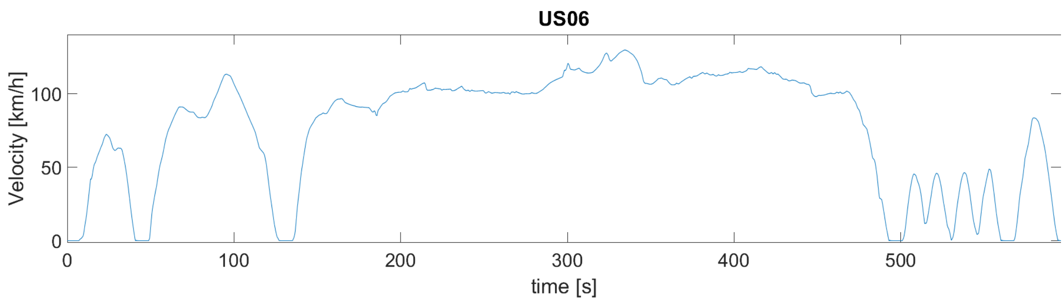

Figure 5.7 US06 cycle

As seen in the results presented in Figure 5.8, the drive cycle starts directly by demanding power values reaching approximately 80kW. The RB-EMS and the Mirai EMS respond to such an amount of demand by increasing the fuel cell power to 75kW, however the value is 65kW for the MPC-based EMS. This behavior is common for the whole drive cycle, so under high amounts of requests, the battery's share is higher in the MPC-based EMS result than the values obtained by the other EMSs. This is an outcome of the efficiency maximization, however comes with a price of drops in the SOC. After the SOC is allowed to decrease to pull the fuel cell power to lower values for efficiency purpose, the MPC-based EMS seeks the opportunity to charge the battery in regions where the power demand is relatively small. Thanks to this tendency, the fuel cell is utilized more efficiently but battery utilization is raised. At this point, the peak values of the battery power must be evaluated in the results. On the contrary to the total utilization, the battery power could be kept away from its limit by the MPC-based EMS, which is a decision due to the battery power limitation effect thanks to the dynamic adjustment of the SOC weight. The increase in the SOC cost forces the fuel cell power to incline so that the SOC level is prevented from decreasing by lowering the battery's power share. Still, due to the calibration of the maps used for SOC cost calculation, the fuel cell does not tend to charge the battery at such inefficient regions, since both the SOC and efficiency terms cooperate in a balanced way. According to the fuel cell power results, the RB-EMS tends to produce the fuel cell power between the values obtained by the MPC-based EMS and the Mirai EMS, and the highest magnitudes of peak values of the fuel cell are observed in the Mirai EMS. The most spiky result of the battery power is produced by the RB-EMS, however the values are still within the limits. The RB-EMS considers the actual SOC and the battery voltage values to determine the battery limits, but not the battery power as explained in the third chapter. For this reason, although the potential undervoltage or undercharging problems are prevented, the output power still reaches to the limits more frequently than the MPC-based EMS and dynamometer results. This behavior is observed at 50th, 140th, and 500-500th s as in the battery power results. All three methods outcome a similar SOC pattern, but with different magnitudes. Similar to the previous cycles, the MPC-based EMS tended to keep the SOC below than others. The RB-EMS kept the SOC at a higher range than the Mirai EMS, unlike the NEDC and UDDS results.

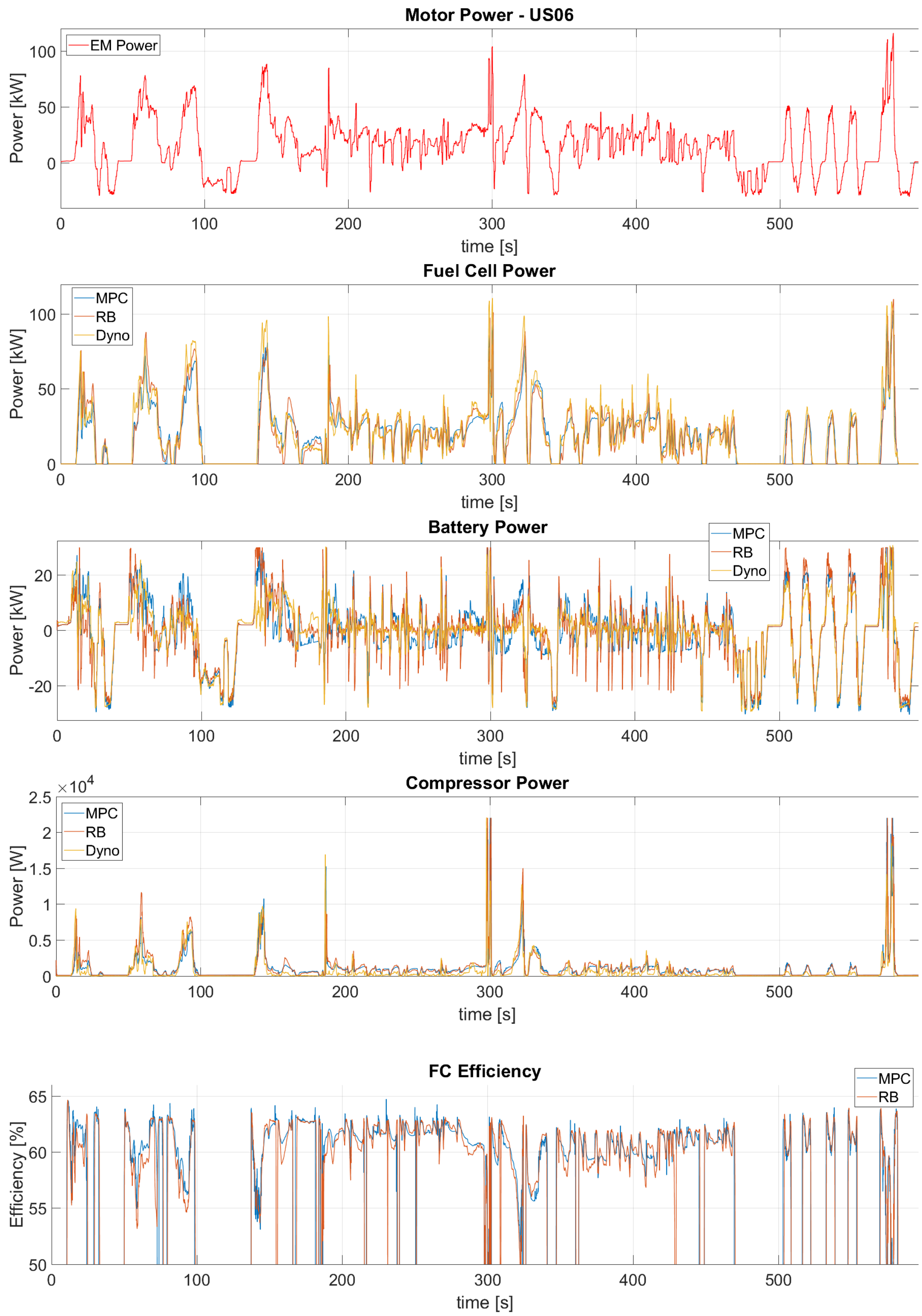

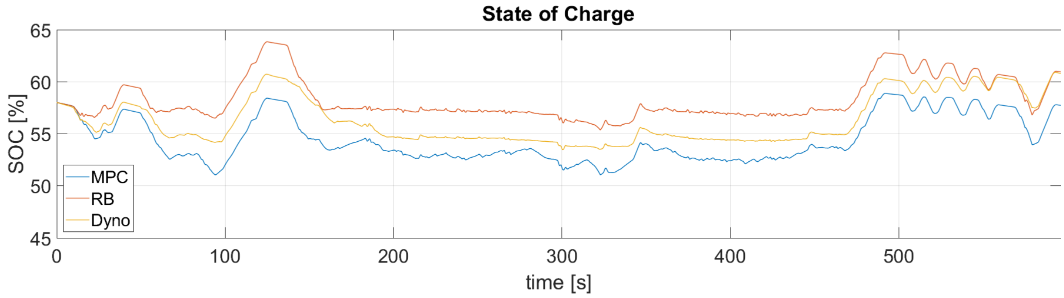

Figure 5.8 Comparision of the system outputs for the RB-EMS, MPC-based EMS, and dynamometer results under US06 cycle

US06 results given in Table 5.4 show that the MPC-based EMS has provided better results in terms of hydrogen consumption, average fuel cell efficiency, and accumulation of the fuel cell power change with the values of 145.0g, 60.74%, and 3857.2kW respectively. On the other hand, the total battery energy is smaller for the Mirai EMS with 1129.7Wh, followed by the RB-EMS with 1336.1Wh, then by the MPC-based EMS with 1458.0Wh. As discussed earlier, the battery power output is kept away from the limit by both the MPC-based EMS and the Mirai EMS, which is important for the sake of the battery's health. The highest magnitude of SOC error at the end of the cycle is produced by the MPC-based EMS with 2.27%, which are 0.95% and 0.79% for the RB-EMS and the Mirai EMS respectively. The lowest value of the fuel cell energy is obtained by the MPC-based EMS, followed by the RB-EMS. Parallelly, the model result of the Mirai EMS for the compressor power is the highest according to the numerical results in Table 5.4.

Table 5.4 Power source outputs for the dynamometer test, RB-EMS, and MPC-based EMS under US06 cycle

Result	Dynamometer	RB	MPC	Unit
EM Energy Net	2851.9			Wh
Hydrogen Consumption	161.2	148.8	145.0	g
	157.3*			
Average FC System Efficiency	Not Available	60.36	60.74	%
FC Energy	3247.2	3114.4	3049.2	Wh
Compressor Energy	115.1	190.8	173.8	Wh
	216.6*			
FC Power Change Accumulation	5578.0	4462.1	3857.2	kW
SOC Initial	58	58	58	%
SOC Final	60.79	60.95	57.73	%
BAT Energy Output	498.0	616.8	673.3	Wh
BAT Energy Input	-631.7	-719.4	-784.7	Wh
BAT Energy Total (absolute)	1129.7	1336.1	1458.0	Wh
BAT Energy Net	-133.7	-102.6	-111.6	Wh

5.1.5 HWFET

HWFET is a pure highway scenario requesting continuous power from the sources. Also, since it does not contain any hard regenerative braking scenario except the end of the cycle, it is suitable for evaluating the steady-state response of the SOC and the fuel cell system efficiency. Although the acceleration and deceleration requests would cause large amounts of power in high-speed traveling, the rate of change in speed is limited in HWFET, so the power demand varies from -30kW to 40kW.

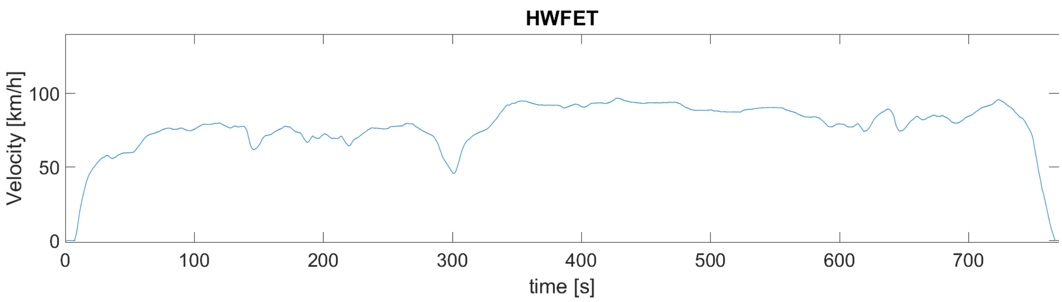

Figure 5.9 HWFET cycle

The cycle directly starts with an acceleration until the velocity reaches around 80km/h, then the vehicle travels at a cruising speed of 90km/h approximately. According to Figure 5.10, the transient response of the Mirai EMS is faster compared to the others, resulting in a slower decrease in the SOC at the first acceleration. After the fuel cell starts operation, the RB-EMS sharply increases the fuel cell power and starts charging the battery. This causes the fuel cell to operate farther from the maximum efficiency point. At the same instant, the MPC-based EMS tends to stay close the the maximum efficiency point and allows the SOC to decrease. However, the first acceleration does not cause an important difference between the magnitudes of the battery outputs among the EMSs. Likely to the previous results, later the fuel cell is utilized at relatively lower power levels where the efficiency is not low, to compensate for the energy loss in the battery. The dynamometer test and the MPC-based EMS simulation results are similar in the course of the SOC level, however, the RB-EMS kept it above the SOC curves obtained by the others. The tendency to charge the battery during the peak power supply causes to fuel cell to work at less efficient regions as shown in Figure 5.10. The largest magnitudes in the battery power output are observed in the RB-EMS results, however it still courses at values far from the limits. None of the designed EMSs performed any undesired behavior while controlling the SOC at continuous power demands, so the SOC curves are steady in all results. In addition to this, the MPC-based EMS achieved a higher efficiency value throughout the driving.

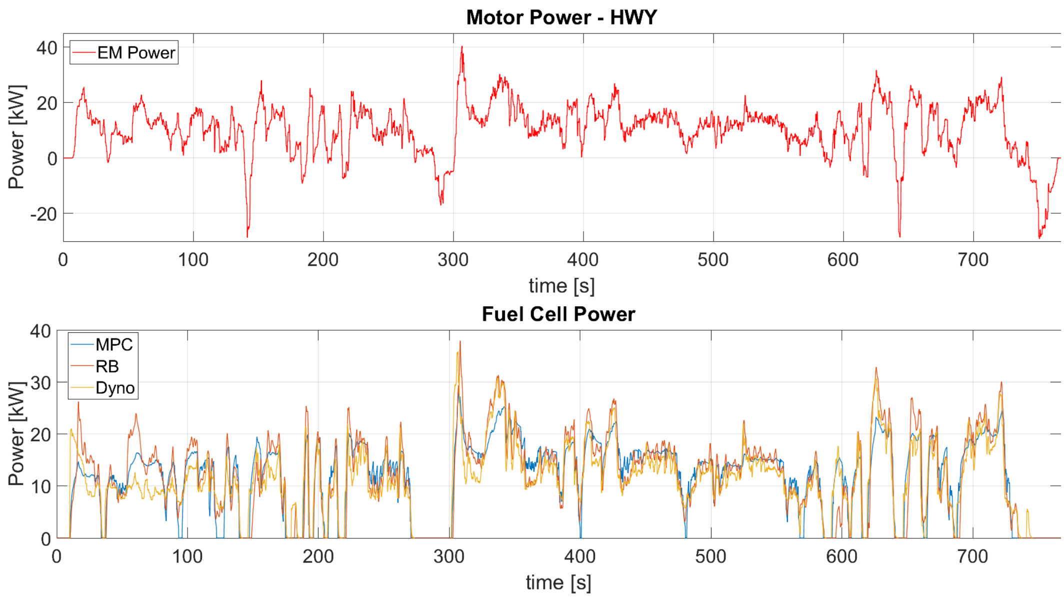

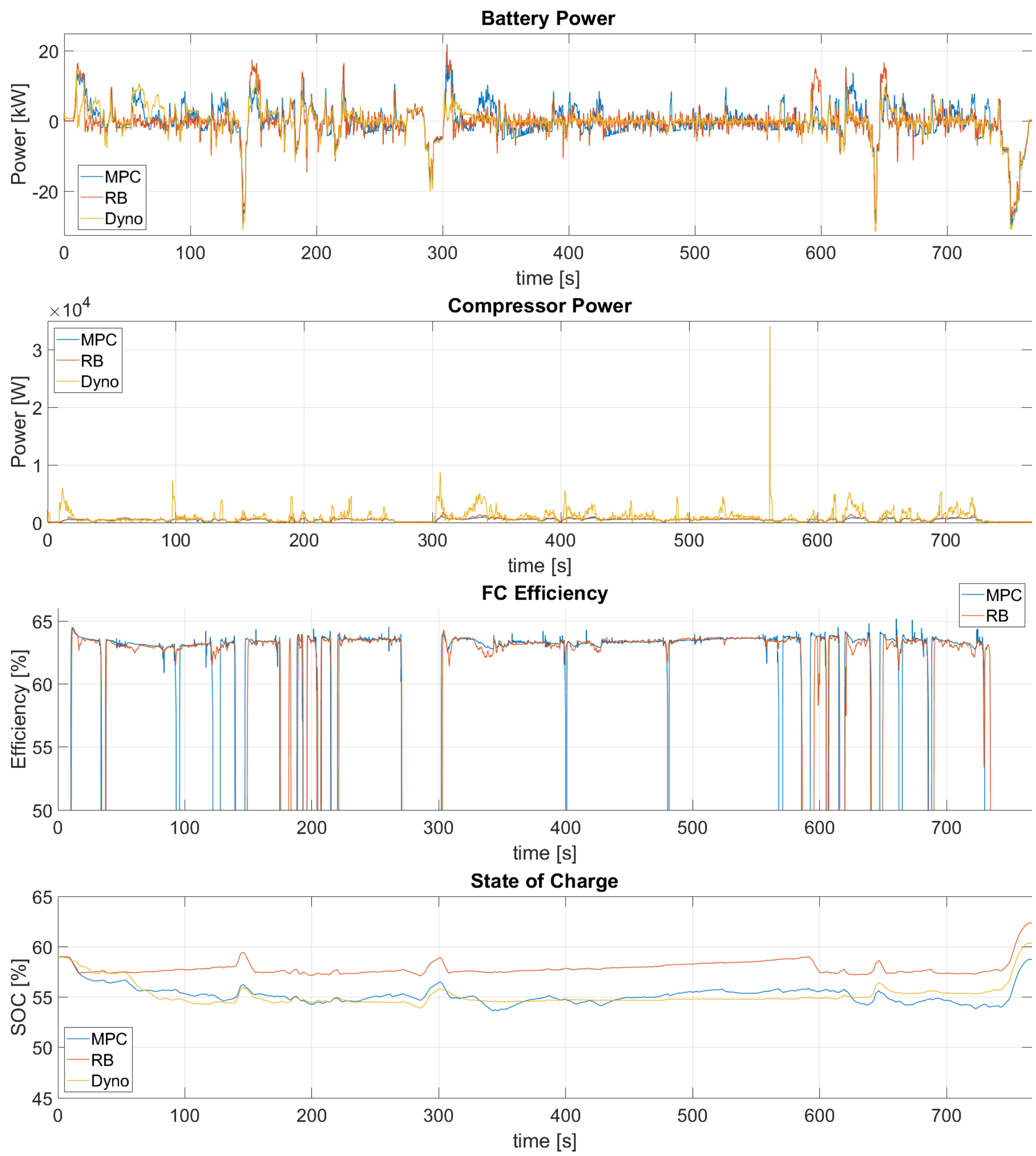

Figure 5.10 Comparision of the system outputs for the RB-EMS, MPC-based EMS, and dynamometer results under HWFET cycle

According to the results given in Table 5.5, although an efficient operation is performed by the MPC-based EMS, the fuel consumption is still higher than the model result of the Mirai EMS. While the fuel consumption result of the MPC-based EMS is very close to the experimental result with a difference of 0.1g hydrogen, the consumption is also decreased by 5.79% compared to the RB-EMS result, and it is 3.42% higher than the model result of the Mirai EMS. Other than the fuel consumption, likely to the other cycles, a smoother output power of the fuel cell is achieved by the MPC-based EMS with 1393.5kW which is 446.6kW and 382.5kW lower than the RB-EMS and the dynamometer results respectively. For the same EMS, the highest utilization of the battery is produced. This is because the MPC-based EMS tends to allow the SOC to decrease to not move far away from the efficiency target, and charges the battery at efficient regions to recover the SOC. Nevertheless, the battery output power did not exceed 18kW, which is still lower than the maximum magnitude created by the RB-EMS. Therefore, a balanced utilization of the battery is obtained by the MPC-based EMS even if the total energy consumption of the battery result is the highest for it. All methods show the flattest SOC results in HWFET. Lastly, as observed in the previous cycles, the compressor power model produces results significantly different from the experimental result. Yet, the model result of the Mirai EMS and the others are very close to each other, with a maximum difference of 6.9Wh between the Mirai EMS and the RB-EMS.

Table 5.5 Power source outputs for the dynamometer test, RB-EMS, and MPC-based EMS under HWFET cycle

<table>
<tr><th>Result</th><th>Dynamometer</th><th>RB</th><th>MPC</th><th>Unit</th></tr>
<tr><td>EM Energy Net</td><td colspan="3">1947.5</td><td>Wh</td></tr>
<tr><td rowspan="2">Hydrogen Consumption</td><td>109.1</td><td rowspan="2">115.7</td><td rowspan="2">109.0</td><td rowspan="2">g</td></tr>
<tr><td>105.4*</td></tr>
<tr><td>Average FC System Efficiency</td><td>Not Available</td><td>63.12</td><td>63.32</td><td>%</td></tr>
<tr><td>FC Energy</td><td>2311.1</td><td>2536.1</td><td>2395.4</td><td>Wh</td></tr>
<tr><td rowspan="2">Compressor Energy</td><td>202.9</td><td rowspan="2">103.0</td><td rowspan="2">100.0</td><td rowspan="2">Wh</td></tr>
<tr><td>96.1*</td></tr>
<tr><td>FC Power Change Accumulation</td><td>1776.0</td><td>1840.1</td><td>1393.5</td><td>kW</td></tr>
<tr><td>SOC Initial</td><td>59</td><td>59</td><td>59</td><td>%</td></tr>
<tr><td>SOC Final</td><td>60.36</td><td>62.35</td><td>58.74</td><td>%</td></tr>
<tr><td>BAT Energy Output</td><td>233.0</td><td>265.0</td><td>354.2</td><td>Wh</td></tr>
<tr><td>BAT Energy Input</td><td>-286.7</td><td>-354.7</td><td>-401.1</td><td>Wh</td></tr>
<tr><td>BAT Energy Total (absolute)</td><td>519.7</td><td>619.7</td><td>755.5</td><td>Wh</td></tr>
<tr><td>BAT Energy Net</td><td>-53.6</td><td>-72.4</td><td>-47.0</td><td>Wh</td></tr>
</table>

6. Conclusion

The study conducted within the thesis is concluded in this chapter first, then it is followed by presenting the recommendations for future works based on the findings throughout the study.

6.1 Concluding Remarks

This thesis has three main focuses which are modeling the electrical powertrain system of a fuel cell hybrid vehicle, design and implementation of a rule-based energy management strategy and a model predictive controller-based energy management strategy, and comparison of the RB-EMS and MPC-based EMS results under five different cycles by considering the dynamometer test results of a commercial FCHEV: Toyota Mirai.

An electrical powertrain model of a fuel cell hybrid electric vehicle is created for the purpose of representing the power outputs of the first-generation Toyota Mirai. To achieve this, the parameters of the powertrain components in Cruise-M are tuned based on the specifications of the reference vehicle. To reduce the modeling error due to unknown factors in the components, such as mechanical losses from the electric motor to wheels and electric motor efficiency, only the electrical layer of the powertrain is focused rather than the full powertrain or the vehicle model. By this means, the deviations between the experimental data and the model outputs are aimed to be minimized, thus, a more fair comparison between our FCHEV model and the Toyota Mirai is performed. In this way, a testbed that is able to show potential differences and similarities between the tendencies of the developed EMSs and the experimental results is presented. The outputs of the components, which are the fuel cell, compressor, and battery, are determined by demanding directly the electric motor power output of the Mirai, which is directly taken from the experimental data shared by the testing authority. In the simulation, the EMS sends the fuel cell current demand through the motor side of the fuel cell's DC/DC converter. Based on the operating voltage of the DC bus which is 650V and the current target of the fuel cell, the power at the DC/DC converter's motor side is determined. Using this power demand at the motor side, the output current of the fuel cell is calculated based on its operating voltage so that the power demand at the motor side of the converter is met considering the efficiency. Synchronously, the rest of the power becomes the battery's target and the battery always meets the rest of the power demand through the same process through its DC/DC converter.

Obtaining the electrical powertrain of the FCHEV is followed by the design of the RB-EMS. The strategy is firstly tested on the FCHEV model developed in Cruise-M to evaluate the representability of the model, and reliability of the RB-EMS in terms of feasibility and realizability of the control decisions. To achieve this, the simulation results are compared with the dynamometer test results of the Toyota Mirai. According to the results, it is observed that the model can represent the Toyota Mirai's behavior in terms of the power source outputs and the physical limits. However, the compressor model in Cruise-M yields significant deviations compared to the experimental results. In general, it is understood that the FCHEV model has the potential to achieve even closer results to the Mirai when the unknown parameters of the vehicle are specified in the model. Although the RB-EMS showed a similarity with the experimental results in terms of the power output trends, since the method does not involve any optimization, the best results could not be achieved by this strategy.

Another purpose of the study is to implement a model predictive controller-based energy management strategy with an improved optimization performance through a map-based adjustment of the cost function weights driven according to the system outputs. For this purpose, firstly an MPC controller is implemented by deriving the non-linear system model of the powertrain and obtaining the system constraints. Subsequently, the cost function is structured including the SOC and the system efficiency costs in a quadratic form. In addition to this generic cost function framework which is widely studied, we integrated into the cost function an on-off strategy for the fuel cell that the fuel cell power is penalized when the fuel cell operation is not feasible or unnecessary according to system outputs and operating conditions. Although the efficiency cost has a fixed weight, the SOC term and the threshold values where the fuel cell is enabled/disabled are determined via a feedback loop. The weight of the SOC term is calculated using the SOC and battery power, while the on-off switching points of the fuel cell are obtained depending on the SOC and the power demand. Then three different calibrations are performed based on NEDC, US06, and a combined drive cycle created from various cycles to obtain three different characteristics of the MPC which are smooth, aggressive, and balanced. The balanced configuration of the MPC is selected for the final assessment.

It is observed that in all of the cycles which are NEDC, UDDS, WLTP, US06, and HWFET, the MPC-based EMS produces the overall best results among the EMSs in terms of fuel economy. It is able to reduce the hydrogen consumption in all the cycles. Moreover, the MPC-based EMS can operate the fuel cell at a higher efficiency level compared to RB-EMS. Since the average efficiency results of the dynamometer test are not available, a comparison between the designed EMSs and the Mirai EMS could not be performed. However, the battery utilization of the MPC-based EMS is higher than the other strategies, except for the UDDS results. The higher battery usage can be attributed to the working principle of the MPC-based EMS. Due to the on-off strategy, it does not start to operate the fuel cell until the power demand exceeds a threshold determined depending on the SOC. On the other hand, once it starts operation, it continues to operate at a high-efficiency region until the power demand decreases below a threshold determined depending on the SOC. In this way, the improved fuel economy returns higher battery utilization. Apart from the SOC dependency for the dynamical adjustment of the SOC term weight, the battery output power is another factor impacting on this weight calculation, and consequently the battery is prevented from operating close to its power limits. As the battery power approaches the maximum limit, the EMS becomes more sensitive to SOC decrease and forces the fuel cell to become more agile and lower the battery's power share to slow down the SOC decrease. The results have shown that all of the strategies are able to keep the SOC in a certain range. Furthermore, the MPC-based EMS results show that the strategy allows the SOC to cruise below compared to the other strategies, however the final value of the SOC is still sufficiently close to the target value. According to the results, the final SOC value is the closest in NEDC and WLTP, while it is the farthest in UDDS and US06. This is because the UDDS and US06 challenge the EMS by requesting power that has relatively more aggressive oscillations due to deviations in the velocity especially at the end of these cycles. Since there are significant differences between the compressor model results and Mira's compressor outputs, a fair evaluation could not be performed. In all cycles except HWFET, a considerably lower amount of energy is consumed on the compressor of the Mirai. Still, closer values are obtained by all EMSs when the experimental data of the fuel cell power is applied to fuel cell system model to produce compressor power outputs through the simulation. Thus, the difference in results does not come from the power allocation decisions of the EMSs, but from model differences. In result, the EMS performance could be improved by introducing the feedback mechanism for determining the cost function parameters.

6.2 Recommendations and Future Work

In future studies, the following improvements are aimed to be performed regarding the FCHEV model and the MPC-based and RB- EMSs.

- The electrical powertrain model is recommended to be upgraded to a full-vehicle model to serve a platform where several scenarios can be realized independently of the electric motor data which is pre-existing. In this way, the model would accept the demand in terms of velocity reference, thus the scope of the study can be enlarged.
- The electric motor model with a realistic efficiency map is recommended to be introduced to the electrical powertrain model in order to increase its accuracy in obtaining the electrical power demand from the mechanical power data.
- By evaluating the changes in degradation indicators such as SEI layer thickness, plated metallic Li layer thickness, inner cell resistance, film layer thickness for the battery, and electrochemical surface area for the fuel cell, which are available for the electrochemical battery and fuel cell model of the Cruise-M, the health protectability of the EMSs are recommended to be assessed extensively.
- The RB-EMS has the potential to perform more successfully with the improvements in two main points. Firstly, the calibration for the battery limit calculation should be obtained more accurately to utilize the battery sufficiently far from its limits. To achieve this, a global optimization method such as the genetic algorithm can be used for adjusting the calibration values defined in the maps. Secondly, in the boost mode, the fuel cell power should be determined by considering the fuel cell system efficiency to improve the fuel economy.
- Using a global optimization method to calibrate the maps for the weight selection is recommended to tune the parameters of the MPC-based EMS to the best values. In this way, the performance of the EMS will be potentially improved. Moreover, even though the weights of the cost function are dynamically determined based on the powertrain states and the optimization performance is improved as a consequence, further flexibility and adaptivity is necessary to overcome the overfitting problem and react to environmental changes. For this purpose, a driving pattern recognition algorithm should be integrated into the EMS to identify the driving conditions and adapt the controller parameters based on the actual driving characteristics.

Bibliography

[1] Toyota Mirai Technical Specifications vs. FCHV, 2014. [Online]. Available: https://mag.toyota.co.uk/toyota-mirai-technical-specifications-vs-fchv-adv/.

[2] Emissions Database for Global Atmospheric Research. GHG Emissions of All World Countries, 2023. [Online]. Available: https://edgar.jrc.ec.europa.eu/report_2023.

[3] Y. Zhou. *Predictive energy management for fuel cell hybrid electric vehicle*. Doctoral thesis, Université Bourgogne Franche-Comté, November 2020.

[4] Zhao C., Wang Lei, Zhou Y., Pan B., Wang R., Wang Limei, and Yan X. "Energy management strategies for fuel cell hybrid electric vehicles: Classification, comparison, and outlook". *Energy Conversion and Management*, 270:116179, 2022.

[5] A. Bouramdane. "Assessing the environmental impact of hydrogen fuel cell technologies (PEMFCs, SOFCs, AFCs): a cradle-to-gate attributional life cycle analysis". *Green Economics*, pages 82–110, 2023.

[6] P. Roy and Kumar S. Srivastava. "Nanostructured anode materials for lithium ion batteries". *Journal of Materials Chemistry A*, 3:2454–2484, 2015.

[7] AVL List GmbH. *AVL Cruise M*. 2022. Version: R2. Graz. Available: https://www.avl.com/en/simulation-solutions.

[8] Argonne National Laboratory. D3 2016 Toyota Mirai. [Online]. Available: https://www.anl.gov/taps/d3-2016-toyota-mirai. Last visited: 27 May 2024.

[9] U.S. Energy Information Administration. Use of Energy Explained, 2023. [Online]. Available: https://www.eia.gov/energyexplained/use-of-energy/transportation.php.

[10] Matulka R. The History of the Electric Car, 2023. [Online]. Available: https://www.energy.gov/articles/history-electric-car.

[11] New South Wales Government. Charging an Electric Vehicle, 2019. [Online]. Available: https://www.transport.nsw.gov.au/projects/electric-vehicles/charging-an-electric-vehicle.

[12] D. De Wolf and Y. Smeers. "Comparison of Battery Electric Vehicles and Fuel Cell Vehicles". *World Electric Vehicle Journal*, 14(262):1–13, 2023.

[13] M. Waseem, M. Amir, G. Lakshmi, S. Harivardhagini, and M. Ahmad. "Fuel cell-based hybrid electric vehicles: An integrated review of current status, key challenges, recommended policies, and future prospects". *Green Energy and Intelligent Transportation*, 2(6):100–121, 2023.

[14] F. Leach, Kalghatgi G., Stone R., and Miles P. "The scope for improving the efficiency and environmental impact of internal combustion engines". *Transportation Engineering*, 1:100005, 2020.

[15] Xiaosong H., Zou C., X. Tang, T. Liu, and L. Hu. "Cost-Optimal Energy Management of Hybrid Electric Vehicles Using Fuel Cell/Battery Health-Aware Predictive Control". *IEEE Transactions on Power Electronics*, 35(1):382–392, 2020.

[16] Wang Y., Z. Sun, and Z. Chen. "Energy management strategy for battery/supercapacitor/fuel cell hybrid source vehicles based on finite state machine". *Applied Energy*, 254:113707, 2019.

[17] K. Song, F. Li, X. Hu, L. He, W. Niu, S. Lu, and T. Zhang. "Multi-mode energy management strategy for fuel cell electric vehicles based on driving pattern identification using learning vector quantization neural network algorithm". *Journal of Power Sources*, 389:230–239, 2018.

[18] M. Iqbal, J. Laurent, A. Benmouna, M. Becherif, H. S. Ramadan, and Claude F. "Ageing-aware load following control for composite-cost optimal energy management of fuel cell hybrid electric vehicle". *Energy*, 254:124233, 2022.

[19] M. Kumar, S. Sen, A. K. Prajapati, and S. Diwania. "A comprehensive power management approach for hydrogen fuel-cell-based hybrid EVs using PID controller". In *2023 IEEE IAS Global Conference on Renewable Energy and Hydrogen Technologies (GlobConHT)*, pages 1–6, 2023.

[20] R. Luca, M. Whiteley, T. Neville, P. R. Shearing, and D Brett. "Comparative study of energy management systems for a hybrid fuel cell electric vehicle - A novel mutative fuzzy logic controller to prolong fuel cell lifetime". *International Journal of Hydrogen Energy*, 47(57):24042–24058, 2022. Hydrogen Society.

[21] D. Li, B. Xu, J. Tian, and Z. Ma. "Energy management strategy for fuel cell and battery hybrid vehicle based on fuzzy logic". *Processes*, 8(8), 2020.

[22] Y. Zhou, A. Ravey, and M. Péra. "Real-time cost-minimization power-allocating strategy via model predictive control for fuel cell hybrid electric vehicles". *Energy Conversion and Management*, 229:113721, 2021.

[23] D. Fares, R. Chedid, Panik F., S. Karaki, and R. Jabr. "Dynamic programming technique for optimizing fuel cell hybrid vehicles". *International Journal of Hydrogen Energy*, 40(24):7777–7790, 2015. Hydrogen and Fuel Cell Systems for Clean Energy Applications.

[24] Y. Huangfu, P. Li, S. Pang, C. Tian, S. Quan, Y. Zhang, and J. Wei. "An improved energy management strategy for fuel cell hybrid vehicles based on

Pontryagin's Minimum Principle". *IEEE Transactions on Industry Applications*, 58(3):4086–4097, 2022.

[25] H. Yang, C. Zhang, X. Gong, Y. Hu, and H. Chen. "Energy management strategy of fuel cell hybrid electric vehicle based on dynamic programming". In *2020 Chinese Automation Congress (CAC)*, pages 3134–3139, 2020.

[26] P. Li, Y. Huangfu, C. Tian, S. Quan, Y. Zhang, and J. Wei. "An improved energy management strategy for fuel cell hybrid vehicles based on the Pontryagin's Minimum Principle". In *2021 IEEE Industry Applications Society Annual Meeting (IAS)*, pages 1–6, 2021.

[27] L. Xu, M. Ouyang, J. Li, F. Yang, L. Lu, and J. Hua. "Application of Pontryagin's Minimal Principle to the energy management strategy of plugin fuel cell electric vehicles". *International Journal of Hydrogen Energy*, 38(24):10104–10115, 2013.

[28] H. Jiang, L. Xu, J. Li, Z. Hu, and M. Ouyang. "Energy management and component sizing for a fuel cell/battery/supercapacitor hybrid powertrain based on two-dimensional optimization algorithms". *Energy*, 177:386–396, 2019.

[29] C. Hou, M. Ouyang, L. Xu, and H. Wang. "Approximate Pontryagin's minimum principle applied to the energy management of plug-in hybrid electric vehicles". *Applied Energy*, 115:174–189, 2014.

[30] S. Ahmadi and S. M. Bathaee. "Multi-objective genetic optimization of the fuel cell hybrid vehicle supervisory system: fuzzy logic and operating mode control strategies". *International Journal of Hydrogen Energy*, 40:12512–12521, 07 2015.

[31] J. Ribau, J. Sousa, and C. Silva. "Reducing the carbon footprint of urban bus fleets using multi-objective optimization". *Energy*, 93, Part 1:1089 – 1104, 12 2015.

[32] A. Del Pizzo, S. Meo, G. Brando, A. Dannier, and F. Ciancetta. "An energy management strategy for fuel-cell hybrid electric vehicles via particle swarm optimization approach". *International Review on Modelling and Simulations*, 7(4):543–553, 2014.

[33] Z. Chen, R. Xiong, K. Wang, and B. Jiao. "Optimal Energy Management Strategy of a Plug-in Hybrid Electric Vehicle Based on a Particle Swarm Optimization Algorithm". *Energies*, 8(5):3661–3678, 2015.

[34] A.P. Pourhashemi and S. M. Mehdi Ansarey M. "Ant colony optimization applied to optimal energy management of fuel cell hybrid electric vehicle". In *2012 IV International Congress on Ultra Modern Telecommunications and Control Systems*, pages 497–503, 2012.

[35] R. Koubaa and L. Krichen. "Ant colony optimization based optimal energy management for an FC/UC electric vehicle". In *2016 17th International Conference on Sciences and Techniques of Automatic Control and Computer Engineering (STA)*, pages 363–367, 2016.

[36] C. Zheng, S. Cha, Y. Park, W. Lim, and G. Xu. "PMP-based power management strategy of fuel cell hybrid vehicles considering multi-objective optimization". *International Journal of Precision Engineering and Manufacturing*, 14, 05 2013.

[37] M. Jain, C. Desai, and Sheldon S. Williamson. "Genetic algorithm based optimal powertrain component sizing and control strategy design for a fuel cell hybrid electric bus". In *2009 IEEE Vehicle Power and Propulsion Conference*, pages 980–985, 2009.

[38] O. Hegazy and J. Van Mierlo. "Particle Swarm Optimization for optimal powertrain component sizing and design of fuel cell hybrid electric vehicle". In *2010 12th International Conference on Optimization of Electrical and Electronic Equipment*, pages 601–609, 2010.

[39] A. Ravey, B. Blunier, and A. Miraoui. "Control strategies for fuel-cell-based hybrid electric vehicles: from offline to online and experimental results". *IEEE Transactions on Vehicular Technology*, 61(6):2452–2457, 2012.

[40] S. Quan, Y. Wang, X. Xiao, H. Hongwen, and F. Sun. "Real-time energy management for fuel cell electric vehicle using speed prediction-based model predictive control considering performance degradation". *Applied Energy*, 304:117845, 12 2021.

[41] L. Xu, J. Li, J. Hua, L. Li, and M. Ouyang. "Optimal vehicle control strategy of a fuel cell/battery hybrid city bus". *International Journal of Hydrogen Energy*, 34(17):7323–7333, 2009. IWBT 2008.

[42] W. Zhang, J. Li, L. Xu, and M. Ouyang. "Optimization for a fuel cell/battery/capacity tram with equivalent consumption minimization strategy". *Energy Conversion and Management*, 134:59–69, 2017.

[43] A. Ferrara, M. Okoli, S. Jakubek, and C. Hametner. "Energy management of heavy-duty fuel cell electric vehicles: model predictive control for fuel consumption and lifetime optimization". *IFAC-PapersOnLine*, 53(2):14205–14210, 2020. 21st IFAC World Congress.

[44] Derick F. Pereira, F. Lopes, and Edson H. Watanabe. "Nonlinear model predictive control for the energy management of fuel cell hybrid electric vehicles in real time". *IEEE Transactions on Industrial Electronics*, 68(4):3213–3223, 2021.

[45] Amin, Riyanto T. Bambang, Arief S. Rohman, Cees J. Dronkers, R. Ortega, and A. Sasongko. "Energy management of fuel cell/battery/supercapacitor hybrid power sources using model predictive control". *IEEE Transactions on Industrial Informatics*, 10(4):1992–2002, 2014.

[46] Y. Zhou, A. Ravey, and M. Marion-Péra. "Multi-mode predictive energy management for fuel cell hybrid electric vehicles using Markov Driving Pattern Recognizer". *Applied Energy*, 258:114057, 01 2020.

[47] A. Anbarasu, T. Q. Dinh, and Sengupta S. "Novel enhancement of energy management in fuel cell hybrid electric vehicle by an advanced dynamic model predictive control". *Energy Conversion and Management*, 267:115883, 2022.

[48] Zekeriya E. Eger. "Reinforcement learning based energy management strategy for fuel cell hybrid vehicles", December 2022. Available: https://https://research.sabanciuniv.edu/id/eprint/42949/1/10439555_Eger_Zekeriya_Ender.pdf.

[49] C. Liu and Yi L. Murphey. "Power management for plug-in hybrid electric vehicles using reinforcement learning with trip information". In *2014 IEEE Transportation Electrification Conference and Expo (ITEC)*, pages 1–6, 2014.

[50] Pedro M. Muñoz, G. Correa, Marcos E. Gaudiano, and D. Fernánde. "Energy management control design for fuel cell hybrid electric vehicles using neural networks". *International Journal of Hydrogen Energy*, 42(48):28932–28944, 2017.

[51] B. Liu, X. Wei, Sun C., B. Wang, and W. Huo. "A controllable neural network-based method for optimal energy management of fuel cell hybrid electric vehicles". *International Journal of Hydrogen Energy*, 55:1371–1382, 2024.

[52] C. Zheng, Zhang D., Xiao Y., and W. Li. "Reinforcement learning-based energy management strategies of fuel cell hybrid vehicles with multi-objective control". *Journal of Power Sources*, 543:231841, 2022.

[53] D. Yang, L. Wang, K. Yu, and J. Liang. "A reinforcement learning-based energy management strategy for fuel cell hybrid vehicle considering real-time velocity prediction". *Energy Conversion and Management*, 274:116453, 2022.

[54] X. Tang, H. Zhou, F. Wang, W. Wang, and X. Lin. "Longevity-conscious energy management strategy of fuel cell hybrid electric vehicle based on deep reinforcement learning". *Energy*, 238:121593, 2022.

[55] Y. Huang, H. Hu, T. Tan, C. Lu, and D. Xuan. "Deep reinforcement learning based energy management strategy for range extend fuel cell hybrid electric vehicle". *Energy Conversion and Management*, 277:116678, 2023.

[56] H. Lohse-Busch, K. Stutenberg, M. Duoba, and S. Iliev. Technology assessment of a fuel cell vehicle: 2017 Toyota Mirai.

[57] J. Fu, L. Zeng, J. Lei, Z. Deng, X. Fu, X. Li, and Y. Wang. "A real-time load prediction control for fuel cell hybrid vehicle". *Energies*, 15(10), 2022.

[58] S. Priyono, S. Hardiyani, N. Syarif, A. Subhan, and A. Suhandi. "Electrochemical performance of LiMn2O4 with varying thickness of cathode sheet". *Journal of Physics: Conference Series*, 1191(1):012022, mar 2019.

[59] Toyota Mirai Technical Specifications, February 2022. Available: https://media.toyota.co.uk/wp-content/uploads/sites/5/pdf/220203M-Mirai-Tech-Spec.pdf.

[60] NEXO: Hyundai's hydrogen fuel-cell first, 2021. Available: https://www.hyundai.com/au/en/news/vehicles/nexo-hyundai-hydrogen-fuel-cell-first.

[61] 2021 Clarity Fuel Cell Specifications Features, n.d. Available: https://hondanews.com/en-US/honda-automobiles/releases/release-4f88c507e72a4e7630685979cb04f2cb-2021-clarity-fuel-cell-specifications-features.

[62] M. Doyle, Thomas F. Fuller, and Newman J. "Modeling of Galvanostatic charge and discharge of the lithium/polymer/insertion cell". *Journal of The Electrochemical Society*, 140(6):1526, jun 1993.

[63] P. Zhang, F. Yan, and C. Du. "A comprehensive analysis of energy management strategies for hybrid electric vehicles based on bibliometrics". *Renewable and Sustainable Energy Reviews*, 48:88–104, 2015.

[64] S. Luciani and A. Tonoli. "Control strategy assessment for improving PEM fuel cell system efficiency in fuel cell hybrid vehicles". *Energies*, 15(6), 2022.

[65] Joel A E. Andersson, Gillis J., Horn G., J. B Rawlings, and M. Diehl. CasADi – A software framework for nonlinear optimization and optimal control. *Mathematical Programming Computation*, 11(1):1–36, 2019.

[66] A. Wachter and Lorenz T. Biegler. "On the implementation of an interior-point filter line-search algorithm for large-scale nonlinear programming". *Mathematical Programming*, 106:25–57, 2006.

APPENDIX

Comparison of the RB-EMS and Dynamometer Test Results Under NEDC

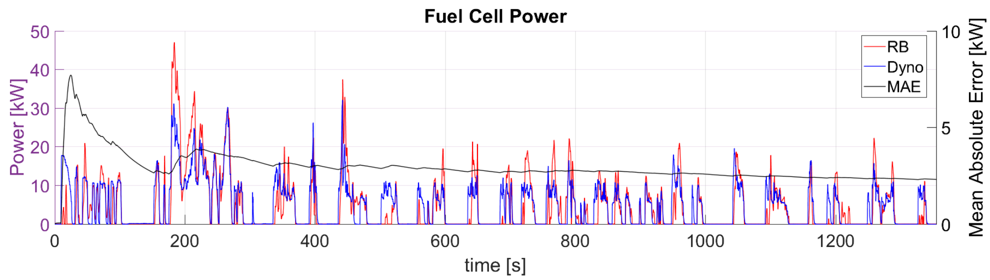

Figure A.1 Fuel cell power results of the RB-EMS and the dynamometer test under NEDC cycle

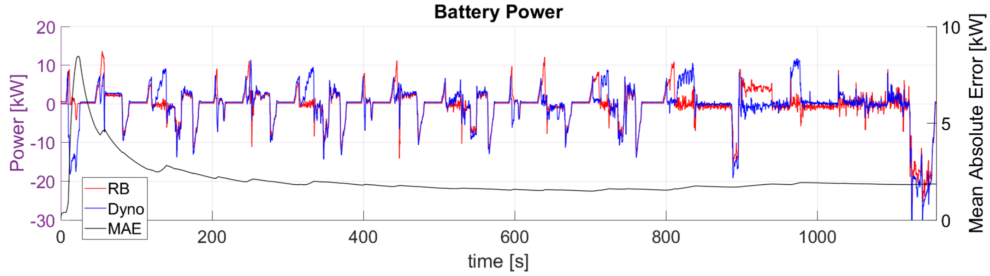

Figure A.2 Battery power results of the RB-EMS and the dynamometer test under NEDC cycle

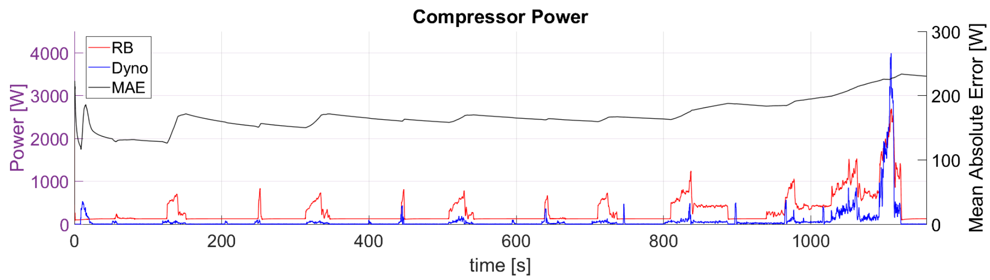

Figure A.3 Compressor power results of the RB-EMS and the dynamometer test under NEDC cycle

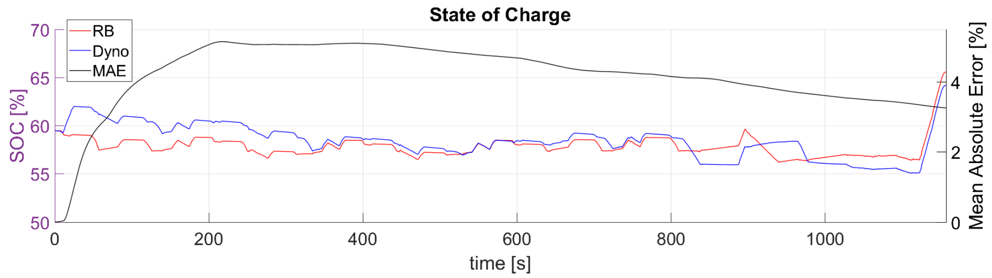

Figure A.4 SOC results of the RB-EMS and the dynamometer test under NEDC cycle

Comparison of the RB-EMS and Dynamometer Test Results Under UDDS

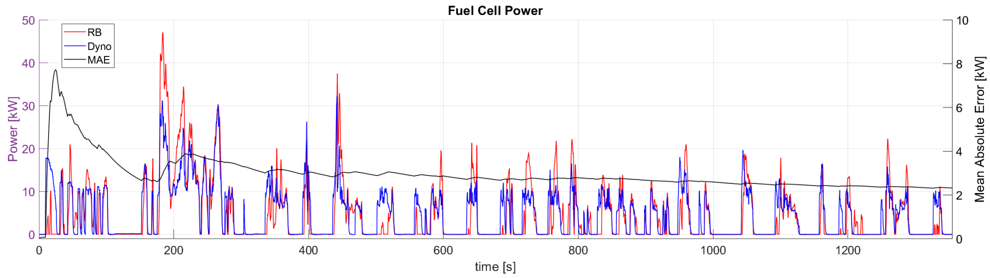

Figure A.5 Fuel cell power results of the RB-EMS and the dynamometer test under UDDS cycle

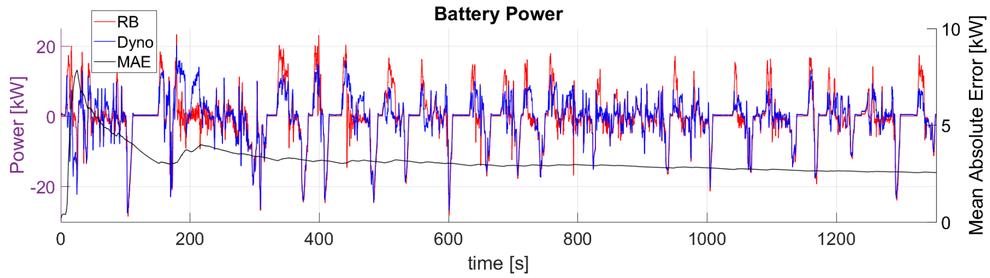

Figure A.6 Battery power results of the RB-EMS and the dynamometer test under UDDS cycle

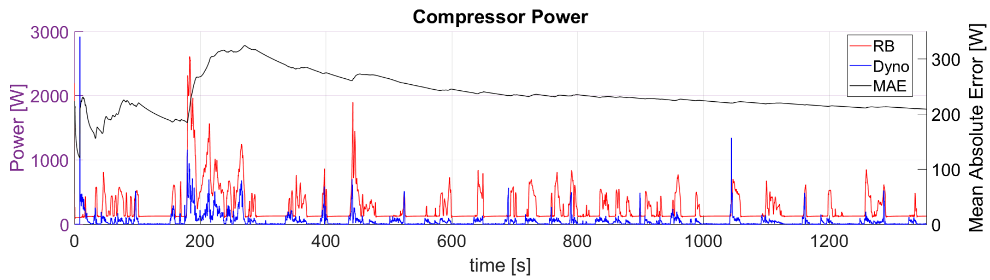

Figure A.7 Compressor power results of the RB-EMS and the dynamometer test under UDDS cycle

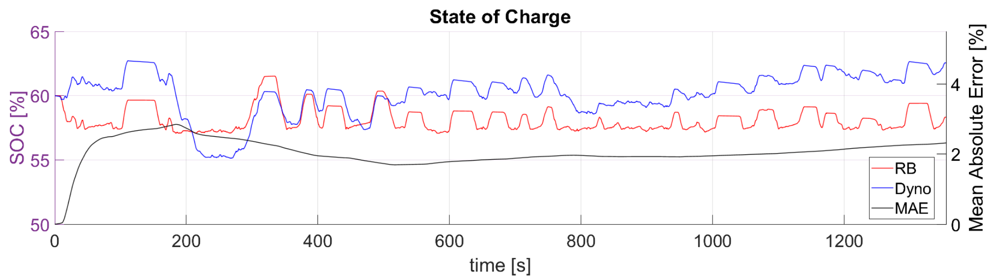

Figure A.8 SOC results of the RB-EMS and the dynamometer test under UDDS cycle

Comparison of the RB-EMS and Dynamometer Test Results Under US06

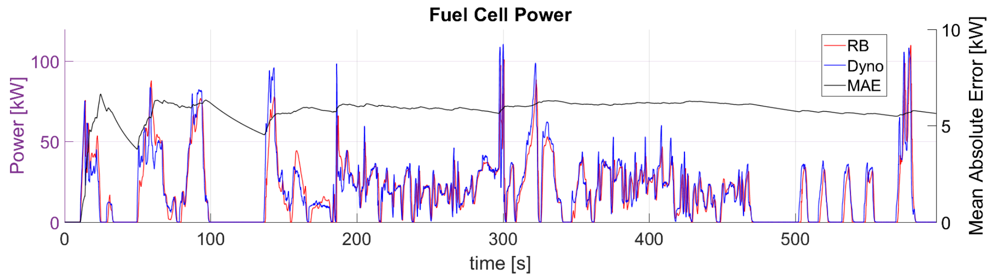

Figure A.9 Fuel cell power results of the RB-EMS and the dynamometer test under US06 cycle

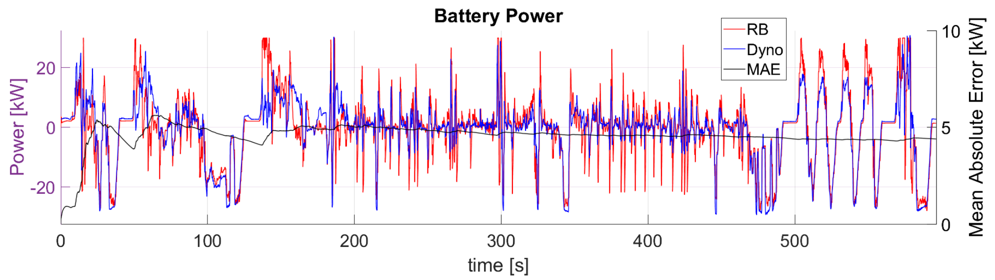

Figure A.10 Battery power results of the RB-EMS and the dynamometer test under US06 cycle

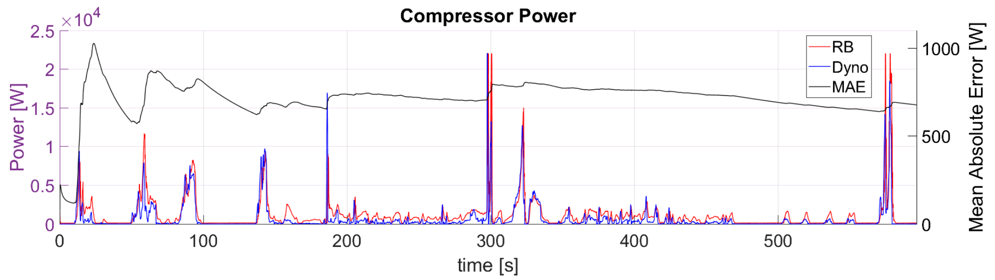

Figure A.11 Compressor power results of the RB-EMS and the dynamometer test under US06 cycle

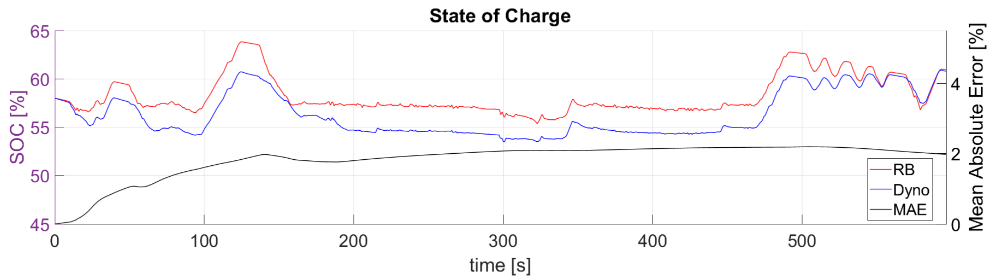

Figure A.12 SOC results of the RB-EMS and the dynamometer test under US06 cycle

Comparison of the RB-EMS and Dynamometer Test Results Under HWFET

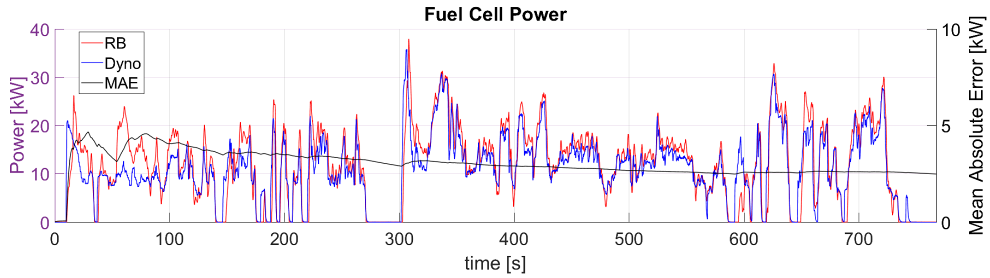

Figure A.13 Fuel cell power results of the RB-EMS and the dynamometer test under HWFET cycle

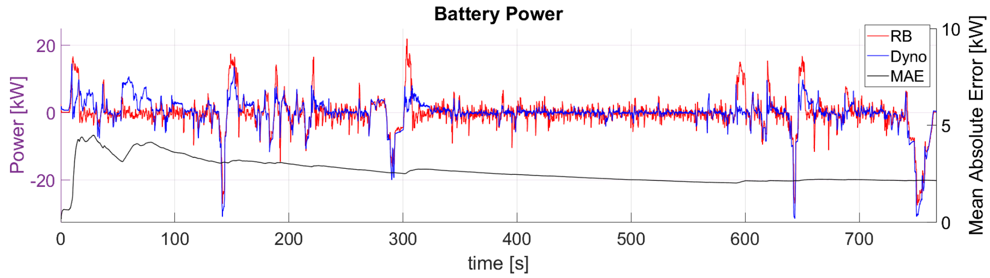

Figure A.14 Battery power results of the RB-EMS and the dynamometer test under HWFET cycle

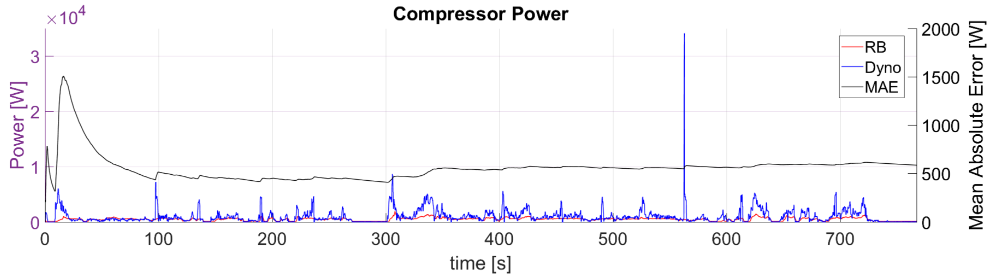

Figure A.15 Compressor power results of the RB-EMS and the dynamometer test under HWFET cycle

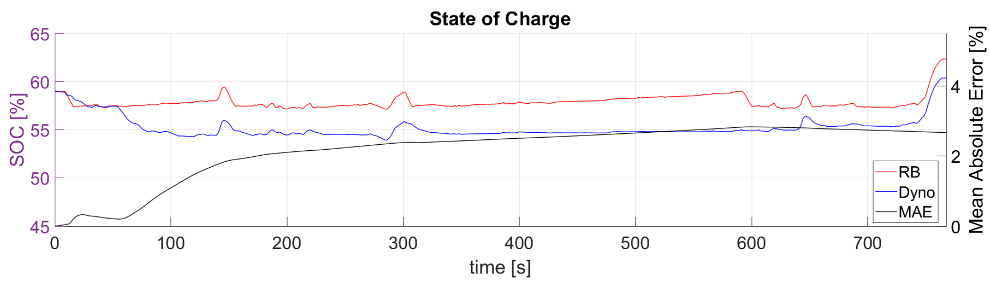

Figure A.16 SOC results of the RB-EMS and the dynamometer test under HWFET cycle